Principles and Application of Transient Electromagnetic Method

by

Hasan Kâmil Aktarakçı

ProQuest Number: 10783880

ProQuest 10783880

T-4331

A thesis submitted to the Faculty and the Board of Trustees of the Colorado School of Mines in partial fulfillment of the requirements for the degree of Master of Science (Geophysics).

Golden, Colorado

Date _March 25, 93_

Signed: _____
Hasan Kâmil Aktarakçı

Approved: _____
Dr. Alexander A. Kaufman
Professor of Geophysics
Thesis Advisor

Golden, Colorado

Date _April 5, 1993_

_____
Dr. Phil Romig
Professor and Head,
Department of Geophysics

ii

ABSTRACT

This thesis describes the application of transient electromagnetic method for mineral exploration. The transient method was introduced at the beginning of 1950s. It was suggested for mining prospecting, oil-gas and geothermal explorations. This method was initiated mainly in the U.S.S.R., the USA and Canada. After intensive development of its theory, equipment and application procedures, the transient method has become a conventional method in a variety of industrial applications. For instance, Geonics developed conventional equipment which have been broadly used in different parts of the World for different application areas.

In recent times, this conventional method is used for hydrocarbon exploration, mining prospecting, ground water exploration and environmental geophysics. Its application can be considered when the object of exploration has different resistivity than surrounding rocks.

In the first part of this thesis, the principles of transient method is described. As is known according to Biot Savart and Faraday laws, the primary magnetic field is generated with a transmitter current and a rapid reduction of the current, and thus also of the primary magnetic field induces an electromotive force. By applying the Ohm's law this electromotive force causes eddy currents that generate a secondary magnetic field. The behavior of the secondary electromagnetic fields are characterized for confined conductors, homogeneous and layered medium separately. In the electric and electromagnetic prospecting the experience shows that the apparent resistivity curves usually more vividly characterize the geologic section than the response of measured field. Therefore, the apparent resistivity in transient method is introduced.

In the second part of this thesis, after the geology and previous geophysical survey

are characterized, a field survey in which author participated, data and interpretation processes are described. The results of this survey demonstrate the ability of the transient electromagnetic method in resolving the depth of the volcanic basement unlike the seismic refraction or aeromagnetic survey. In addition, the changing depth of alluvium and lateral resistivity changes along the profile are able to delineate the prevailing fault system.

TABLE OF CONTENTS

LIST OF FIGURES

LIST OF TABLES

ACKNOWLEDGEMENTS

Chapter 1

PRINCIPLES OF TRANSIENT METHOD OF ELECTROMAGNETIC DEPTH SOUNDING

Introduction

In this chapter, the main principles of transient method will be described. First, the behavior of the transmitter current and primary electromagnetic field will be considered. Then, the secondary electromagnetic field and secondary current (induction current) will be illustrated. Later, the main features of the equipment, system and the method of interpretation will be discussed. And finally, some numerical examples will be given.

1.1 Physical Principles of the Transient Method

In this section, the behavior of the transmitter current and the main feature of the primary electromagnetic field will be illustrated. Later, secondary electromagnetic field will be discussed.

1.1.1 The Primary Transient Field

The Primary Magnetic Field

In the transient method, a direct current in the transmitter loop has following behavior (Figure 1.1b). At the beginning, the current is constant up to a certain time. Then, it is reduced to zero during a very short time which is called a ramp time, before the current is absent. The ramp time depends on equipment, size of the loop and
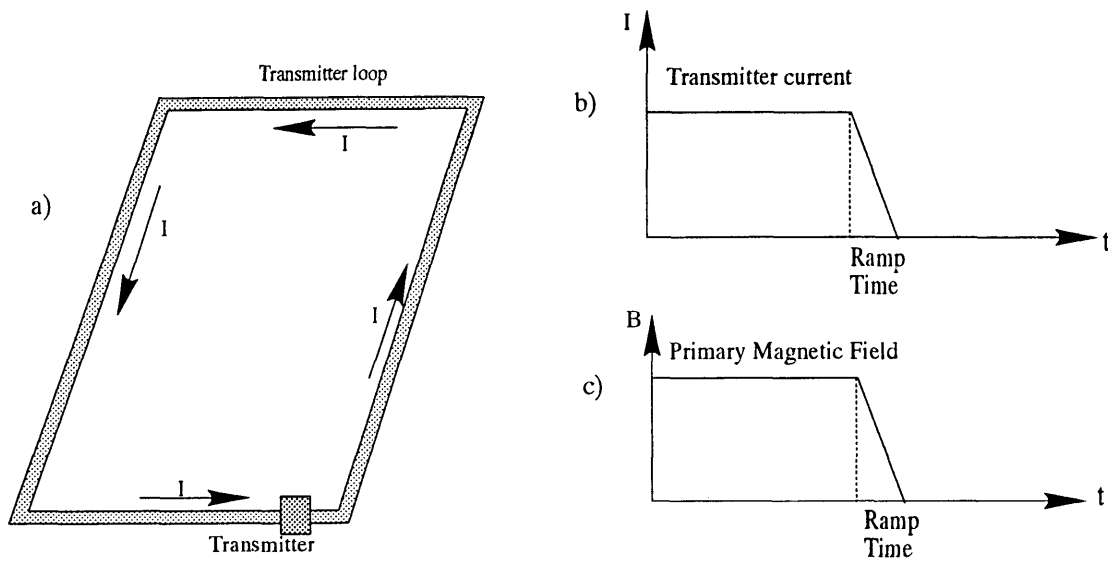
FIG. 1.1. (a) A rectangular transmitter loop of wire with current. (b) A current waveform. (c) A primary magnetic field waveform.

magnitude of the current. For example, a ramp time in the EM-37 equipment is 300 μs for 20 amps into 300m × 600m transmitter loop. Another example of the ramp time is that when the size of the loop or the magnitude of the transmitter current are large, the ramp time will be long.

According to Biot-Savart's law, the magnetic field is generated with current. The main feature of the primary magnetic field is shown in Figure 1.1c. As seen in the Figure 1.1c, the primary magnetic field behaves like transmitter current. When the current goes rapidly to zero, the primary magnetic field also goes rapidly to zero. Measurement is made after the ramp time. There is no primary magnetic field during the measurement time, unlike the other conventional electromagnetic methods. As follows from Biot-Savart's law, vector lines of the primary magnetic field are perpendicular to current lines. In other way, the primary magnetic field is perpendicular to horizontal plane. (Figure 1.2a).
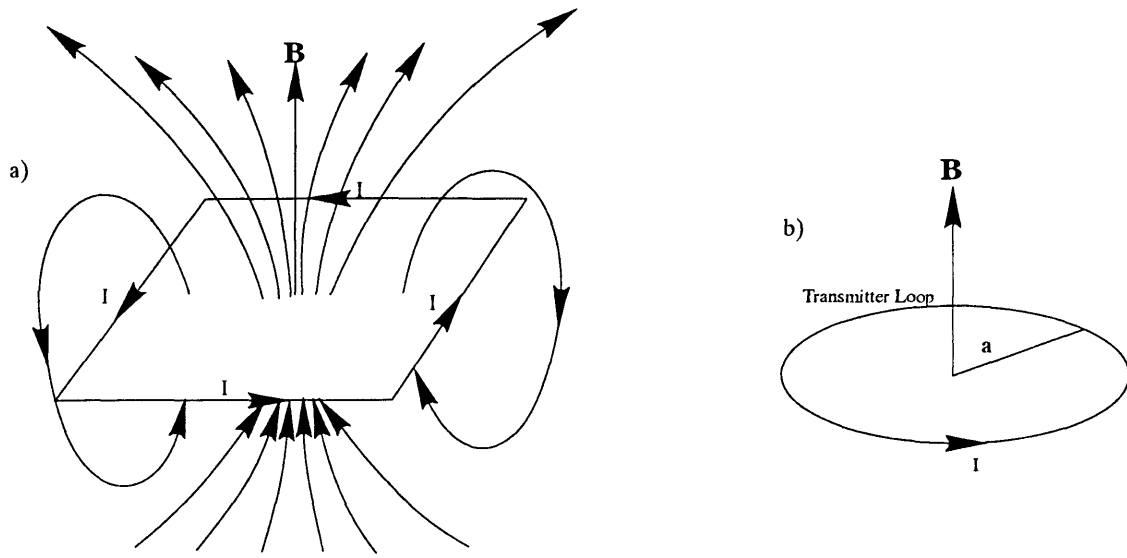
FIG. 1.2. (a) Behavior of the primary magnetic field around the transmitter loop.
(b) The primary magnetic field on the center of the loop.

Now, the behavior of the primary magnetic field which is generated by current in the loop will be evaluated. As an example, suppose the transmitter current is 20 amps and for simplicity, the transmitter loop is a circle with 100m radius. (See Figure 1.2b). The vertical component of the primary magnetic field on the center of the transmitter loop is calculated in following way:

$$B_z^o = \frac{\mu_o I}{2a} \qquad (1.1)$$

where $\mu_o = 4\pi \times 10^{-7} H/m$ is the magnetic permeability and B_z^o is the vertical component of the primary magnetic field on the center of the loop.

$$B_z^o = \frac{4\pi \times 10^{-7} \times 20}{2 \times 100} = 125.6 \times 10^{-9} Tesla \approx 125\gamma \qquad (1.2)$$

For comparison, the magnetic field of the earth is around 50,000 γ. However, the primary magnetic field generated by the current in the loop changes in very short time; the change can be detected.

Before the primary electric field is investigated, change of the primary magnetic field with depth will be evaluated. According to Biot-Savart's law, the primary magnetic field decreases with increasing distance from the current flow. The changing of the primary magnetic field with depth is illustrated in following way:

$$B_z = \frac{\mu_o I a^2}{2(a^2 + z^2)^{3/2}} = \frac{\mu_o I}{2a(1 + \frac{z^2}{a^2})^{3/2}} \tag{1.3}$$

When the z is equal to zero, the vertical component of the primary magnetic field is called (B_z^o) as in the equation 1.1. The ratio of them can be written in following form:

$$\frac{B_z}{B_z^o} = (1 + \frac{z^2}{a^2})^{-3/2} \tag{1.4}$$

Therefore, the behavior of the primary magnetic field changing with depth is seen in Figure 1.3 with 100m, radius of the current loop. As seen in the Figure 1.3, the magnitude of the field decreases with increasing depth. At the small depths, the field is not changing too quickly. Instantly, the magnetic field changes rapidly with increasing depth after a certain depth, it changes slowly.

The Primary Electric Field

The main role of the primary magnetic field is to generate an electric field. As it is seen in the Figure 1.4a, the primary magnetic field changes during only ramp time, therefore primary vortex electric field arises during this time (Figure 1.4b). In fact,
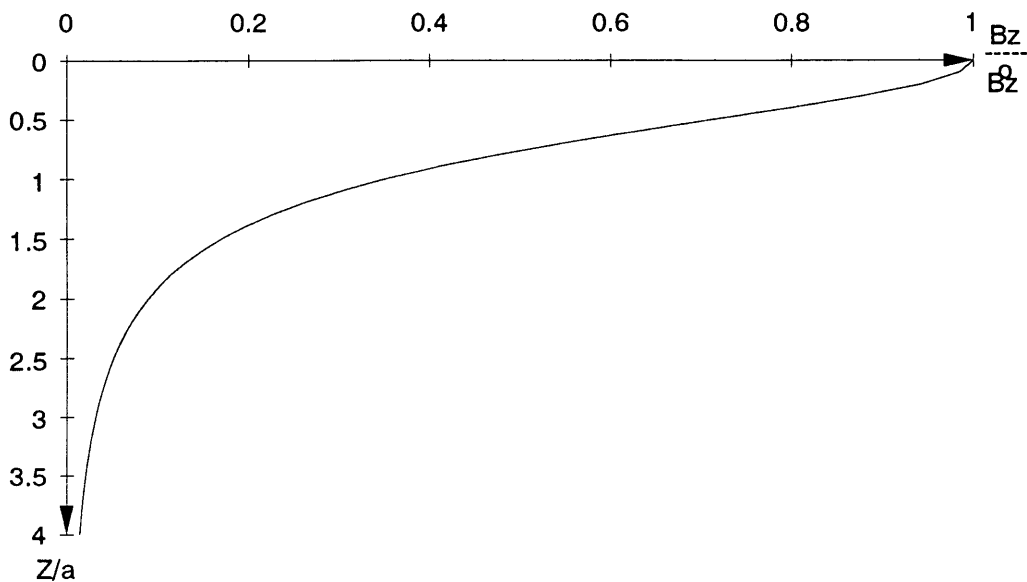
FIG. 1.3. Behavior of the primary magnetic field with depth.

a rapid reduction of the primary magnetic field induces an electromotive force (emf) which is described in the equation 1.5.

$$\varepsilon = \oint_L \vec{E}.\vec{dl} = \int_s \dot{\vec{B}}.\vec{ds} = -\frac{\partial \Phi}{\partial t} \qquad (1.5)$$

Where Φ is the magnetic flux, $\vec{E}$ is the electric field defined at each point along a closed contour, L. The magnitude of the emf is proportional to the time rate of change of the flux. The primary electric field appears only during the ramp time (Figure 1.4b). In addition, it is constant during this time because it is directly proportional to rate of change of flux. It is proper to notice that the receiver is open during the ramp time therefore, there is no measurement during the ramp time.

When a transmitter loop is located on the horizontal plane, the primary magnetic field is located vertical to the plane. But from the symmetry of the magnetic field, the
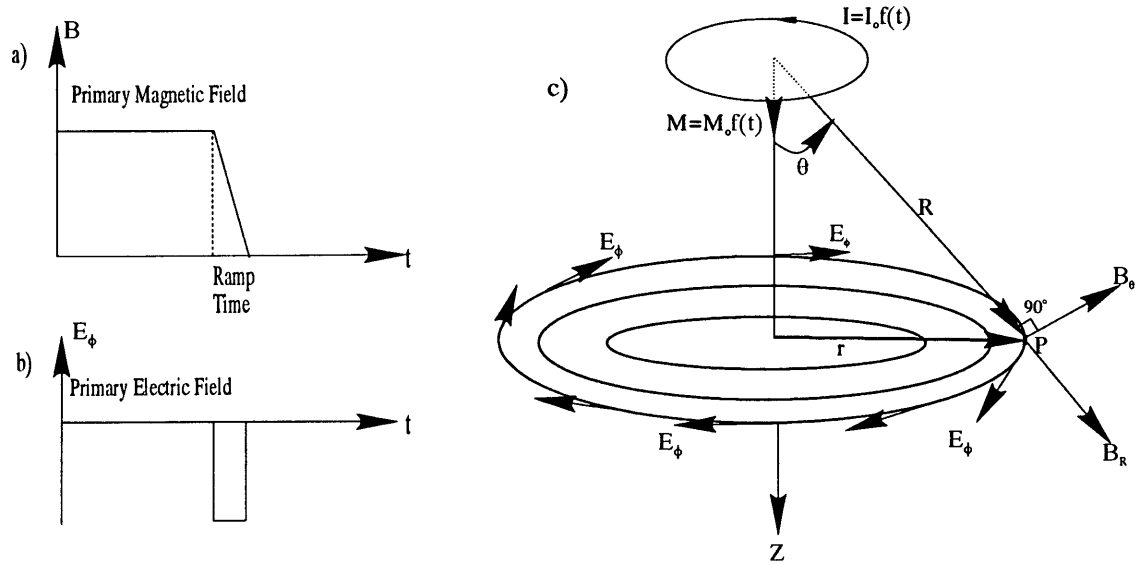
FIG. 1.4. (a) A primary magnetic field wave form. (b) Variation with time of the primary electric field. (c) Magnetic dipole situated in a spherical coordinate system.

electric fields are horizontal circles which are centered on the z axis (Figure 1.4c). The behavior of the electric field is evaluated as a function of coordinates. For simplicity, the point P is chosen is relatively far away from the current loop. As usual, this distance is at least two or three times larger than the radius of the loop. Thus, the current loop behaves as a magnetic dipole with a moment directed along the Z axis and situated at the origin of a spherical coordinate system (Figure 1.4b). The primary magnetic field according to Biot-Savart's law at the point P:

$$B_R = \frac{2\mu_o M_o}{4\pi R^3} \cos\theta f(t) \quad , \quad B_\theta = \frac{\mu_o M_o}{4\pi R^3} \sin\theta f(t) \quad and \quad B_\phi = 0 \qquad (1.6)$$

The vortex electric field arising as a result of Faraday law has only tangential component, E_ϕ;

$$E_\phi = -\frac{\mu_o M_o}{4\pi R^3} r f'(t) \qquad (1.7)$$
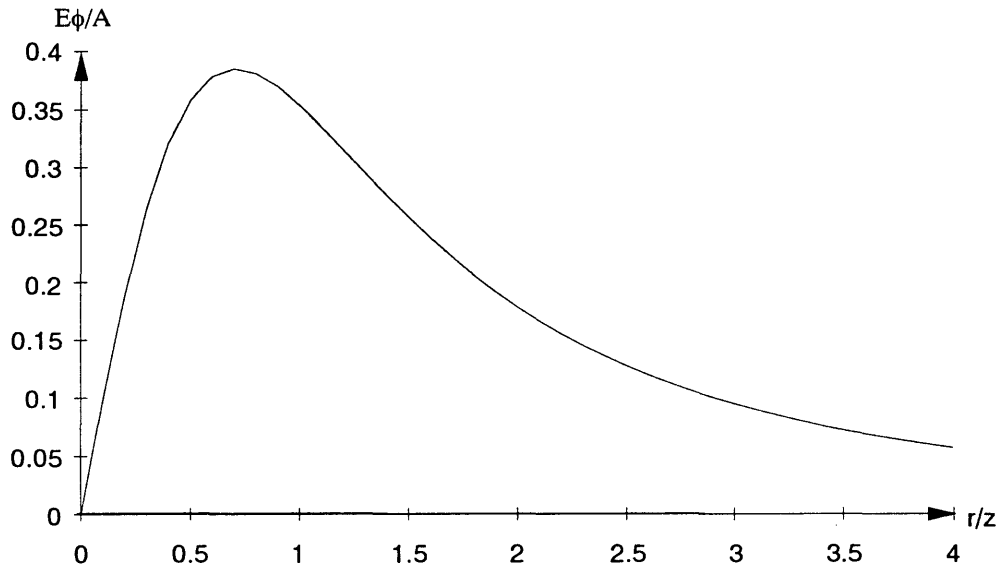
FIG. 1.5. The behavior of the tangential component of the electric field.

where $r = R \sin \theta$ and $R = \sqrt{r^2 + z^2}$ This equation can be also written in following way:

$$E_\phi = -\frac{\mu_o M_o f'(t)}{4\pi z^2} \frac{r/z}{(1 + (r/z)^2)^{3/2}} = A \frac{r/z}{(1 + (r/z)^2)^{3/2}} \tag{1.8}$$

As seen in Figure 1.5, there is no a primary electric field on the Z axis where r is equal to zero. It starts to increase with increasing r/z up to a certain distance, r. Then, it starts to decrease with increasing distance r. It is clear that the constant, A, is proportional to the inverse square of the vertical distance, z, therefore, the magnitude of the primary magnetic field decreases with increasing vertical distance, z (Figure 1.5).

In conclusion, the main role of the transmitter will be summarized. It creates the primary magnetic field which is related with the current and the size of the transmitter loop in which it flows. This primary magnetic field induces an primary electric field during only the ramp time. That is illustrated in following way:

$$I_t \rightarrow B_p \rightarrow \dot{B}_p \rightarrow E_p$$

where I_t is the transmitter current, B_p is the primary magnetic field, $\dot{B}_p$ is the rate of change of the magnetic field and E_p is the primary electric field. In following section, the secondary current which is caused by this primary electric field will be described.

1.1.2   The Secondary Transient Field

In this section, the behavior of secondary field measured in transient method will be discussed. It is convenient to consider the field in different area of applications. First of all, the field will be investigated in a confined conductor which is an example of an ore body. Later, it will be discussed for a uniform and layered half space.

The Behavior of Field Caused by a Confined Conductor

As it was seen in the previous section, the primary electric field is appeared only during a ramp time. If there is an conductor beneath the transmitter loop, the charges start to move along the electric field. This movement of charges (current) creates the secondary magnetic field and thus also the secondary electric field. As theory shows that at the first time, the current arises on the surface of the conductor if the ramp time is extremely small. This phenomena is called skin effect (Figure 1.6a). During the ramp time, there is an interaction among these surface currents that depends on not only the primary but also the secondary electric field. At the end of this time, the primary fields vanishes. The surface currents are distributed in such way that they create the magnetic field inside the conductor which is equal to the primary magnetic field. However, the magnetic field outside of the body will be completely different from the primary magnetic field. When the primary field disappears, the surface currents do not have any support; thus, they start to diffuse into the conductor
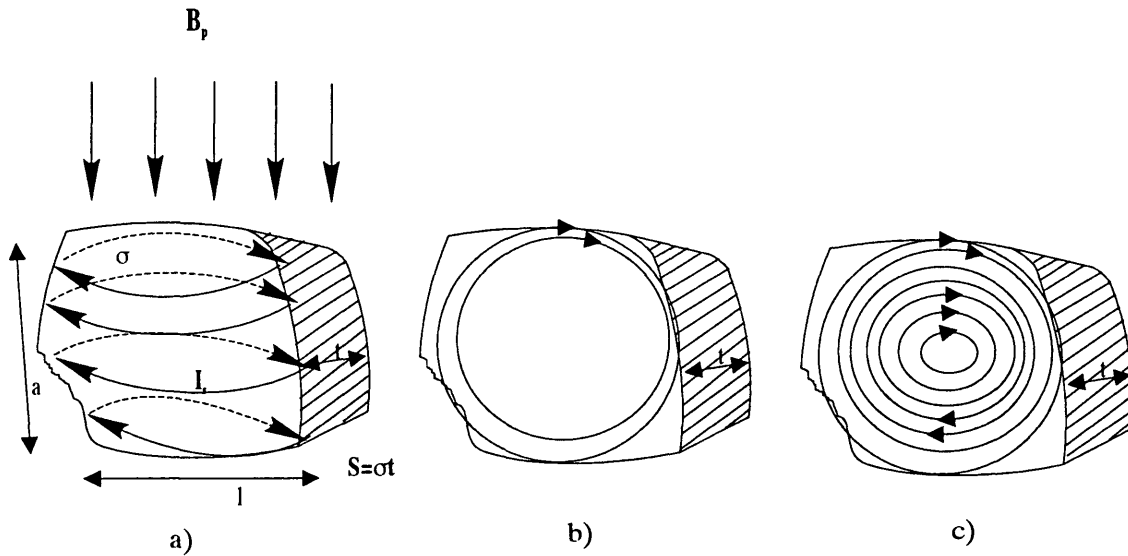
FIG. 1.6. Schematic illustration of current flow in arbitrary shaped conductor at various times.

(Figure 1.6b). This phenomena is called diffusion of currents and the electromagnetic field. For instance, the electrical field satisfies following equation.

$$\nabla^2 \vec{E} = \mu_o \sigma \frac{\partial \vec{E}}{\partial t} \qquad (1.9)$$

It is called heat equation because the same phenomena is observed during heat diffusion. The magnitude of the surface currents and the magnetic field start to decrease with increasing time since electromagnetic energy is transferred into heat. According to Faraday's law this change of the magnetic field create an electric field inside the conductor and the currents correspondingly appear inside of the conductor. This processes is sufficiently complicated and requires solution of the Maxwell's equations.

Now, the secondary field caused by induced currents in a conductor will be discussed. Suppose the current in the transmitter behaves as a step function. In

reality, the behavior of the current different from a step function, for instance, there is a ramp time. As well known, the magnetic field caused by induced currents can be written in following form:

$$B_x(t) = B_o \sum_{n=1}^{\infty} a_{nx} e^{-t/\tau_n}$$
$$B_y(t) = B_o \sum_{n=1}^{\infty} a_{ny} e^{-t/\tau_n}$$
$$B_z(t) = B_o \sum_{n=1}^{\infty} a_{nz} e^{-t/\tau_n} \tag{1.10}$$

where B_o is the primary field , a_n are geometric factors and τ_n are parameters. Geometric factors, a_n, depend on:

- size of the loop

- shape of the conductor

- size of the conductor

- location of the conductor

- location of the transmitter loop

- location of the receiver loop.

But, they are independent on the conductivity of the body. The parameters, τ_n, are related with the conductivity, shape and size of the body. It is essential that they do not depend on the current on the transmitter, the position and the size of transmitter and receiver loop. Moreover, they do not depend on position of the conductor. In most cases the coefficients for each components satisfy following inequality:

$$a_{1x} > a_{2x} > a_{2x} > a_{4x} > ...$$
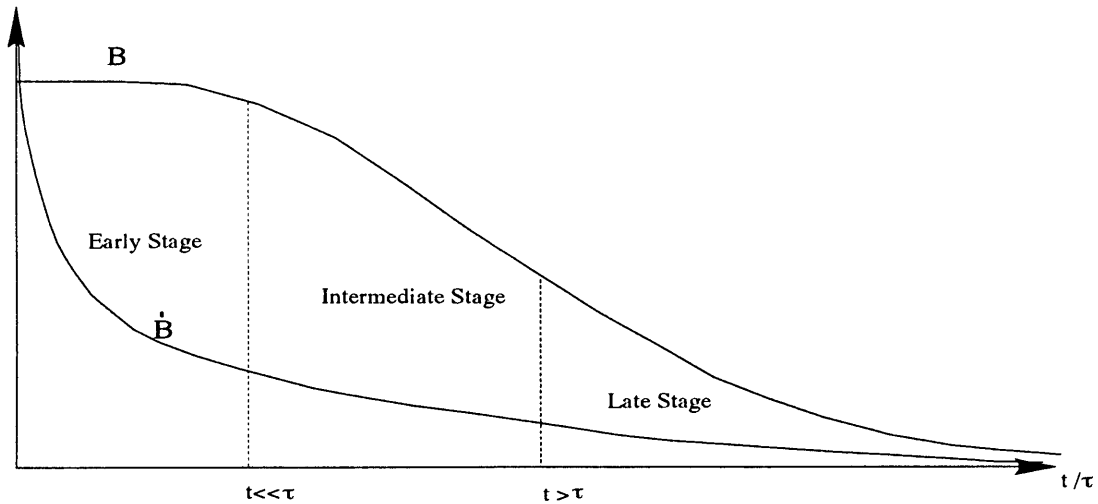
FIG. 1.7. Schematic illustration of the time constant.

$$\tau_1 > \tau_2 > \tau_3 > \tau_4 > ... \tag{1.11}$$

The largest parameter, τ_1, is usually called the time constant, τ, of the conductor, i.e. $\tau = \tau_1$. It is a very important parameter because it allows to make a judgment about geoelectric parameters of a conductor which causes the anomaly. The typical behaviors of the magnetic field and its derivative with time are shown in Figure 1.7. As it is seen in the Figure, it is natural to distinguish in three different parts of time response of the electromagnetic field.

The early stage: During this range of time, when $t \ll \tau$, the currents are mainly located on the surface of the conductor and the secondary magnetic field depends on the geometric coefficients, a_n. Since they do not depend on conductivity of the body and the position of body, the secondary fields do not contain any information which is related with conductivity of the body. However, the behavior of the electromotive force is different from the behavior of the mag-

netic field. Unlike the magnetic field, the electromotive force slightly depends on a conductivity of conductor body in this stage. Moreover, during this stage, the induced currents are usually located near the Earth's surface and this range of time does not have any practical interest.

The intermediate stage: Unlike the early stage, the magnetic field starts to depend a conductivity and the geometric parameters in this stage. The relationship between the field and the parameters is relatively complicated when especially the surrounding medium is sufficiently conductive.

The late stage: With increasing time, the secondary magnetic field will be observed in the late stage when the time of measuring, t, exceeds the time constant, τ. As it is seen in the equality 1.11, with increasing time influence of the first constant is dominant. Therefore, the behavior of the field is described by a first term of the sum in the equation 1.10.

$$B_x(t) = B_o a_{1x} e^{-t/\tau}$$
$$B_y(t) = B_o a_{1y} e^{-t/\tau}$$
$$B_z(t) = B_o a_{1z} e^{-t/\tau} \tag{1.12}$$

These equations are very simple and this fact greatly facilitates the interpretation. The remarkable feature of these equations is that they are represented with the product of two terms, geometric parameters and the exponential term, on the right side of the equation 1.12. The exponential term does not depend on the intensity of the primary field or the position of the observation point, but is only function of the time, t, and time constant, τ. In order to prove this

SPHERE

a)

$$\tau = \dfrac{\mu_o \, \sigma \, a^2}{\pi^2}$$

σ = Conductivity

a = Sphere Radius

THIN PLATE

b)

$$\tau_p = \dfrac{\mu_o \, S \, l_1}{8.02}$$

l_2/l_1	1	2	4
τ/τ_p	0.77	0.94	1.00

Cylinder

c)

$$\tau = \dfrac{\sigma \, \mu_o \, a^2}{5.78}$$
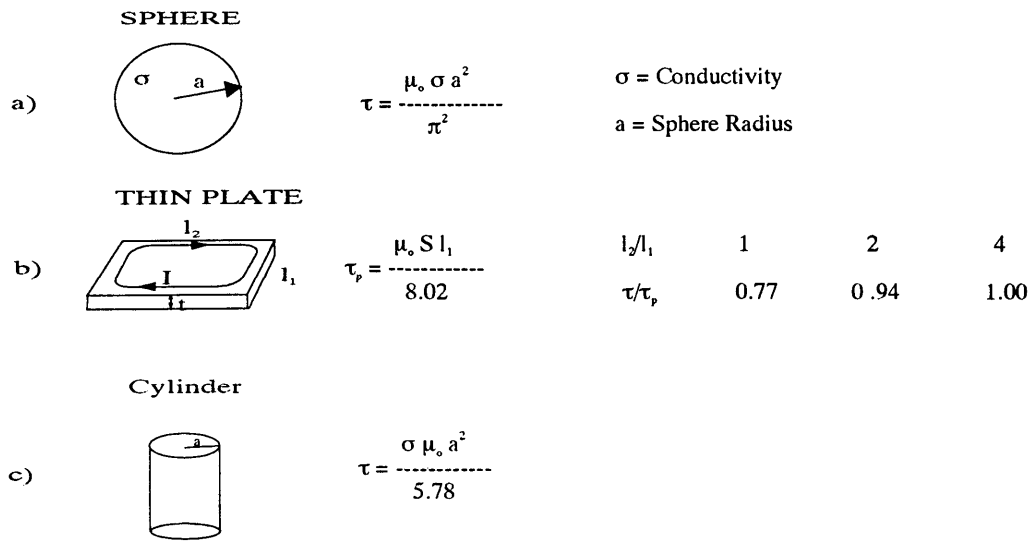
FIG. 1.8. The time constants for different geometric shapes.

fact, we consider the ratio of the two first term in the equation 1.10.

$$\frac{a_2 \, e^{-t/\tau_2}}{a_1 \, e^{-t/\tau_1}} = \frac{a_2}{a_1} e^{\frac{-t}{\tau_1}(\frac{\tau_1}{\tau_2}-1)}$$

(1.13)

According to the equation 1.13, the coefficient, $\left(\frac{\tau_1}{\tau_2}-1\right)$ is positive and therefore, the exponential term is getting smaller with increasing time. In other words, with increasing time at the late stage, the influence of second term becomes relatively small. In the same manner, it is valid for the other terms. Therefore, at the late stage, the field practically defined by first term.

Taking into account importance of the time constant, the table of this parameter is given in the Figure 1.8. Let us illustrate some values of the time constant for several cases:

Cases 1 For example, the radius and resistivity of a sphere are (Figure 1.8a):

$a = 30m$, ρ=0.1 ohm-m

The time constant for such a sphere can be found $\tau \approx 1.1$ msec.

Case 2 The resistivity of thin conducting plate is 0.05ohm-m and its thickness,t, is 1m (Figure 1.8b). The time constant can be calculated for different ratio of sides of the plate.

l_2/l_1	1	2	4
τ	$0.048 msec$	$0.058 msec$	$0.062 msec$.

Case 3 A cylinder with the circular cross-section; a=20m is its radius and its resistivity is $\rho = 0.05 ohm - m$ (Figure 1.8c).

The time constant can be found $\tau \approx 1.7 msec$.

These numerical examples allows us to understand the time range of the measurement. Usually the determination of numerical values of geometric parameters and time constant requires a solution of boundary value problem and currently there are several programs which are used by finding these parameters.

Let us illustrate the behavior of the magnetic field along a profiling when the primary field has the form of a step function. Suppose a sphere with a radius a is embedded in an insulating space and the source of the primary magnetic field is a horizontal loop with a current, I, flowing in it (Figure 1.9a). As is known, the field can be described for the late stage in following way:

$$B_z = \frac{3B_o a^3}{\pi^2 R^3} e^{-t/\tau} (3Cos^2\theta - 1)$$

$$B_x = \frac{9B_o a^3}{\pi^2 R^3} e^{-t/\tau} Sin\theta Cos\theta \quad if \quad t >> \tau \tag{1.14}$$

where a is the radius of the sphere, B_o is the primary magnetic field which is described in the equation 1.3. Also, it is convenient to represent the equation 1.14 as in following
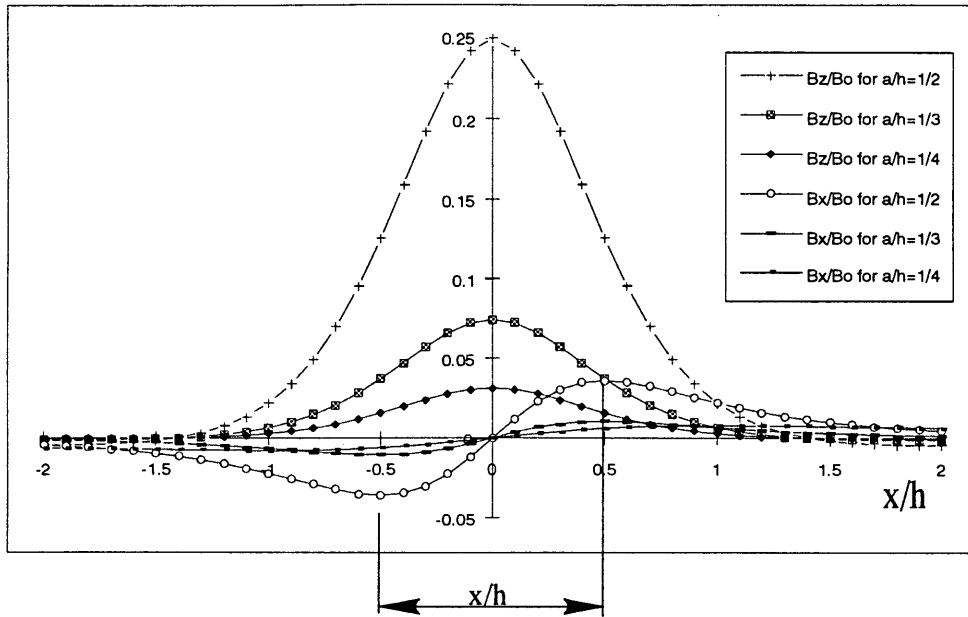
b)
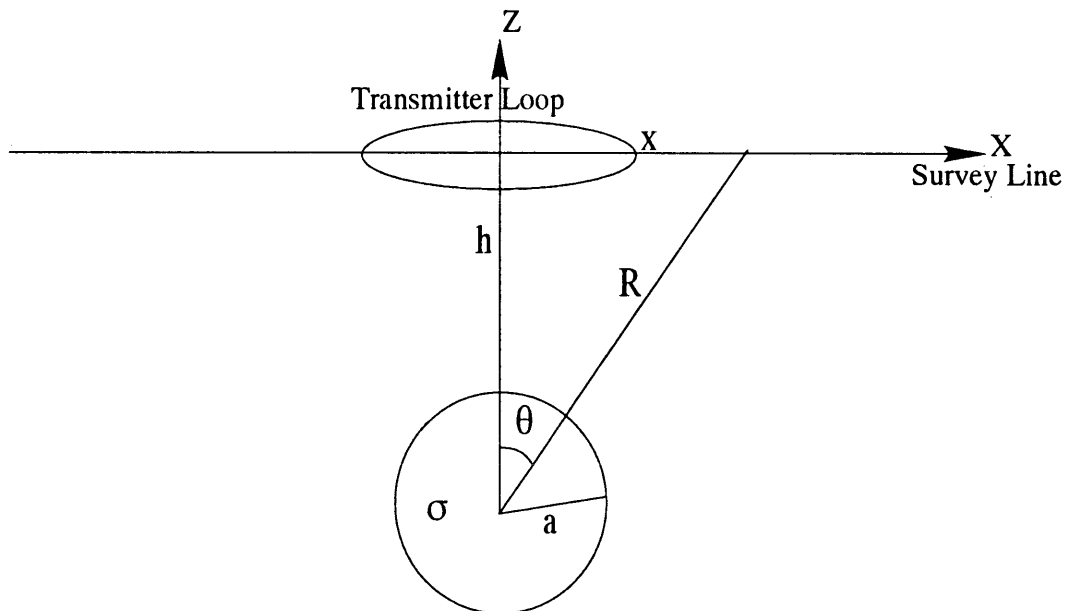
a)

FIG. 1.9. (a)The geometry of the source and the conductor sphere. (b)The behavior of magnetic field above the target.

way:

$$\frac{B_z}{B_o} = \frac{3e^{-t/\tau}}{\pi^2} \frac{a^3}{h^3(1 + (x/h)^2)^{3/2}} \left(\frac{3}{1 + (x/h)^2} - 1\right)$$

$$= A(a/h)^3 \frac{1}{(1 + (x/h)^2)^{3/2}} \left(\frac{3}{1 + (x/h)^2} - 1\right) \tag{1.15}$$

and for horizontal component;

$$\frac{Bx}{B_o} = \frac{9e^{-t/\tau}}{\pi^2} \frac{a^3}{h^3(1 + (x/h)^2)^{3/2}} \frac{x}{1 + (x/h)^2}$$

$$= B(a/h)^3 \frac{1}{(1 + (x/h)^2)3/2} \frac{1}{(r/h) + (h/r)} \tag{1.16}$$

The results of calculation of the vertical and the horizontal components of the magnetic field (B_z, B_x) are given as a function of the depth, radius of the conductor sphere and the distance for a survey line through the center of the transmitter loop. As is seen from these curves:

1) In approaching to the center of the transmitter loop, at the beginning, the horizontal component of the magnetic field decreases and reaches a minimum then, it becomes equal zero exactly above the conductor. Later it start to increase until a maximum point then, it goes zero. The amplitude of the field decreases with increasing the depth of the target. Furthermore, the distance between the maximum and minimum position of the field is directly related with the depth of the target and is exactly equal the depth (Figure 1.9b).

2) The vertical components of the magnetic field has a maximum in the center of the loop and gradually decays to zero with increasing distance from the transmitter loop. The amplitude of the maximum is a function of the depth of the sphere.

As was mentioned above for more complicated bodies there are different program

which allows the calculations.

Next we will evaluate the signals caused by a secondary magnetic field. Suppose the measurement is made at the center of the transmitter loop above the sphere (Figure 1.9a).

- The radius of the transmitter loop,   r=100m

- The transmitter current,   I=20amps

- The radius of the conductor sphere,   a=30m

- The depth of the conductor,   h=60m

- The resistivity of the conductor, ρ=1 ohm-m

- The measurement time, $t = 2\tau$

- The receiver moment is $M_r = nS = 1m^2$, where n is the number of turn and S is the receiver loop area.

In such case, the electromotive force can be calculated by using the following equation:

$$B_o = \frac{\mu_o I r^2}{2(r^2 + h^2)^{3/2}}$$

$$B_z = \frac{6B_o a^3}{\pi^2 h^3} e^{-t/\tau}$$

$$\varepsilon = \dot{B_z} M_r \tag{1.17}$$

$$V = -\rho \frac{3I r^2 a e^{-2}}{(r^2 + h^2)^{3/2} h^3} \tag{1.18}$$

thus, the electromotive force will be $V = 0.0071$ millivolts. As the experience

shows, the noise caused by natural magnetic field and cultural noise is changed approximately in following way:

$$10^{-12} < \dot{B}_z < 10^{-8} \ v/m^2.$$

In this section, the behavior of the secondary field was discussed for a conductor sphere which is important for the mining exploration.

1.2 Physical Principles of Transient Sounding

In the previous section, the behavior of the electromagnetic fields caused by currents in confined conductors was investigated. Now, we will consider the behavior of electromagnetic fields generated by induced currents in layered medium. This study will help us to understand the physical principles of the transient sounding. Let us start from the case of a uniform medium.

1.2.1 The Field in a Uniform Medium

Suppose the primary field, caused by a small current loop (Magnetic dipole), behaves as a step function (Figure 1.4a). It is natural to distinguish four stages in the vicinity of any observation point located at a distance R from the dipole:

Stage-I When the transmitter current is switched on, the electromagnetic wave arises in the vicinity of the dipole and this wave travels away from the dipole with a velocity V:

$$V = \frac{1}{\sqrt{\varepsilon\mu}} = \frac{C}{\sqrt{\varepsilon^*\mu^*}}, \tag{1.19}$$

where ε is a dielectric constant, μ is a magnetic permeability of a medium and $C = 3 \times 10^8 m/sec$. Therefore, the wave arrives to a receiver at the instant
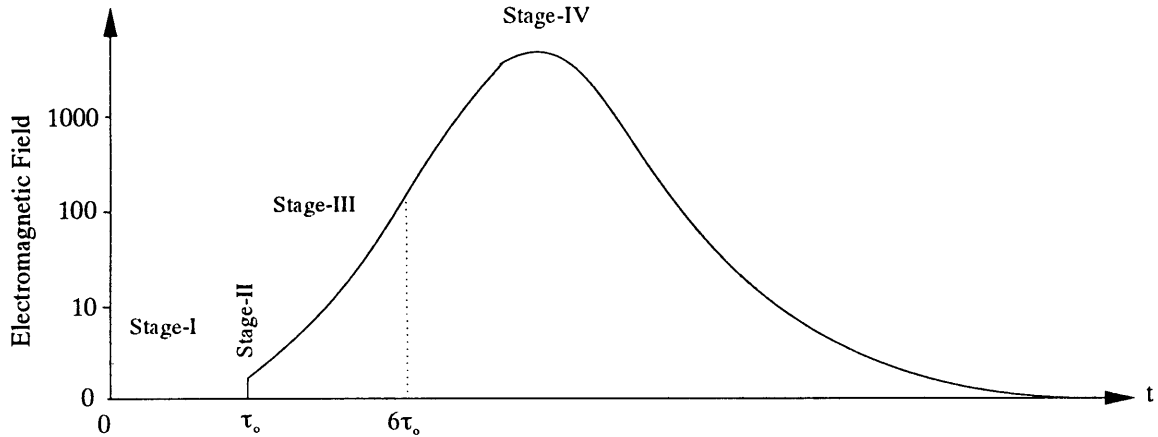
FIG. 1.10. Schematic illustration of behavior of the electromagnetic field after the transmitter current is turned on.

$t = \tau_o$ (Figure 1.10):

$$\tau_o = \frac{R}{V} = \frac{R}{C}\sqrt{\varepsilon_r},\tag{1.20}$$

if $\mu = \mu_o$. Let us evaluate τ_o time for the cases of practical interest. For example, if the distance R from the transmitter to the receiver is equal to 100m then, the time τ_o will be

$$\tau_o = \frac{100m}{3 \times 10^8} = 10^{-6}sec = 1\mu sec\tag{1.21}$$

This means that the electromotive force in the receiver equals to zero during the first stage.

Stage-II This stage describes the moment $t = \tau_o$ when the wave arrives at the observation point and it is called first arrival (Figure 1.10). The magnitude of the first arrival depends on not only a distance, a dielectric constant, a

magnetic permeability but also a conductivity of medium. As theory shows, in a nonconductive medium, the magnitude of signal can be relatively large, but in a conductive medium at a sufficiently large distance, this signal becomes very small. It decreases exponentially with a conductivity.

Stage-III When the wave arrives at the observation point, it quickly changes with time. For this reason, the field is caused by not only the conduction currents but also the displacement currents. Therefore, it depends on both a conductivity and a dielectric constant. Usually this range of time lasts during $(6\text{-}10)\tau_o$. For instance, if $\tau_o = 1\mu sec$, the time will be 6 or 10 μsec at the end of this stage. So it shows very short time interval. Usually, the measurements in a conventional equipment start later than this time. For example, the first channel of Geonic's EM-37 begins to measure after around $100\mu sec$.

It is proper to notice that there are area of geophysics where the measured field is caused by both the conduction and the displacement currents. These area are the radar system, the dielectric logging in borehole and shadow method for detecting ore bodies among two tunnels or bore holes.

Stage-IV During this stage, the electromagnetic fields is independent on dielectric constant. However they depend on a conductivity, a magnetic permeability of medium and a separation as well as time. In this stage, the diffusion of the electromagnetic field is observed (Figure 1.10) and it is called quasi-stationary field. This field, measured in transient sounding, will be considered in detail.

Let us investigate the behavior of a conduction current during the quasi-stationary field of a magnetic dipole in a uniform full-space medium.

Behavior of Conduction Current

The physical principles of the transient sounding is similar to that for the transient method for search of confined conductors, since in both cases the diffusion of the currents is observed. Unlike the mining prospecting where the field caused by an induced currents in a confined conductor is considered, we will investigate the behavior of field in layered medium. To illustrate the quasi-stationary field in such medium, first of all we will analyze the simplest model which does not have any interfaces (uniform medium). It is convenient to start a discussion from a study of the distribution of conduction currents. Again, we assume that the transmitter current is turned on. According to Faraday's law, at the first moment, the induction currents appear near the transmitter unlike the case that they appear on the surface of a confined conductor when the surrounding medium is insulator. At this moment, the magnitude of induced currents is equal to the magnitude of current of the transmitter, but it is opposite direction. Inasmuch as the transmitter current is constant, it does not support the induced currents. For this reason, they start to decrease because electromagnetic energy is transformed into heat. Because of this change of the current, the alternating magnetic field arises and its change with time creates induced electric field and therefore the currents in the medium. With increasing time, the induction currents and the field appear at greater distances from the transmitter. Suppose the magnetic field caused by this currents is measured in some distance, R, from the transmitter as shown in the Figure 1.11. It is obvious that the change of distribution of currents with time makes influence on the depth of investigation. In order to show this relation, let us consider the distribution of currents in the medium at some distance from the transmitter. As seen in the Figure 1.12, at the beginning, the density of currents is equal to zero then, it starts to increase and reach to a maxi-
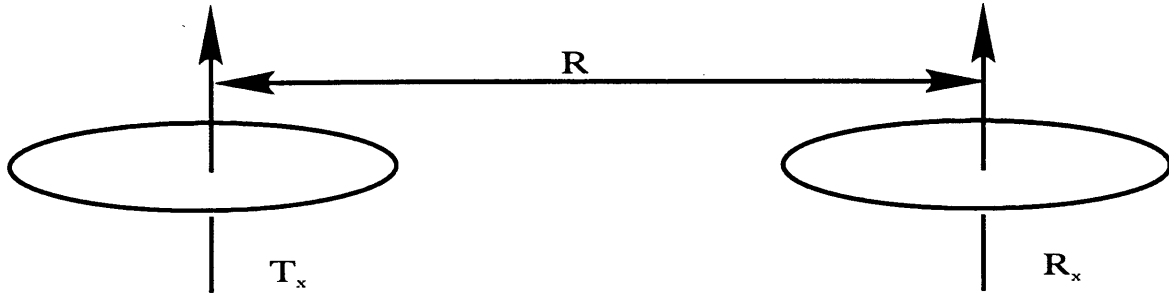
FIG. 1.11. The position of the transmitter and the receiver.
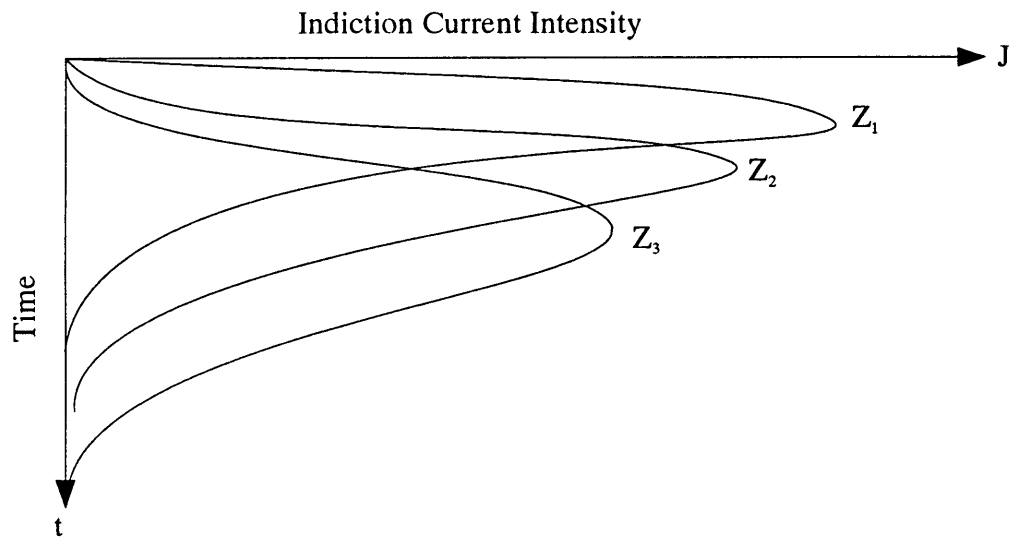
FIG. 1.12. Schematic illustration of the current intensity versus with depth.

mum and later it goes to zero. When separation is small, all transient response occurs at relatively quickly. During the early times the currents appear near the transmitter therefore the magnetic field contains information about shallow part of the medium. Since with increasing time the currents appear in greater depth, therefore the magnetic field caused by the induced currents contain information about deeper part of the medium. This is the main concept of the transient sounding. Of course there are other factors which also effect to the magnetic field such as the distribution of the resistivity with depth and the separation between a transmitter and receiver. Now let us look at the influence of a resistivity and separation on the transient response of the field. As an example, the Figure 1.13 shows the transient response of the field for uniform medium in different resistivity and separation. As seen in the Figure 1.13a, if the resistivity of medium increases, the electromagnetic energy is more rapidly transformed into heat therefore the diffusion is observed relatively quickly. On the other hand, if the medium is conductive, the diffusion process lasts longer. The Figure 1.13b shows how the separation between the transmitter and receiver makes influences on the behavior of the field. For instance, with increasing distance between the transmitter and the receiver, all main feature of the field start to observe in larger time. It is related with the fact that with increasing separation the relative contribution of currents located in greater depth becomes stronger.

We investigated the magnetic field and currents in a uniform medium and demonstrated their behaviors in accordance with the diffusion phenomena. It is clear that the same diffusion phenomena effect is observed in layered medium. For instance, suppose there is a two layer medium with more conductive upper layer (Figure 1.14). At the first moment the conduction currents will be near the transmitter. Therefore, the field measured by the receiver contains information from the first layer. Of course,
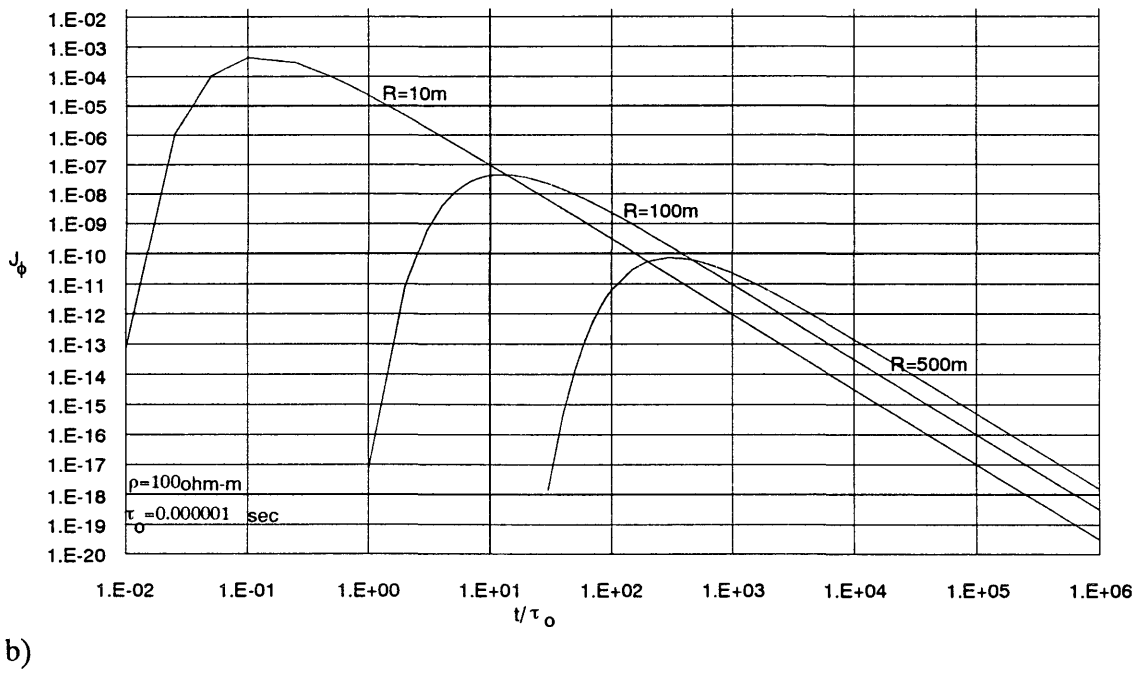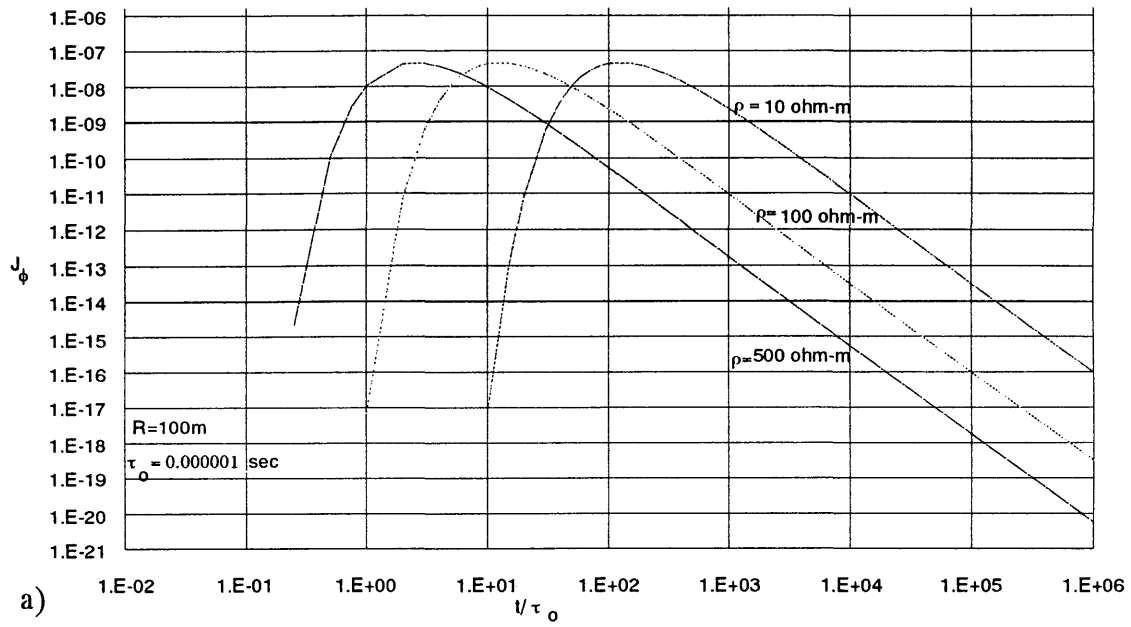
FIG. 1.13. Behavior of the function $(u^5/R^4)e^{-u^2/2}$ as a function of t/τ_o.
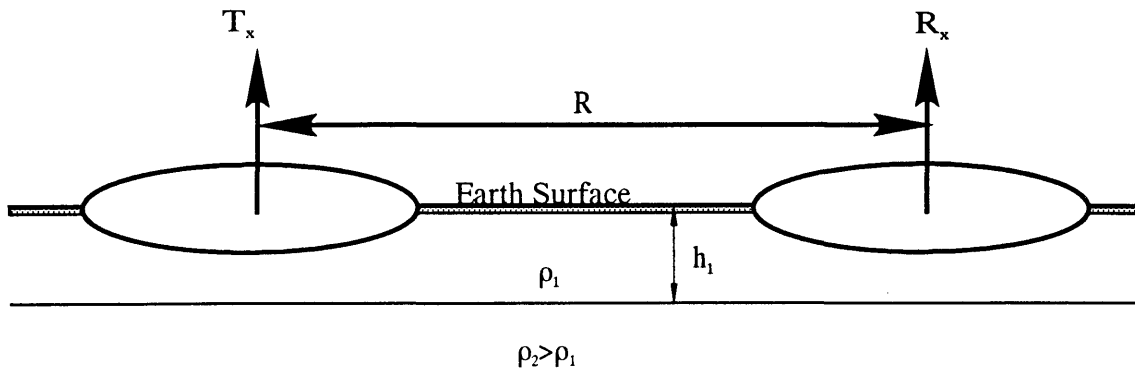
FIG. 1.14. Location of a transmitter and a receiver on the two layer medium.

if the upper layer is more conductive, the currents in this layer remain longer and vice versa. Then, with increasing time the magnitude of the currents becomes more significant at a greater depth. Finally, due to diffusion, the currents appear at the basement and we get information about its resistivity. In other words, the upper layer becomes transparent. It is obvious that the same conclusion can be arrived for many layered medium. This analysis shows that depth investigation in the transient sounding is independent on the separation between the receiver and the transmitter. Unlike the Schlumberger sounding, the transient sounding allows to perform a study of the resistivity of depth regardless how small separations and this fact gradually improves its lateral resolution. Now, let us characterize the behavior of the electromagnetic field in a layered medium.

1.2.2 Behavior of the Electromagnetic Field in the Layered Medium

As is well known the interpretation of the transient sounding consists of comparison between the measured and calculated field and the later is based on solution

of boundary value problem (forward problem). Usually in order to calculate the field we solve the boundary value problem in the frequency domain. Then, making use of the Fourier integral, the transient response is calculated. The solution of the forward problem allows to calculate spectrum and it consists of several steps. First of all electrical and magnetic field must satisfy Helmholtz equation which describes the behavior of the field inside of the layers:

$$\bigtriangledown^2 \vec{E_i} + k_i^2 \vec{E_i} = 0$$
$$\bigtriangledown^2 \vec{B_i} + k_i^2 \vec{B_i} = 0 \tag{1.22}$$

where $k_i^2 = \gamma \mu i w$, w is circular frequency $(2\pi f)$ and subscribe i shows ith layer in the medium. Second condition requires a continuity of tangential components of the electric and magnetic fields at interfaces:

$$E_t^i = E_t^{i+1}, \quad B_t^i = B_t^{i+1} \quad when \quad z = h_i$$

where h_i is the thickness of the ith layer and t indicates any tangential components. The third condition shows that the field tends to the primary field when the point of observation approaches to the source:

$$\vec{E} \longrightarrow \vec{E_o} \quad when \quad R \longrightarrow 0$$
$$\vec{B} \longrightarrow \vec{B_o} \quad when \quad R \longrightarrow 0$$

where $R = \sqrt{r^2 + z^2}$. The fourth condition requires that the field must tends to zero at infinity:

$$\vec{E} \longrightarrow 0 \quad when \quad R \longrightarrow \infty$$
$$\vec{B} \longrightarrow 0 \quad when \quad R \longrightarrow \infty$$

In most practical cases, we can assume that the source of primary magnetic field is horizontal current's loop and when it is relatively small it can be treated as a magnetic

dipole. For this reason, the vector lines of the induced currents which appear in the medium are located in horizontal plane. They are circles and their centers are located on the Z-axes. Therefore they create the electromagnetic field which is described by two component of the magnetic fields, B_r, B_z, and one component of the electrical field which is E_ϕ. The electromagnetic field caused by a magnetic dipole in layered medium is defined as;

$$E_\phi = \frac{iw\mu M}{2\pi} \int_0^\infty \frac{m^2}{m + m_1/R_n} J_1(mr)dm$$

$$B_r = \frac{M}{2\pi} \int_0^\infty \frac{m_1 m^2}{m + m_1/R_n} J_1(mr)dm$$

$$B_z = \frac{M}{2\pi} \int_0^\infty \frac{m^3}{m + m_1/R_n} J_o(mr)dm \qquad (1.23)$$

where $m_1 = \sqrt{m^2 - k_1^2}$, m is the separation constant, J_o, J_1 are the Bessel's function of the first kind of order zero and one respectively and

$$R_n = coth\{m_1 h_1 + coth^{-1}(m_1/m_2)coth[m_2 h_2 + coth^{-1}(m_2/m_3)coth(m_3 h_3...)]\}$$

As was pointed out early, as soon as its spectrum is known, the integral Fourier is used for calculation of the transient response of electromagnetic field. Let us notice that there are at least two exceptions where there is no need to apply the Fourier integral. These cases include the field of a magnetic dipole on the surface of uniform half-space medium and above a conductive plane in a free space.

Now, we will describe the behavior of magnetic field on the surface of layered medium and assume that the source of the field is vertical magnetic dipole on the earth surface. It is proper to notice that the information about electrical field caused by a magnetic dipole can be used when we measure the vertical component of magnetic field at the center of the loop. Let us start with a uniform half space medium.
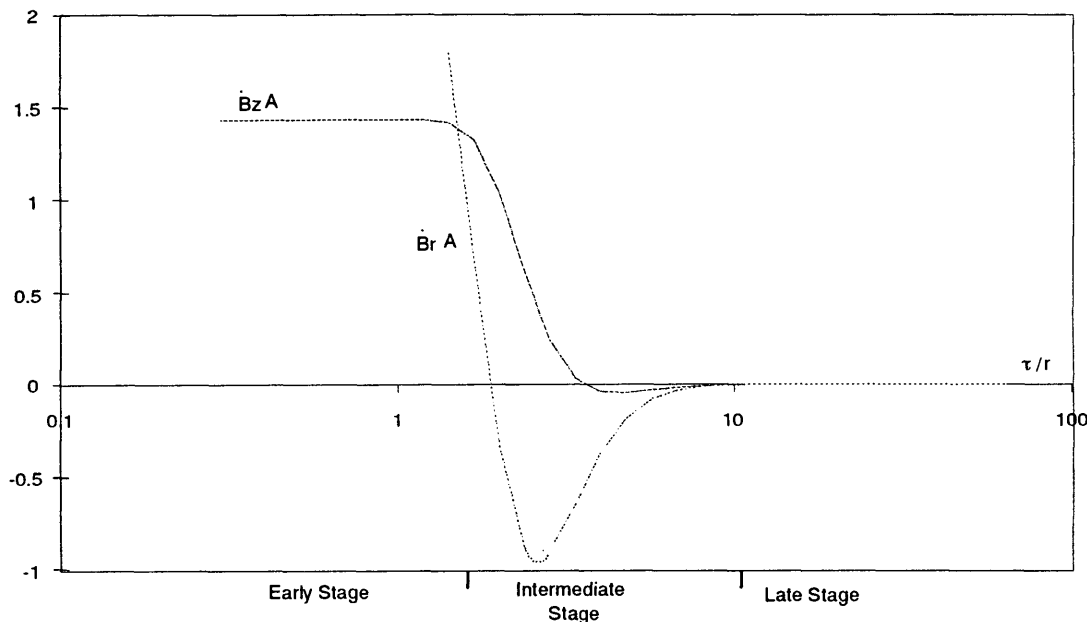
FIG. 1.15. Variation of the time derivatives of the radial and vertical components of magnetic field as a function of scaled time and distance $(A = r^5/M\rho)$

In most practical cases the receiver measures the electromotive force due to the secondary magnetic field and for this reason first we will show its behavior on the surface of a uniform half-space. The behavior of the time derivatives of the radial and vertical components of the magnetic field as a function of a ratio, τ/r, are shown in Figure 1.15. The R is a distance between a transmitter and a receiver and τ is described as:

$$\tau = \sqrt{2\pi\rho t \times 10^7} \qquad (1.24)$$

First we will show the vertical component of magnetic field as seen in the Figure 1.15. When the τ/r is small, the function $\dot{B}_z$ practically does not change. With increasing time it starts to decrease gradually and further with increasing of time it reaches zero and changes sign. After it reaches a minimum, it goes zero. The behavior of

function $\dot{B}_r$ is completely different at early stage. Unlike $\dot{B}_z$ when τ/r tends to zero $\dot{B}_r$ increases extensively. With increasing τ/r it decreases then becomes zero and later it reaches minimum and then asymptotically tends to zero. The minimum of the $\dot{B}_r$ takes place earlier time than that for $\dot{B}_z$. It is useful to distinguish three stages of the transient response of a time-derivative of magnetic field: early, intermediate and late stages (Figure 1.15). When the parameter τ/r is smaller than unit or 2, the early stage takes place. The field for early stages can be approximately defined in following form:

$$\frac{\partial B_z}{\partial t} \approx -\frac{9M\rho}{2\pi r^5} \quad if \quad \tau/r < 2$$
$$\frac{\partial B_r}{\partial t} \approx -\frac{3M}{2\pi r^4}\sqrt{\frac{\mu\rho}{\pi t}} \quad if \quad \tau/r < 1 \quad\quad\quad (1.25)$$

As seen in the equation 1.25 the time derivative of magnetic field, $\dot{B}_z$, is proportional to the resistivity of medium. When the conductivity of medium increases, the induced currents stay longer therefore the early stage will be observed for the large values of the ratio τ/r. It is also clear that with increasing a resistivity the signal becomes bigger. At this stage both component of field relatively quickly decrease with distance. For example, the vertical component of field changes as $1/r^5$. Unlike the vertical component of the field, the horizontal component of field decays slowly with distance, $1/r^4$. This analysis shows that the horizontal component of field is dominant.

In the opposite case, when the parameter $\tau/r \gg 1$, late stage is observed and the behavior of the field has completely different character. As follow from the exact solution both derivatives are described by following equations:

$$\frac{\partial B_z}{\partial t} \approx \frac{\mu M}{20\pi\sqrt{\pi}}\frac{(\mu\sigma)^{3/2}}{t^{5/2}}$$

$$\frac{\partial B_r}{\partial t} \approx \frac{\mu M}{64\pi} r \frac{(\mu \sigma)^2}{t^3} \quad if \quad \tau/r > 16 \tag{1.26}$$

Unlike the early stage the voltage induced in a horizontal receiver coil decays as $t^{-5/2}$ and the derivative of horizontal component of magnetic field is smaller ($\dot{B}_r < \dot{B}_z$). The electromagnetic field is characterized by a relatively high sensitivity to a change in conductivity of medium during this stage:

$$\dot{B}_z \sim \sigma^{3/2} \quad and \quad \dot{B}_r \sim \sigma^2 \tag{1.27}$$

It is important to emphasize that the measurements at late stage are usually more sensitive to ground resistivity than the measurements at early stage and very often the measurements performed at the late stage provide an information about the distribution of conductivity and a greater depth.

Let us show the behavior of time-derivative of vertical component of the magnetic field for different resistivities and distances between a transmitter and a receiver. As seen in the Figure 1.16a the changing of resistivity does not change the shape of the curve but early time as well as two other stages is observed greater times with decreasing a resistivity. Similar behavior is observed in the case of the changing distance when the resistivity is constant (Figure 1.16b).

Next let us consider a behavior of transient field in the presence of a thin conducting layer. Very often this model of a medium is useful for understanding of the method for its applications in ground water geophysics as well as oil geophysics. For instance, when salt water penetrates into a aquifer, it is important to find a boundary between fresh and salt water and the part of the layer saturated by salt water can be treated as a thin conducting layer. Similar situation occurs when the part of oil reservoir is filled by salt water. Now let us show the behavior of field in case of a
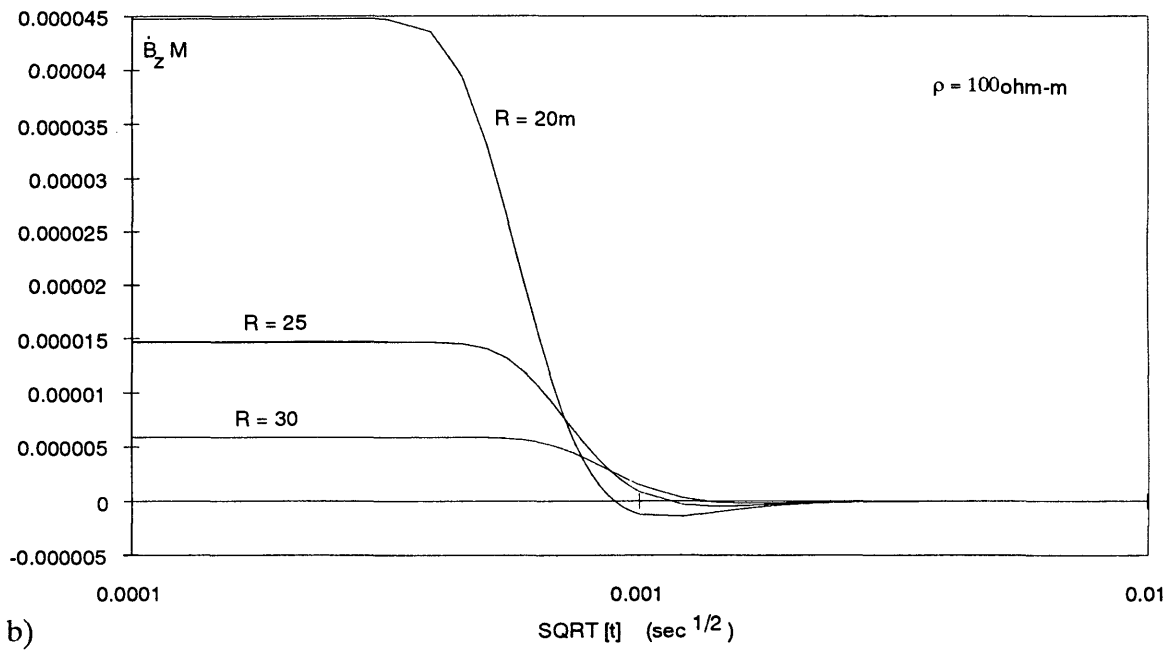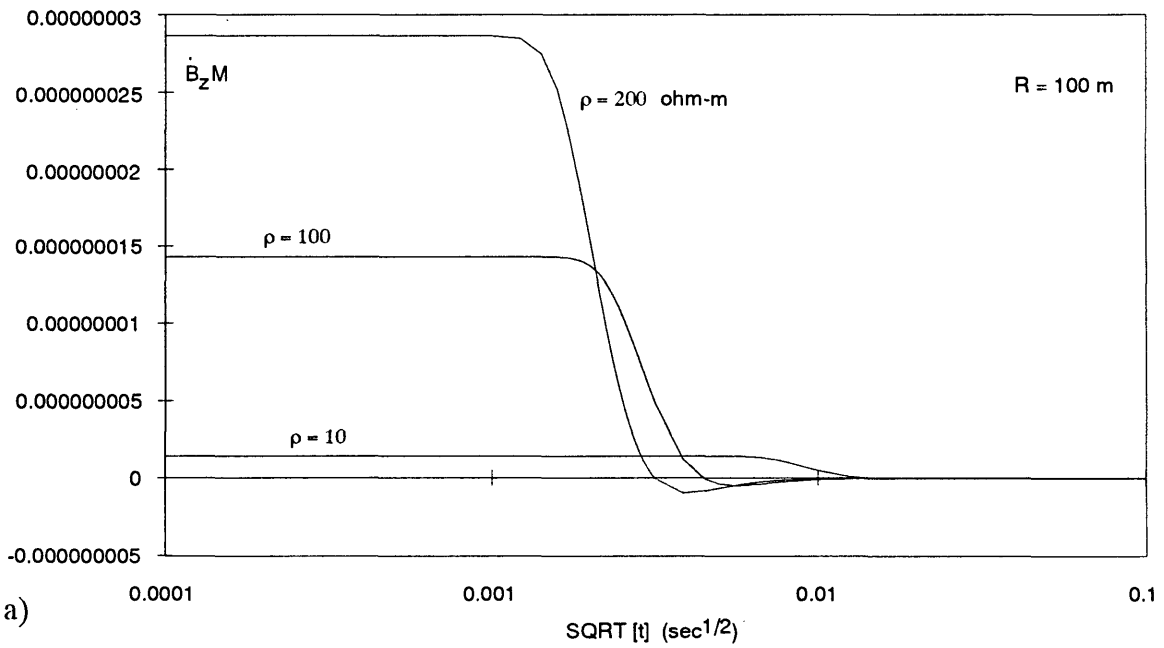
FIG. 1.16. The behavior of time-derivative of the magnetic field versus with (a) resistivity, (b) distance.
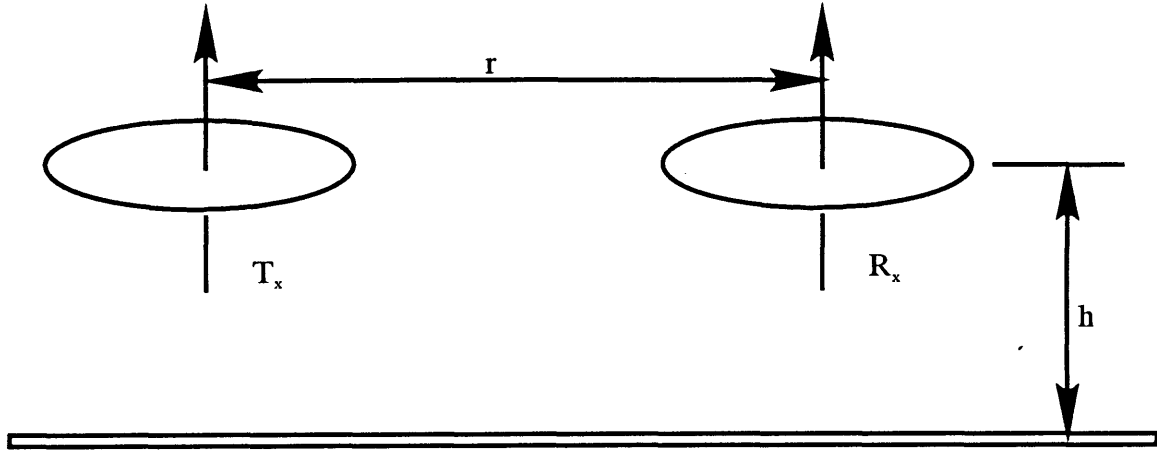
FIG. 1.17. Thin Plate.

thin conductive layer. Suppose, a horizontal conductive thin plate is located in a free space as shown in Figure 1.17. As theory shows that the time-derivative of the vertical and horizontal component of magnetic field can be written in following form:

$$\dot{B}_z = -\frac{2M}{4\pi r^4 \mu S}\frac{(\tau_s + 2h_o)[9 - 6(\tau_s + 2h_o)^2]}{[1 + (\tau_s + 2h_o)^2]^{7/2}}$$

$$\dot{B}_r = \frac{6M}{4\pi r^4 \mu S}\frac{[1 - 4(\tau_s + 2h_o)^2]}{[1 + (\tau_s + 2h_o)^2]^{7/2}} \tag{1.28}$$

$$and \qquad \tau_s = \frac{2t}{\mu S r} \tag{1.29}$$

where $h_o = \frac{h}{r}$ and S is longitudinal conductance. As an example, the behavior of the time-derivative of vertical component of magnetic field is shown in the Figure 1.18. At the beginning the field is constant then with increasing τ_s it increases and reaches a maximum. Later it decreases with increasing the parameter τ_s and then it changes polarity and reaches a minimum value and then goes to zero. If the parameter τ_s is less than $2h_o$, $\tau_s < 2h_o$, the early stage is observed. Usually the late stage starts,
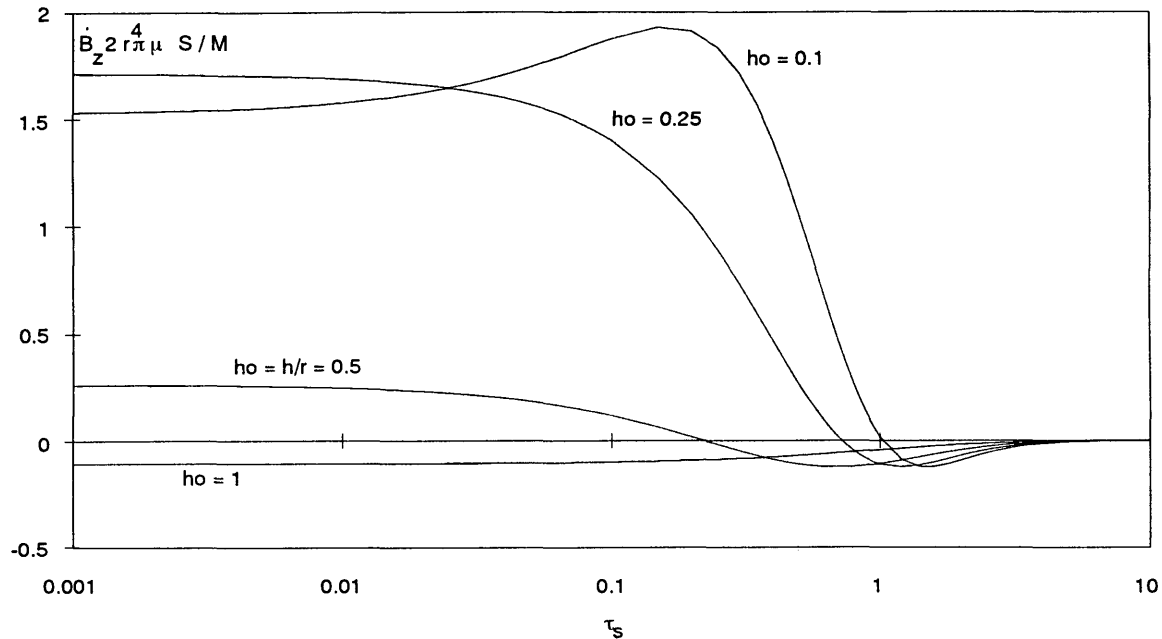
FIG. 1.18. The behavior of the time-derivative of horizontal component of the magnetic field as a function of normalized time.

when the $\tau_s \gg 2h_o$. At this stage the time-derivative of the vertical component of magnetic field can be described in following form:

$$\dot{B}_z \simeq \frac{-3MS^3\mu^4}{16\pi t^4} \qquad (1.30)$$

As seen in the equation 1.30 the $\dot{B}_z$ is independent of a separation, r, like it was observed for a uniform half-space medium (eq. 1.26). The result can be carried out for a n-layered medium. It should be noticed that a transient response of a thin sheet is singularly sensitive to the conductivity-thickness product being proportional to S^3. For instance, if the S is changed 10%, the results is changed 30%. Furthermore at the late stage the field decreases much more rapidly with time then that for uniform half-space medium.

In the previous paragraphs, the transient responses have been investigated for relatively simple models of the medium as being a uniform space, a uniform half-space and a thin conducting layer. Now we will show the behavior of the transient field for horizontally layered medium. As it is seen in the Figure 1.19a the behaviors of the time-derivative of vertical component of the magnetic field for the different ratio of resistivities in case of two layers medium are similar to each other. Only, their amplitude change with different ratio of resistivities. The Figure 1.19b shows the behaviors of $\dot{B}_z$ for three horizontally layered medium. In four cases, H $(\rho_1 > \rho_2 < \rho_3)$, A $(\rho_1 < \rho_2 < \rho_3)$, K $(\rho_1 < \rho_2 > \rho_3)$ and Q $(\rho_1 > \rho_2 > \rho_3)$ type of curves, their behaviors are similar to each other. There are slightly differences among them but it is not clear to identify the types of the sections.

Now let us outline the main features of the interpretation of transient method. The main purpose of interpretation is to determine the thickness and resistivity of sub-surface layers. This process is called a solution of the inverse problem. As is well known the solution of the inverse problem is unique for a horizontally layered medium. In other words if the field is measured without error, we could define exactly all parameters of the medium. However, in reality the medium is different from the horizontally layered medium. Also the measurements are performed with some errors which are caused by two main factors, *geologic* and *man-made as well as natural noise.* An example of the geologic noise is any lateral changes of resistivity in the layered medium. At the same time there is other type of error which is caused by another noise. For instance, the electrical power lines, pipelines, fences, telephone lines, the separation between a transmitter and a receiver and their orientation, and natural electromagnetic field, etc. cause the noise. For this reason the solution of the inverse problem is ill-posed. It means in general we can define only some of parameters
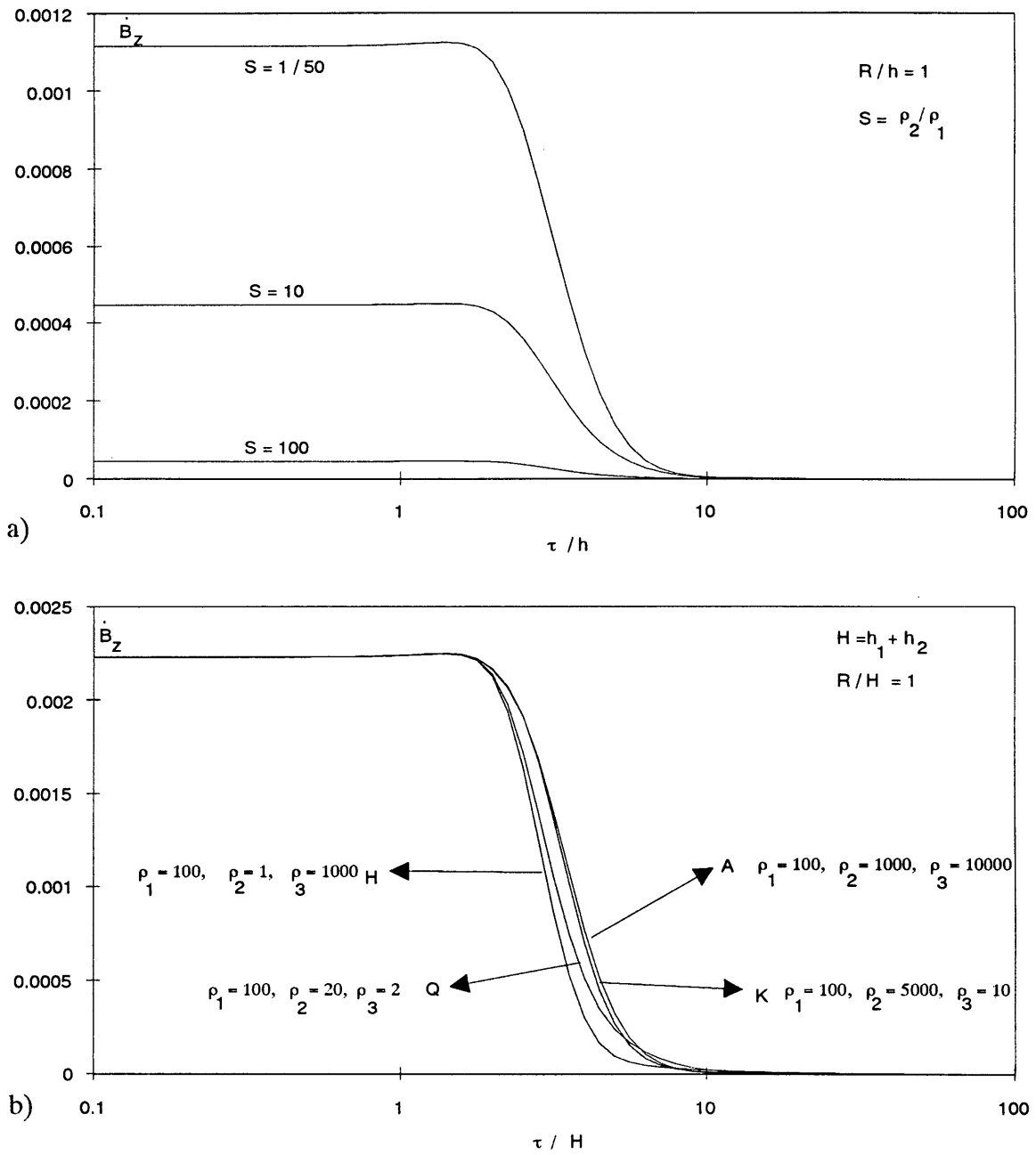
FIG. 1.19. The late stage behavior of the time-derivative of vertical component of the magnetic field for (a) two layers (b) three layers medium.

of the section with some accuracy while other parameters can not be practically determined. Taking into account this fact the interpretation consists of several steps. First step is first guess about the values of parameters of the medium and we assume them by having some geologic and geophysical information. In this step the transient response is calculated by using the approximated values of the parameters (solution of the forward problem). Then the calculated and measured field are compared. If there is a difference, which exceeds the error between the measured and calculated field, all parameters of the first guess or some of them are changed in such way that a better fit to these data achieved. This process repeats several times when the difference among them becomes smaller than the error. As a result of this procedure we can distinguish two set of parameters of the medium. Some of them are defined with reasonable accuracy and are useful for interpretation of geology. These parameters define a model of the medium. At the same time, there are other parameters which are defined poorly, and they can not be used trustfully. In principle we can perform the interpretation by using the transient response of electromagnetic field however usually these curves do not show the type of section (Figure 1.19). In fact, as it was shown above the shape of the curves can be same for different types of a section.

In the electric and electromagnetic prospecting the experience shows that the apparent resistivity curves usually more vividly characterize the geoelectric section than the responses of measured field. This allows us to determine the parameters of first guess more accurately. Moreover, some parameters can be directly defined from the apparent resistivity curves. For this reason, usually the interpretation in the transient method as well as in other electrical method is based on the use of the apparent resistivity curves. In the next section, the main features of these curves will be described.

1.3 Definition and Calculation of Apparent Resistivity

As is known the apparent resistivity in transient method is usually introduced in two ways and they are based on the behavior of the transient field at the early and the late stages respectively. In most practical cases, i.e., ground water, engineering, mining geophysics, performing shallow soundings, we use the apparent resistivity based on the late stage behavior. In order to introduce the apparent resistivity, let us consider the behavior of the field at the late stage on the surface of uniform half-space medium. As it was shown before the measured field at the center of the loop for the late stage is

$$\frac{\partial B_z}{\partial t} = -\frac{\mu M}{20\pi\sqrt{\pi}}\frac{(\mu\sigma)^{3/2}}{t^{5/2}} \tag{1.31}$$

Therefore, the expression for the electromotive force, ε, measured in the receiver is

$$\varepsilon = -\frac{\mu M r}{10\sqrt{\pi}}\frac{(\mu\sigma)^{3/2}}{t^{5/2}} \tag{1.32}$$

Thus, the resistivity of a uniform half-space medium is

$$\rho = (\frac{\mu}{t})^{5/3}(\frac{IrM_R}{10\sqrt{\pi}\varepsilon})^{2/3} \tag{1.33}$$

Using this expression and knowing the time of measurement, electromotive force and the parameters of system, the resistivity for the uniform half-space medium is determined provided that the measurements are performed at the late stage. If the measurements are made within early or late stage on the surface of uniform half space or if the medium is not uniform, the calculated values will differ from that the specific resistivity of the uniform half space and it is called apparent resistivity. We described the apparent resistivity on the center of the loop. In similar manner, we can
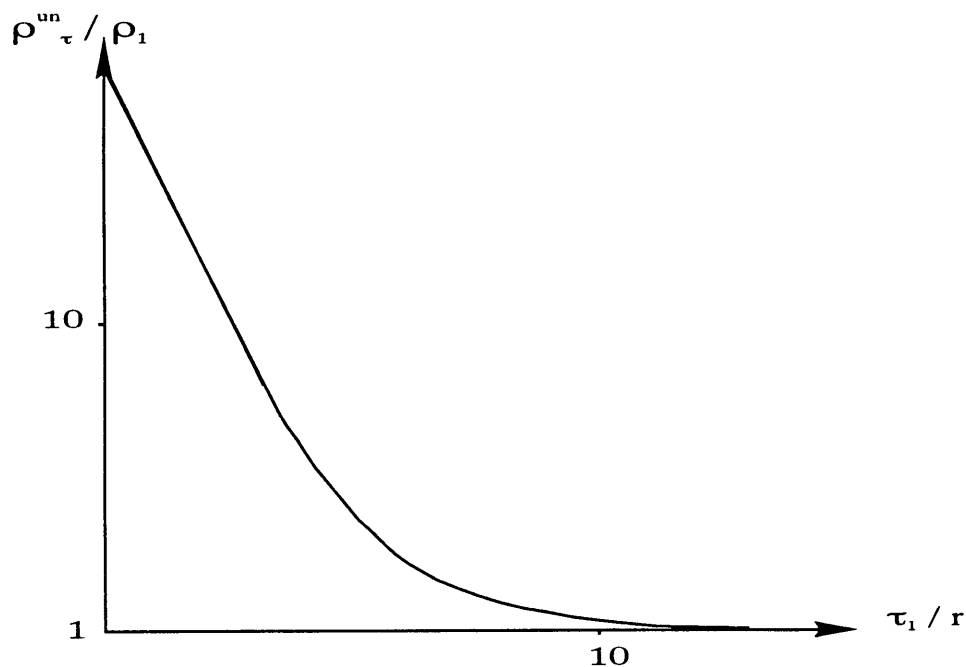
FIG. 1.20. The behavior of late time apparent resistivities, for a uniform half-space as a function of scaled time when the measurements are made at the center of loop.

introduce the apparent resistivity when the transmitter can be treated as a magnetic dipole (dipole-dipole array). As follows from the equation 1.31, the electromotive force, ε, is

$$\varepsilon = \frac{\mu^{5/2}\sigma^{3/2}M_R M_T}{20\pi\sqrt{\pi}t^{5/2}} \tag{1.34}$$

Therefore the apparent resistivity is

$$\rho_a = \left(\frac{\mu^{5/3}M_r^{2/3}}{20^{2/3}\pi}\right)\frac{M_t^{2/3}}{t^{5/3}V^{2/3}} \tag{1.35}$$

where M_R and M_T are the moment of receiver and transmitter respectively.

Now we will consider the behavior of apparent resistivity curves and method which approximately allow to determine the parameters of the medium. First of all

let us consider the behavior of late apparent resistivity curves for a uniform half-space medium. As shown in the Figure 1.20 the apparent resistivity increases unlimitedly when the times goes zero. This behavior directly follows from the behavior of the field at the early stage. With increasing of time the apparent resistivity decreases gradually and as follows from definition it approaches to one at the late stage. If the measurements are performed within the late stage, the apparent resistivity is equal ρ_1 and we do not need to perform any interpretation. If measurements are performed within intermediate and the early stages, the interpretation can be done by comparison between theoretical and experimental curves. As follows from the behavior of the curve at early stage, the slope of the curve is equal 10/3. Taking into account that with decreasing time, the field in a horizontally layered medium coincides with the field in a uniform half space medium. This asymptotic behavior is a general character as soon as the field behavior corresponds to the early stage. Sometimes this slope is used for determination of ρ_1.

Next, consider the late time apparent resistivity curves for two-layer medium. When the ratio ρ_2/ρ_1 is greater than one, the apparent resistivity curves are seen in Figure 1.21. As is seen from this Figure, at early stage all curves merge each other. It means, the influence of basement becomes negligible and the field correspond to that in a uniform half-space medium. With increasing time the induced currents appear in the second layer and the influence of resistivity of this layer increases. Correspondingly, the apparent resistivity gradually approaches to the apparent resistivity of a second layer. When the second layer is much more resistive, we can distinguish three parts of the curves. In the first part, the apparent resistivity curves behave as in a uniform half-space. In the opposite case, in very large time, the apparent resistivity approaches the apparent resistivity of a second layer. Also there is a intermediate
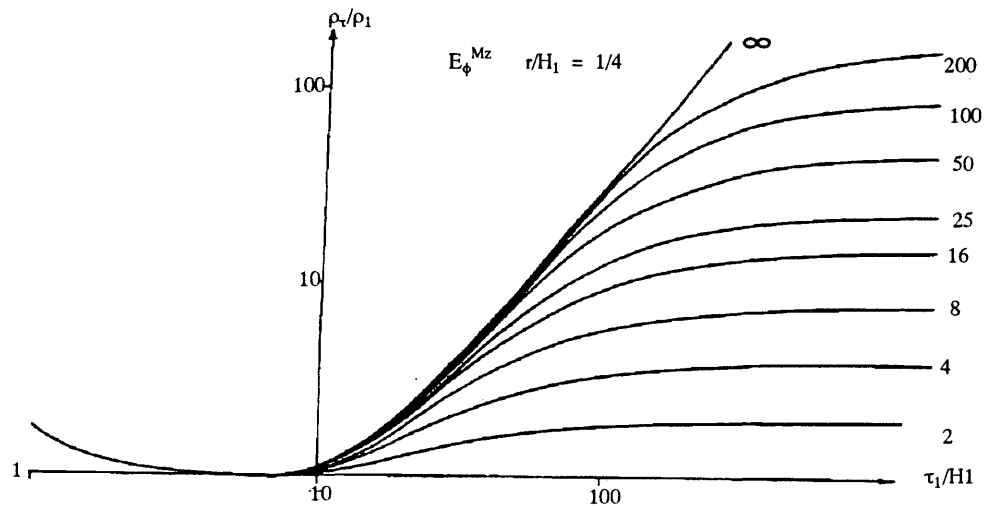
FIG. 1.21. Late-time apparent resistivity curves for a loop-wire configuration for two layers with the second layer relatively resistive. The relative spacing, r/H_1, is 0.25.

range, when the curves merge with each other provided that $\rho_2/\rho_1 \gg 1$. This range is called Zone-S and the induction current almost uniformly distributed in the first layer in the vertical direction. S means a longitudinal conductance and can be written as follows:

$$S = \sigma_1 H_1 \tag{1.36}$$

where σ_1 and H_1 are the conductivity and the thickness of the first layer respectively. Within this range, the field does not depend on ρ_1 and H_1 separately. As theory shows it is a function of longitudinal conductance of the fist layer. Moreover, unlike Schlumberger, frequency soundings the field in transient method is proportional to cube of conductance in this range of time. This fact demonstrates high sensitivity to conductance of this method. As follows from theory, this behavior is observed in
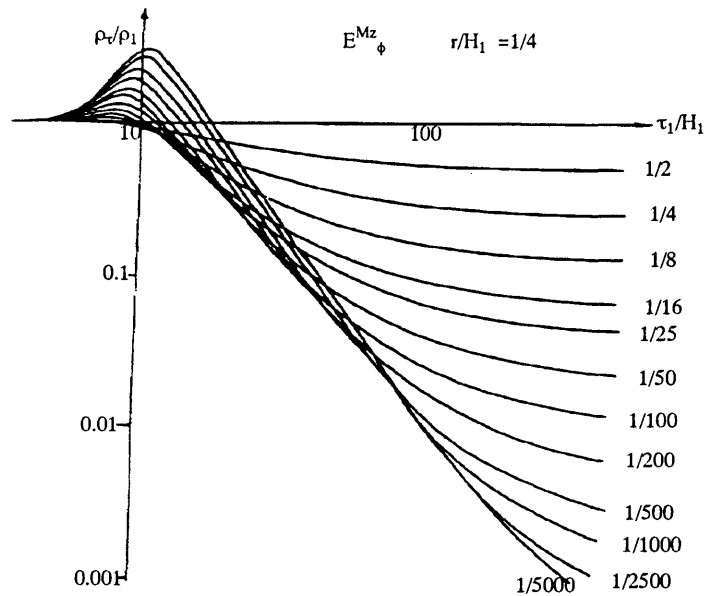
FIG. 1.22. Late-time apparent resistivity curves for two layers with the second layer being relatively conductive. The relative spacing, r/H_1, is 0.25.

general when there are different conductive layers above high resistive basement. In this case, the conductivity of sediment is defined in following way

$$S = \sum \sigma_i H_i \tag{1.37}$$

Very often, in many practical applications of the transient sounding related with mapping basement, the use of this part of the curve is a great practical important. This analysis of the curve allows us to determine approximate parameters of the section. In the Figure 1.21 at early stage, $\tau_1/H_1 < 6$, we can determine the resistivity of first layer. When the ratio of τ_1/H_1 is relatively small, the minimum of the curves

practically takes place around

$$\frac{\tau_1}{H_1} \approx 10 \tag{1.38}$$

and knowing the resistivity, we can determine H_1. When the resistivity of basement relatively high, from the ascending branch we can determine the conductance. From the right part of the curve, it is possible to evaluate ρ_2.

The apparent resistivity curves in case of more conductive basement are shown in Figure 1.22. At the early stage, the curves behave in same way as in the previous case. With increasing time all curves manifest maximum. Then, further increasing time the apparent resistivity gradually decreases and goes to the resistivity of a second layer. Applying the similar approach we can also evaluate the parameters of the type of section.

In conclusion, three layers apparent resistivity curves for different types of the section are shown in the Figure 1.23 and they show different behaviors. For instance, in the case of type-H a minimum is observed. There is similar system of formulas which allow to evaluate the parameters of these sections.
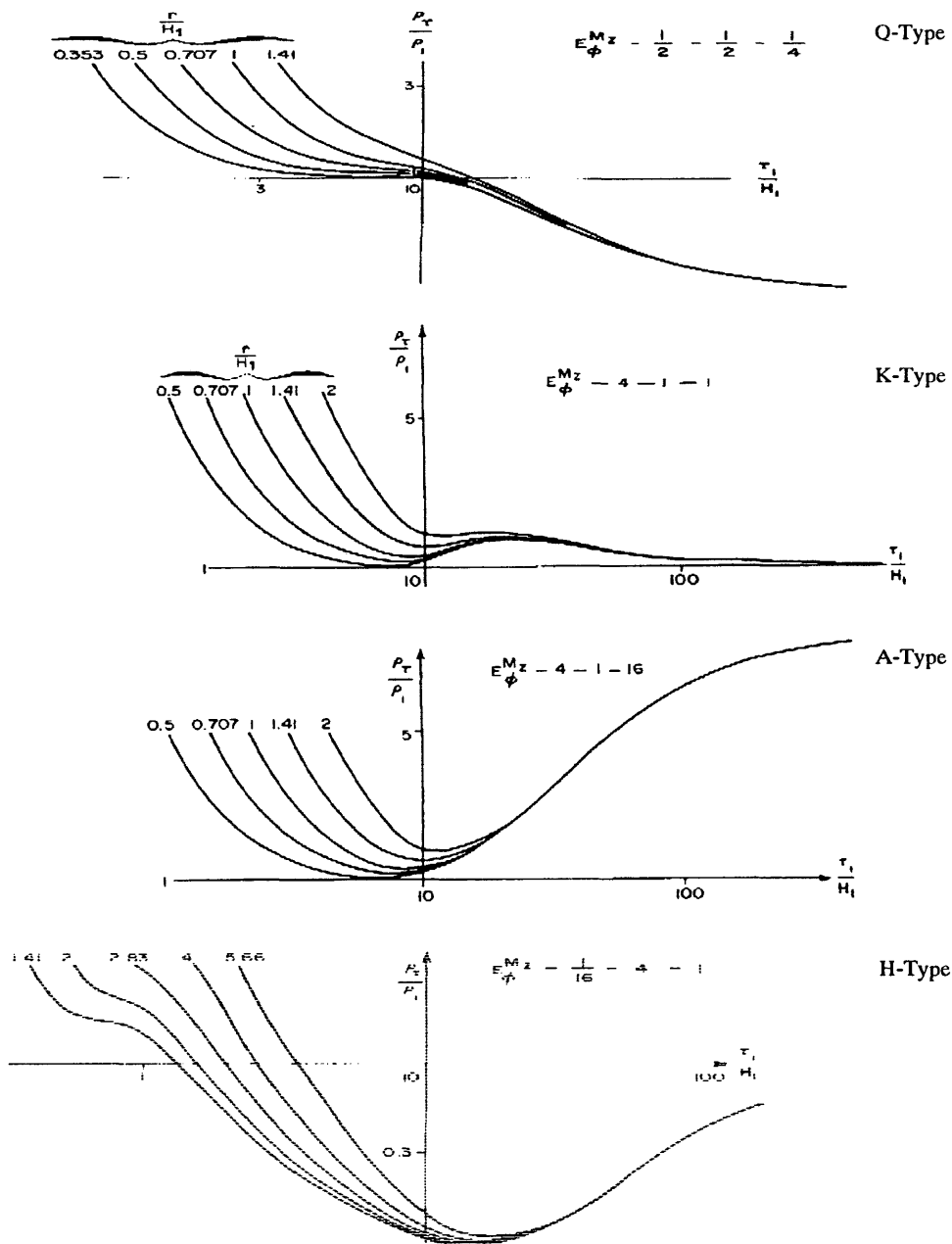
FIG. 1.23. Three-layer late-time (a)type H, (b)type A, (c)type K, (d)type Q apparent resistivity curves for a loop-wire configuration. The label at the top of the plot lists the type of measurement, the ratio of resistivities between the first two layers, the ratio of thicknesses, and last, the ratio of the last-layer resistivity to the first $(E_\phi^{Mz} - \frac{1}{2} - \frac{1}{2} - \frac{1}{4})$. The index on each curve is the ratio of separation, r, to first-layer thickness, H_1.

Chapter 2

DETERMINATION OF EXTENSION OF VOLCANIC MOUNTAINS UNDER BASIN-FILL DEPOSITS

2.1 Introduction

The volcanic basement may contain igneous intrusions which may contain gold. The overlying alluvium is a rapidly-varying assemblage of boulder, gravel, sands and fine grained playa deposits. These heterogeneous rocks make the acquisition of interpretable geophysical data very difficult. Examples are shown of magnetic and refraction seismic exploration followed by the description of a transient electromagnetic survey which accurately defined the basement surface and the overlying geology.

First, the regional and local geology will be described. Second, the results of the part of aeromagnetic and refraction seismic surveys will be shown. Third, the electromagnetic survey will be described in detail: field work, geophysical interpretation and geological interpretation.

2.1.1 Regional Geology

Nevada lies almost entirely within the Great Basin region of the Basin and Range physiographic province (Figure 2.1). It has had a long and complex geologic history that includes major episodes of sedimentation, igneous activity, orogenic deformation and continental rifting. The oldest rocks in Nevada consist of metamorphic and intrusive rocks of Precambrian age. From this time, many changes occurred in the tectonic setting of Nevada with the onset of extensional faulting and the eruption of
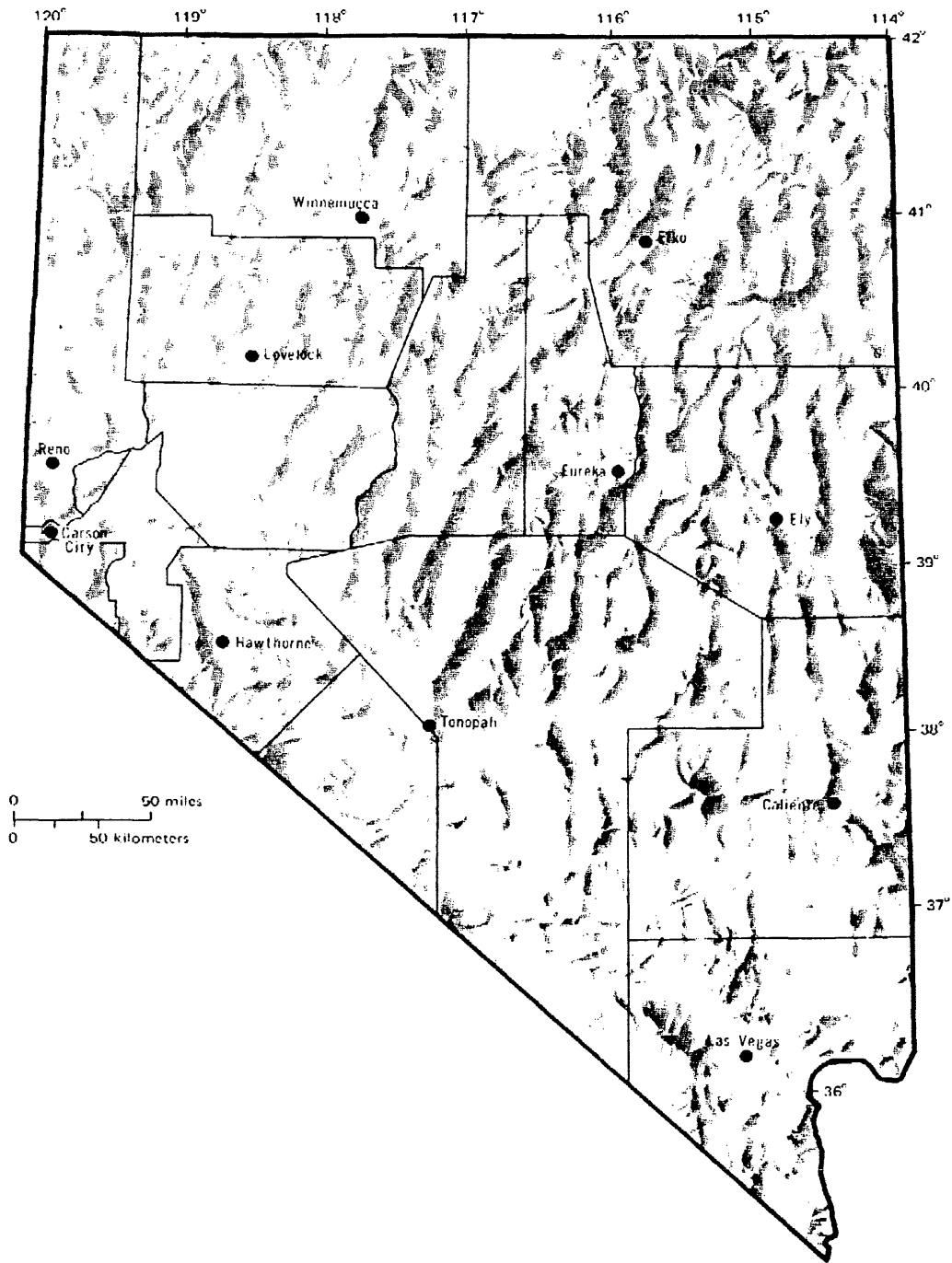
FIG. 2.1. Physiographic map of Nevada.

basalt or bimodal assemblages of basalt and rhyolite. The major basins and ranges were formed by extensional block faulting and continental sediments were trapped in fault-related basins (Stewart, 1980). The state is mainly characterized by a series of generally north-south trending mountain ranges separated by alluviated valleys (Figure 2.1). The study area will be described in detail.

2.1.2   Local Geology

The study area is located in a Basin and Range Province, Nevada. The rocks in the valley have been grouped into consolidated rocks and basin-fill deposits. Basin fill-deposits have been subdivided into playa and non-playa deposits. Consolidated rocks form mountain blocks on the west, north and east boundaries of the basin and underlie the basin fill. The consolidated rocks are predominantly Tertiary rhyolite flows, ash flows, crystal-poor to crystal-rich ash-flow tuffs and intrusive rocks. Basin-fill deposits are composed primarily of Tertiary and Quaternary alluvial, colluvial, eolian and lacustrine sediments. Thin layers of volcanic ash and minor amounts of chemically precipitated minerals and coatings are also present in the basin-fill deposits. Basin-fill deposits, originated by erosion of adjacent mountains, range in grain size from clay in the playa to boulders in the alluvial fans. They generally grade in size from coarse near the mountain blocks to fine towards the center of the basin. The lithology of section A-A' (Figure 2.2) shows the vertical distribution of coarse-grained, and mixed deposits in the basin fill. The location of this section is shown in Figure 2.3. The section was constructed by plotting grain size from interpretation of individual well logs, and then correlating, where possible, the grain-size distributions from well to well.
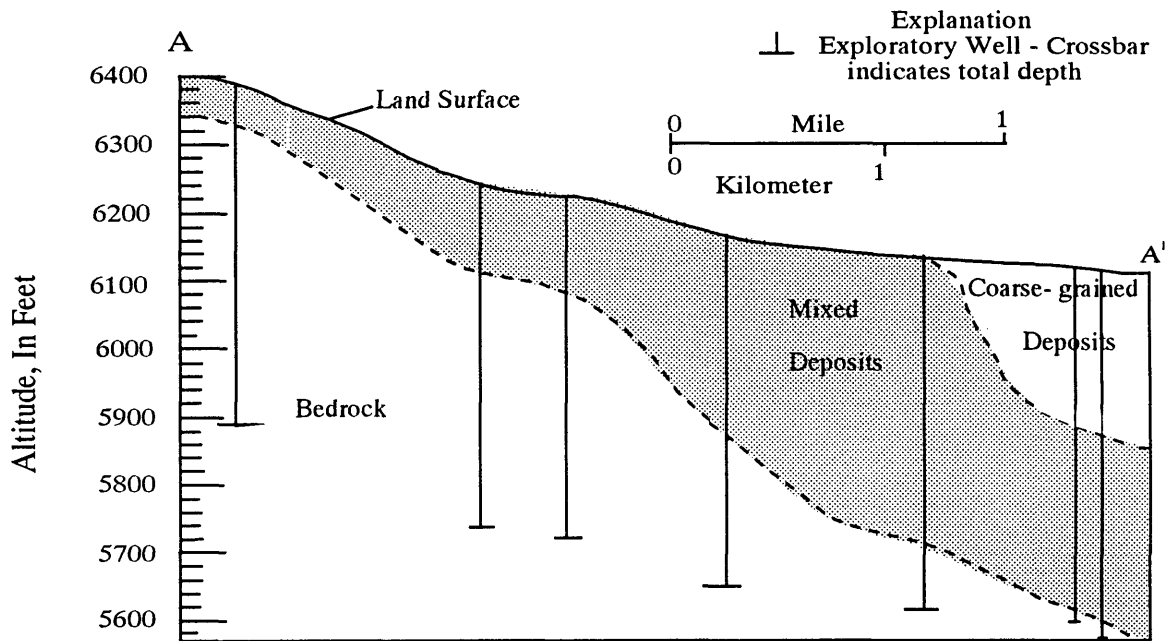
FIG. 2.2. Lithologic of section A-A'.

2.2 Previous Geophysical Surveys

In this section, two geophysical surveys will be described. These surveys were done in 1965 and 1966 by the Geophysics Department of Stanford University. The location map of the geophysical surveys is given in the Figure 2.3. First, the results of an aeromagnetic survey will be shown. Then, the results of a seismic refraction survey will be demonstrated.

2.2.1 Aeromagnetic Survey

An airborne magnetometer survey was conducted in the central part of Nevada, in the summer of 1965. The description that follows is taken from Salehi (1967). The main objective of this survey was to obtain the basement depth under the alluvium of the valley. Flight elevation was maintained at 7500 ft. above sea level through-out
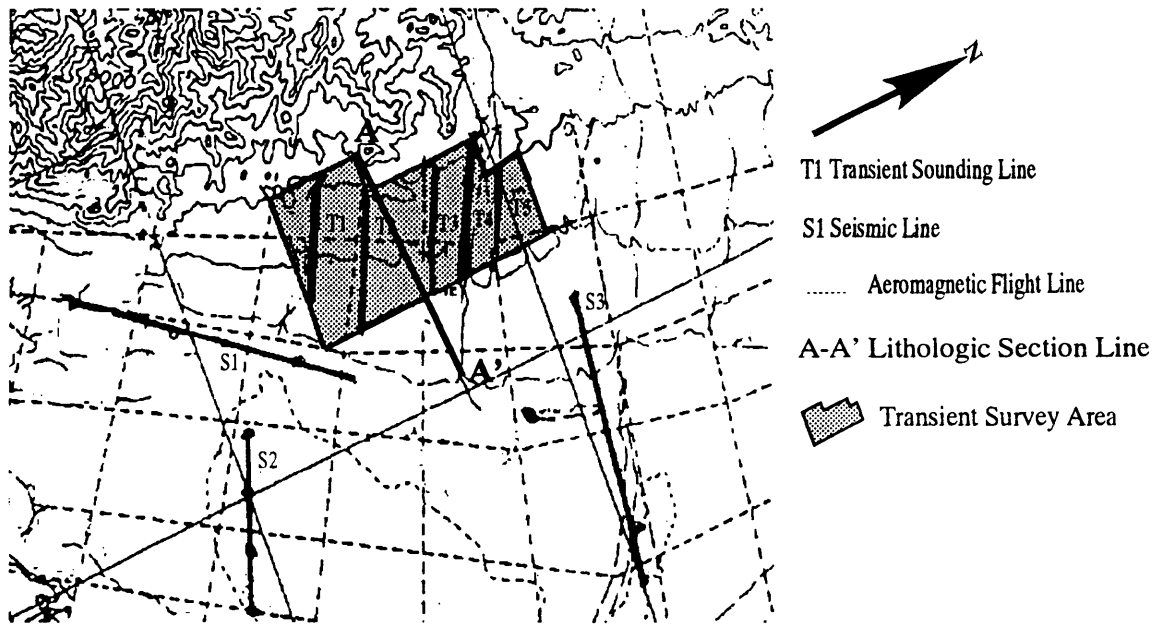
FIG. 2.3. The location map of geophysical surveys (after Salehi, 1967).

the survey. A Varian M49 proton precession magnetometer was used. The original

data is no longer available, only the interpreted results; those results applicable to

the TEM survey are discussed. After correction for the diurnal, the total intensity

map (Figure 2.4a) was prepared by contouring the corrected data at 50 Gamma

intervals taking the reference level as 53000 Gamma. This reference level is the value

for the normal geomagnetic field at the survey location. After the total intensity

map was prepared, the residual and second vertical derivative values using the nine-

point scheme were prepared. Since the main interest in the survey was the study of

the larger magnetic features, presumably related to the basement, a grid interval of

one mile was chosen so that the effect of the smaller near-surface sources would be

attenuated. Figure 2.4 b and c show the residual and second derivative maps. As seen

in the Figure 2.4a, only the section B-B' and C-C' which are located close to the area
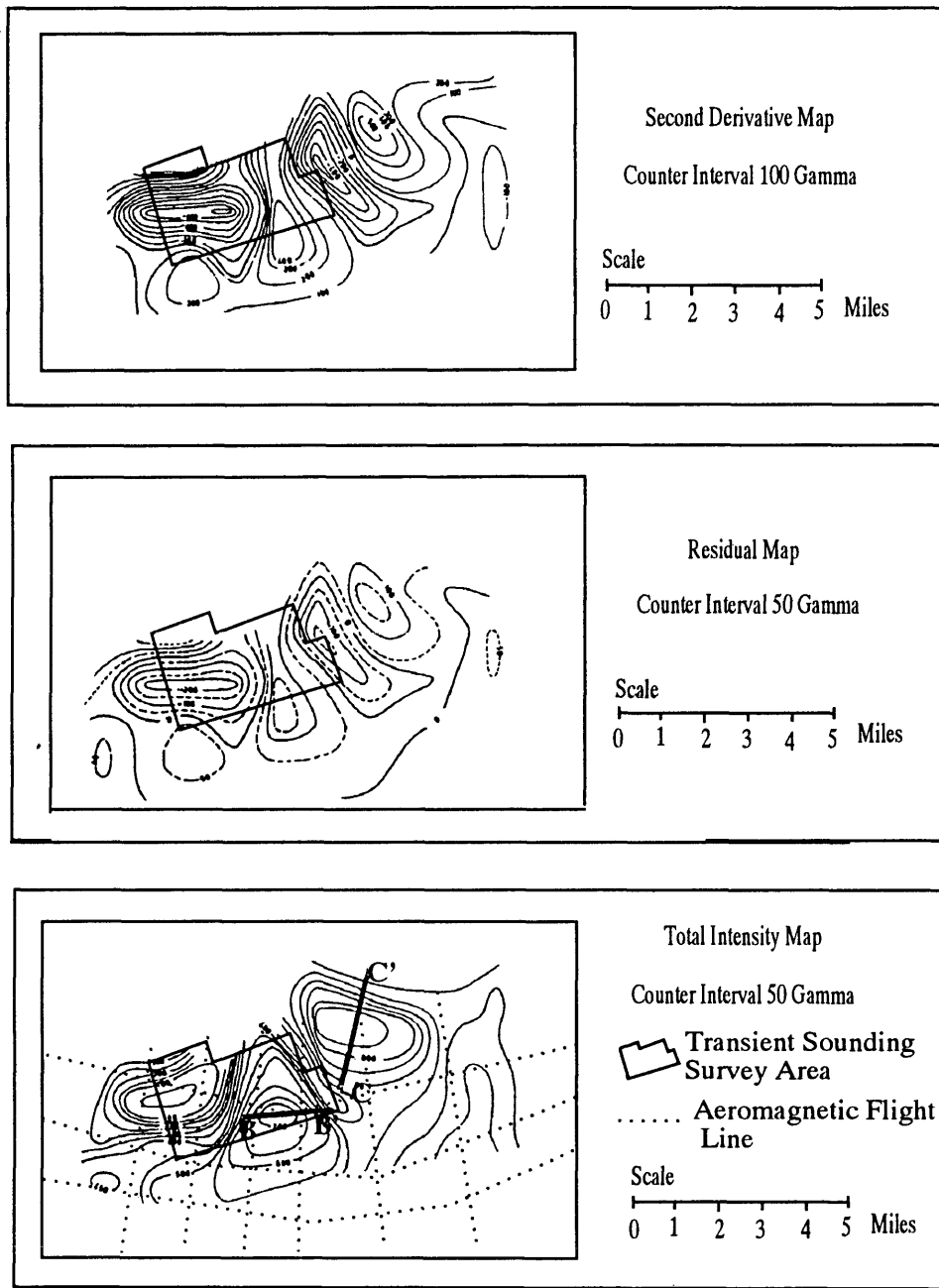
FIG. 2.4. (a) Total magnetic intensity map, (b)Residual map, (c) Second derivative map.

C-C'

b)

B-B'

a)
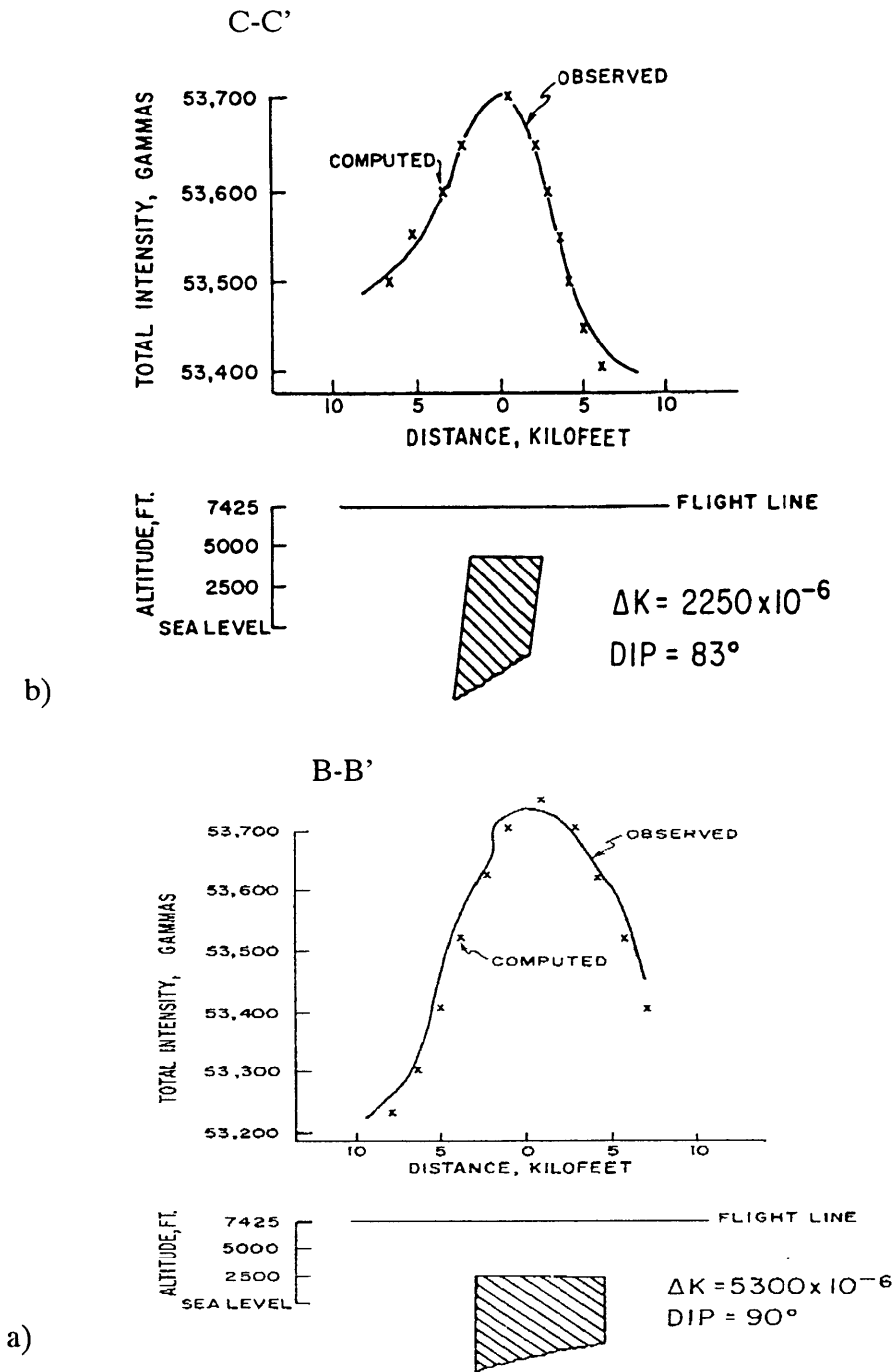
FIG. 2.5. Total magnetic intensity profile with interpretation along line (a)B-B' and (b)C-C'.

of interest will be described in this thesis. The magnetic susceptibility, which is the fundamental rock parameter in magnetic prospecting, was calculated for the sections. The effective magnetic susceptibility contrast, ΔK, was computed from the total intensity map. After the evaluation of the effective magnetic susceptibility contrast, two dimensional model computation was done. Figure 2.5 shows the interpretation of two of the anomalies seen in Figure 2.4 a-c. The solid line is the plot of the observed values and the small crosses represent the computed points. The existence of rock bodies with reverse remanent magnetization, perhaps volcanic plugs, are strongly indicated. The depth to the top of the magnetic bodies was found to be approximately 3700 ft. below the surface.

2.2.2   Seismic Refraction Survey

Three reversed seismic refraction profiles were shot near the study area during September, 1966, to determine the depth of the high velocity basement (Herring, 1967). One of the seismic refraction profiles, located parallel to the probable structural trend, is close to lines 1 and 2 of the transient sounding (Figure 2.7). Only two shot points on this seismic line is around 2000 ft. far from the end of the transient line-1 and 2 (Figure 2.7). Therefore, the seismic refraction result from the section D-D' will be shown. A simple intercept time method of interpretation could not be used because of structural complication. The overlying alluviums have a rapidly-varying lithology, boulder, gravel, sands and fine grained playa deposits. Thus, this heterogeneous rocks have different velocity distribution and give different first break times. Therefore, there are more than one intercept time on the time-distance graph (Figure 2.6). Herring (1966) used the delay time method to determine the depth and dips for this seismic refraction survey. By using all refraction curves along the seismic
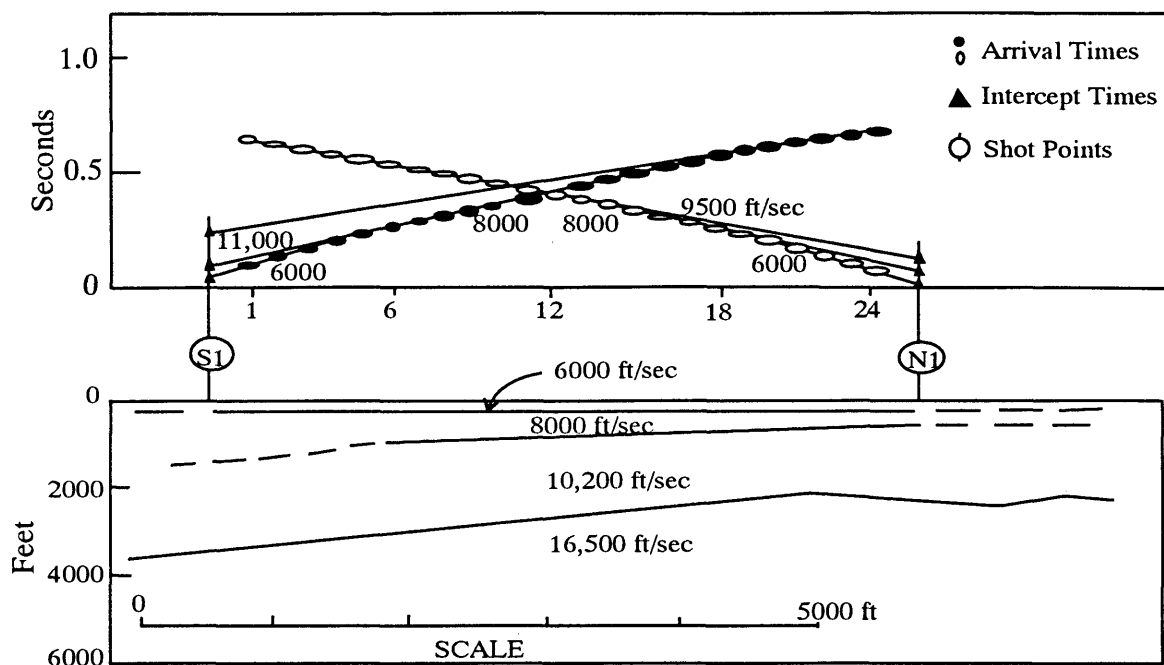
FIG. 2.6. Time distance curve and cross section.

profile, the sediments and volcanic overlying the basement in the area were found from 2000 to 3800 feet thick between shot point S1 and N1 (Figure 2.6).

Neither the aeromagnetic or seismic survey results could give an accurate depth to basement because of the heterogeneous nature of the alluvium. Thus, another type of survey was necessary. As mentioned above, the basin-fill deposits have a complex lithology but they have a strong resistivity contrast with basement. The alluvium has a wide range in electrical resistivity but the basement has a very high resistivity which indicates that an inductive electromagnetic survey might provide the desired depth to basement. The chosen technique was a time domain central loop survey using the Geonic's EM37 equipment.

2.3 Logistics and Data Acquisition
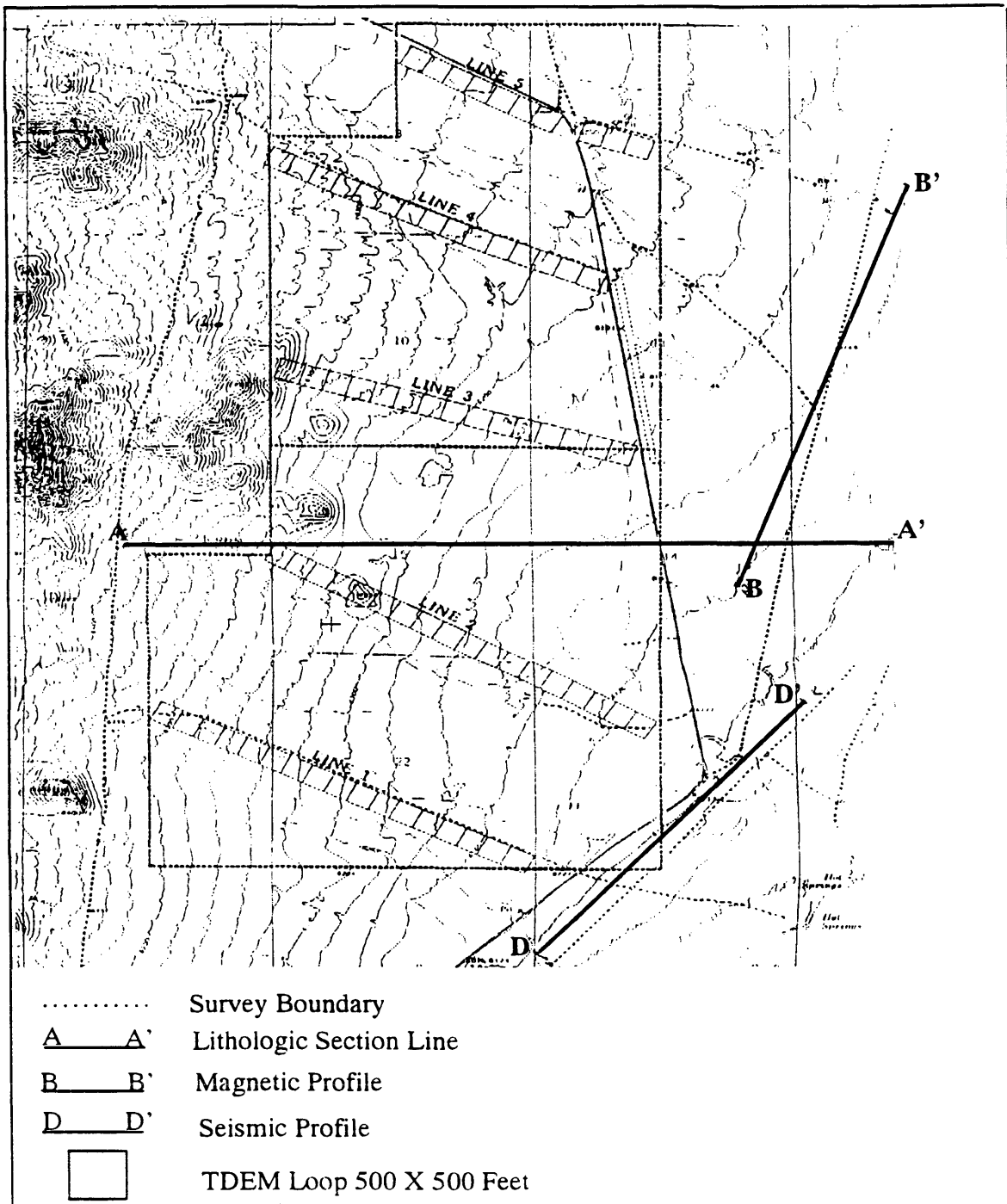
FIG. 2.7. TEM survey location map.

The transient electromagnetic survey was performed by three people: two geo-
physicists and one field helper. The locations of sounding sites were determined along
northeast-southwest lines approximately perpendicular to the anticipated main Basin
and Range faults. These lines are located by use of geologic, gravity and topographic
maps. As is known in TEM, effective exploration depth is partly a function of the
dimensions of transmitter loops. Thus, in the study area, the expected exploration
depth was about 250m therefore, to achieve that, measurements employing 152.5m by
152.5m transmitter loop were used. The lines, which make optimum use of existing
roads and trails, are about 2.3km long and soundings were made at 152.5m intervals.
In addition, the lines are located in such way that they run over topographic features
that might be related to geologic structures. For example, Line-2 was selected to run
over a topographic high that might be due to a bedrock high (Figure 2.7). During the
five days of field work, a total of 75 soundings were acquired over the area of interest
using Geonic's EM-37 transient electromagnetic system. Technical specifications of
the EM-37 are given in Appendix-A. At the start of survey a base control point was
established on the east corner of Line-1. The transmitter and motor-generator were
positioned at a corner of the transmitter loop. After the transmitter and receiver
electronics were synchronized, the receiver coil was placed at the center of the trans-
mitter loop and connected to the recording electronics by a 5m data transmission
cable. The reason of using the central measurement or in-loop configuration was to
measure the maximum amplitude of the field. A square wave current was pulsed
through the wire at 30 Hz base frequency. The receiver measured and recorded the
decay of the vertical magnetic fields. During data acquisition, numerous transient
decays were recorded for each sounding. Readings were acquired at several receiver
gains with opposite receiver polarities for each sounding location to eliminate ambi-

ent electrical noise due to power lines, radio stations and spherics. The measurement duration is a few milliseconds for EM-37, and many pulses of positive and negative polarities are stacked in a short period of time and average to remove noise. Finally, The readings were stored in a DAS-54 solid state data logger and nightly transferred to a personal computer with a 286 processor.

2.4 Data Processing

The data, stored in the DAS-54 logger, are transferred to floppy disks on a computer. The first step in data processing is to average to emfs which are recorded at opposite receiver polarities (see Figure 2.8a). Then, the records at different amplifier gains and frequencies are combined to give a single composite transient decay (see Figure 2.8b).

After the composite transient decay has been calculated for each measuring point, only the late stage apparent resistivities are calculated by using equation 1.35. Basically, the measurement at late stage are usually more sensitive to ground resistivity than the measurement at early stage and very often the measurements performed at the late stage provide better information about the distribution of conductivity at greater depth (see section 1.2.2). The EM37 reads millivolts and milliseconds however, the equation is in terms of volts and seconds and a conversion must be made. The conversion can also been built into a constant:

$$K_{loop} = \frac{\mu^{5/3}M_r^{2/3}}{20^{2/3}\pi}(\frac{1000msec}{sec})^{5/3}(\frac{1000mV}{V})^{2/3}$$
$$= 6.322 \times 10^{-5}M_r^{2/3} \tag{2.1}$$

where M_r is the moment of the receiver and K_{loop} is a constant which depends on
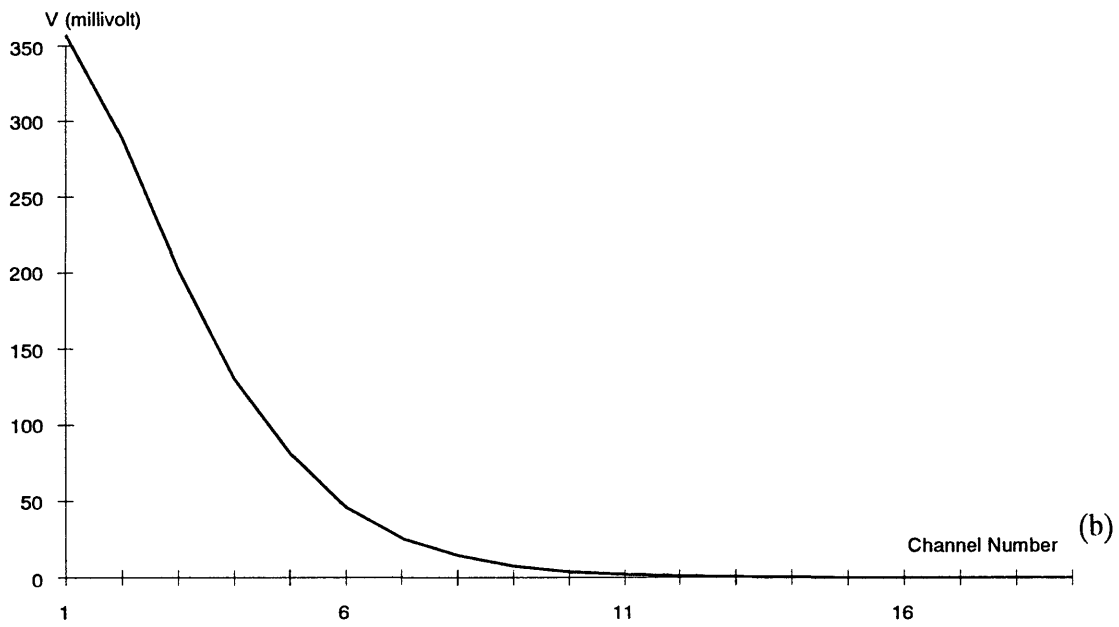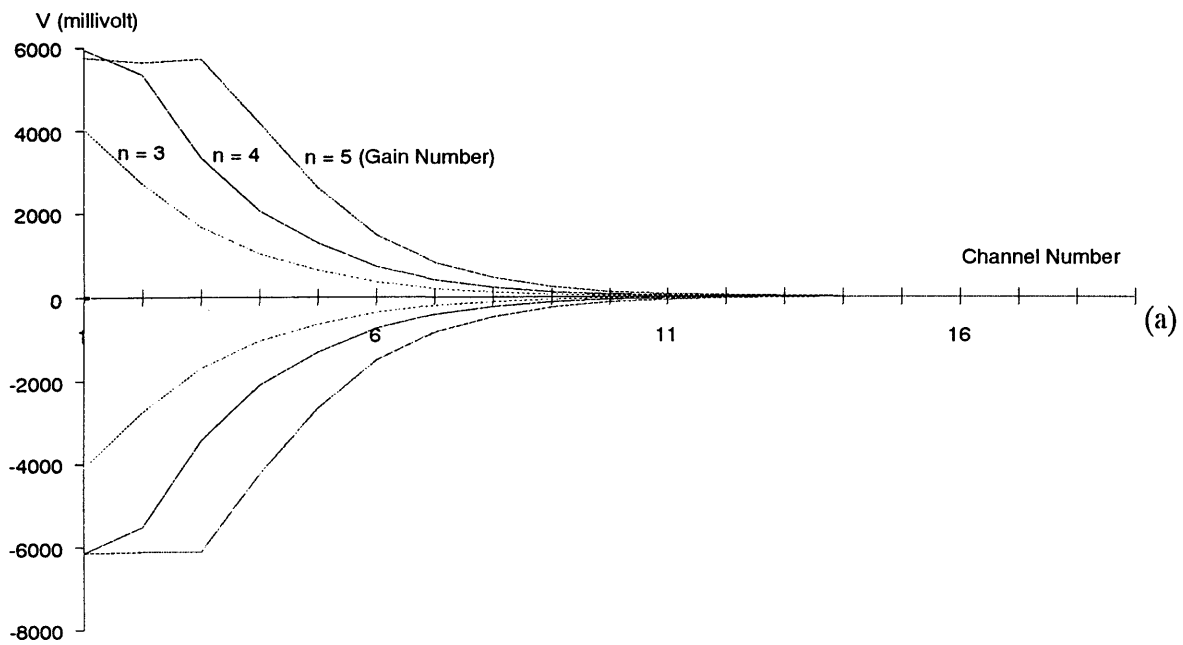
FIG. 2.8. (a) The measured signal at different gain and polarity, (b) the combined signal.

the receiver coil used and on the preamplication factor of 52.1 built into the Geonic's EM-37. Using the constant for different receiver coil's effective area in equation 1.35, the late stage apparent resistivity can be written in the following form:

$$\rho_a(t) = K_{loop} \frac{M_t^{2/3}}{t^{5/3} V^{2/3}} \tag{2.2}$$

where V is the voltage and M_t is the moment of the transmitter. Using the sounding data from Table 2.1 and the parameters from Table 2.2, late stage apparent resistivity, ρ_a, can be calculated in the following way:

1.Convert from a square loop to a circular loop:

r=1.12 L/2 =1.12(250m)=280m

2. $M_t = A_t \times I = \pi(280)^2(17.5amps) = 4.310 \times 10^6$

3. Correct the voltage for the gain

$V = V \ 2^{-G} = 3747 \ 2^{-3} = 468.4$

Substitute into equation 2.2:

$$\rho_a(0.22) = 1.9 \times 10^{-2} \frac{(4.310 \times 10^6)^{2/3}}{(0.22)^{5/3}(468.4)^{2/3}} \tag{2.3}$$
$$\rho_a(0.22) = 104.3 ohm - m$$

Using equation 2.2, the late time apparent resistivities, calculated for all channels, are seen in Table 2.1 and Figure 2.9 for given example. The behavior of late time apparent resistivity curve in the Figure 2.9 looks like the behavior of late time apparent resistivity curve for a uniform half-space medium (see section 1.3). In the next section, the interpretation of the apparent resistivities and the apparent resistivity curves will be discussed.

Table 2.1. Examples of measured voltage and calculated apparent resistivity.

Channel number	Sqrt[t]	Data	Rhoa-Late
1	0.0094	13550.3	202.03
2	0.0105	10433.6	166.29
3	0.0118	7385.6	141.88
4	0.0133	5274.6	119.17
5	0.0148	3747.8	104.81
6	0.0167	2485.0	92.16
7	0.0188	1607.5	83.02
8	0.0210	1048.5	76.33
9	0.0237	641.7	70.75
10	0.0267	393.0	65.94
11	0.0297	258.1	61.20
12	0.0331	159.3	58.82
13	0.0376	91.8	55.54
14	0.0424	54.1	52.94
15	0.0472	33.2	51.24
16	0.0534	19.3	48.79
17	0.0600	8.3	58.06
18	0.0670	6.4	47.80
19	0.0755	3.5	48.00
20	0.0848	1.9	48.98

Table 2.2. Parameters for calculation of apparent resistivity.

Transmitter Loop = 500m×500m	Current, I = 17.5 amps	Frequency = 30Hz
Receiver Coil, A_{rec} = 100 m^2	Time, t=0.22 msec	Gain, G = 3
Voltage, V = 3747 millivolts	Channel number = 5	
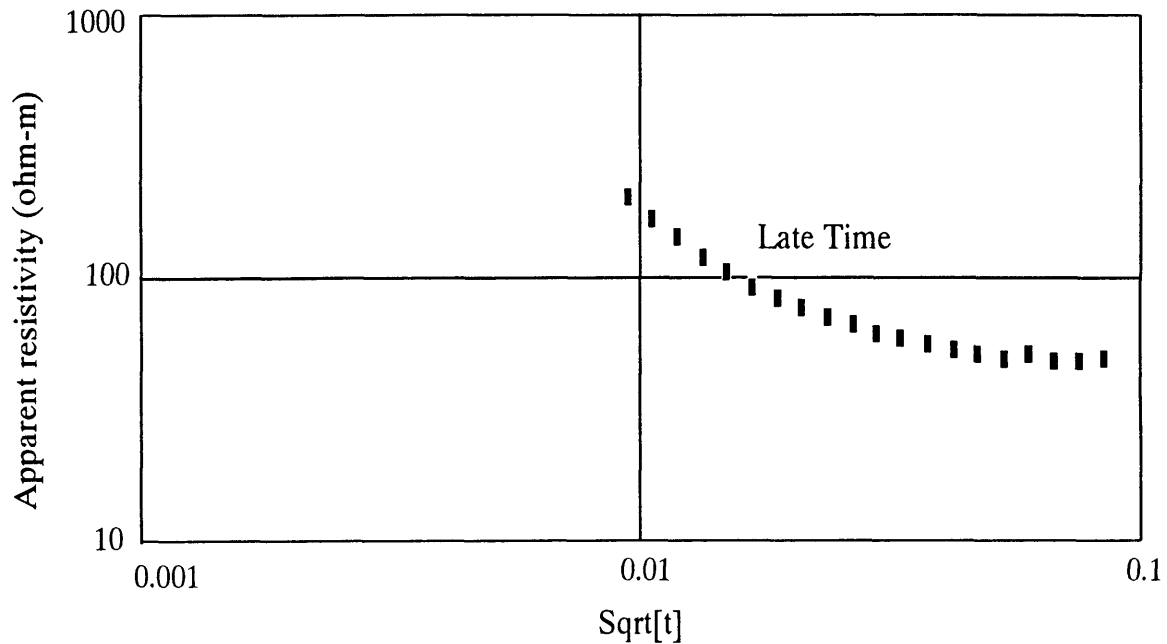
FIG. 2.9. Example of TEM results converted to apparent resistivity using the expression valid for late time (equation 2.2).

2.5 Interpretation of Apparent Resistivities and Curves

First of all, the late-time apparent resistivity contour maps will be plotted to get preliminary idea about the geoelectric section of the study area. Second, the late time apparent resistivity values for each sounding are plotted on a log-log graphic chart and then each sounding curve will instantly be interpreted by the curve matching method. Third, an inversion method will be used to obtain a one-dimensional geoelectric section. The inversion program requires an initial model for the geoelectric section. This model is usually derived from approximate matching of apparent resistivity curves with model curves or from a knowledge of the geologic section obtained from drill holes.

2.5.1 Late-Time Apparent Resistivity Contour Maps

Figures 2.10 through 2.14 show the distribution of late-time apparent resistivity with time along the Line-1 through Line-5 respectively. It might be mentioned that the early times can correspond to the shallow layers and the increasing time can correspond to the increasing depth.

As seen in the Figure 2.10, at early times, apparent resistivity values greater than 50 ohm-m continue along the line. At intermediate times, resistivity values lower than 50 ohm-m probably indicate the presence of unconsolidated rocks which thicken to east. At later times, high resistivity values maybe indicate the presence of consolidated volcanic rocks. A trend of decrease in the resistivity from 1E through 18E is evident from the map.

In the Figure 2.11, at early times, resistivity values lower than 200 ohm-m on the east continue along the line and the high resistivity values on the west go on along the late times. Thus, the high resistive consolidated rocks are located close to surface on the west. After the early times, the high resistivity values expand through under the low resistivity values on the east and the low resistivity values thicken to east. At the late times, the high resistivity values which correspond to the consolidated rocks continue until the station 12E.

The Figure 2.12 shows the low resistivity distribution at early times and the high resistivity distribution at late times. The changing of resistivity trend around the station 12E maybe indicate the presence of a fault and also this trend may shows the locations of the layers along the line.

As seen in the Figure 2.13, at early times, the apparent resistivity values lower than 200 ohm-m continue along the line and the resistivity values greater than 200 ohm-m go on through the late times. In other words, the high resistivity distribution
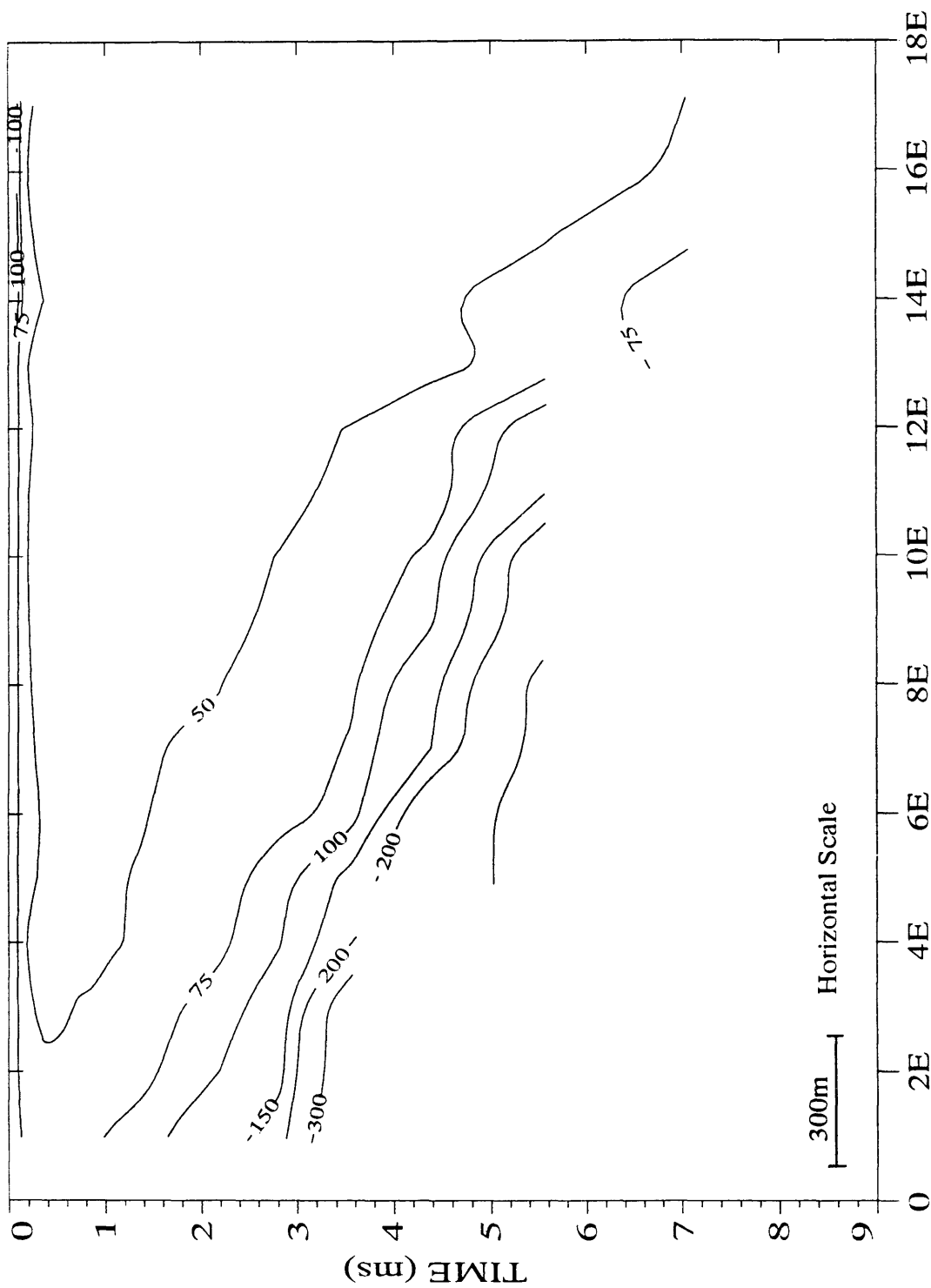
FIG. 2.10 Late time apparent resistivity contour map of Line-1. Contour values in ohm-m.
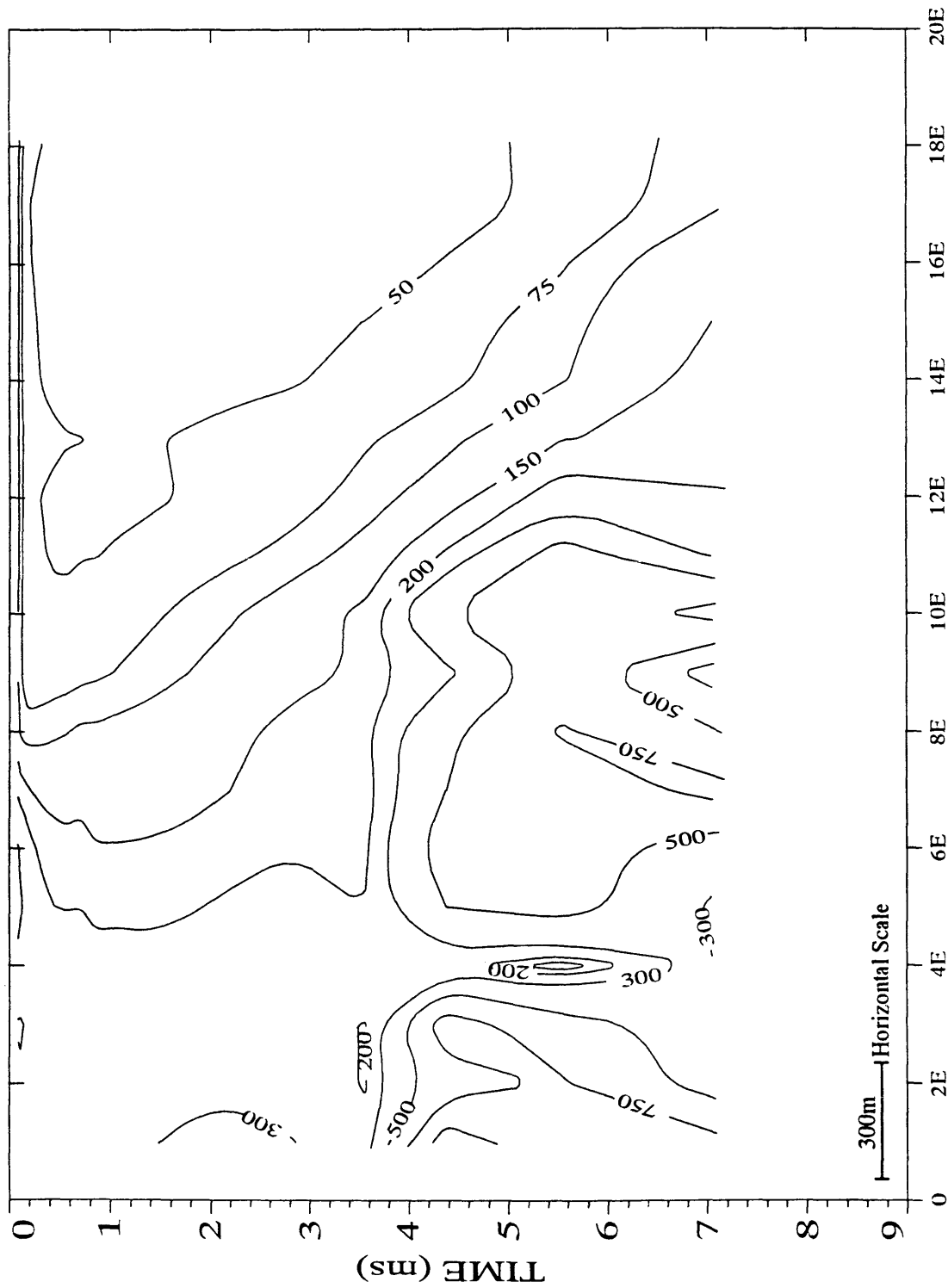
FIG. 2.11 Late time apparent resistivity contour map of Line-2. Contour values in ohm-m.
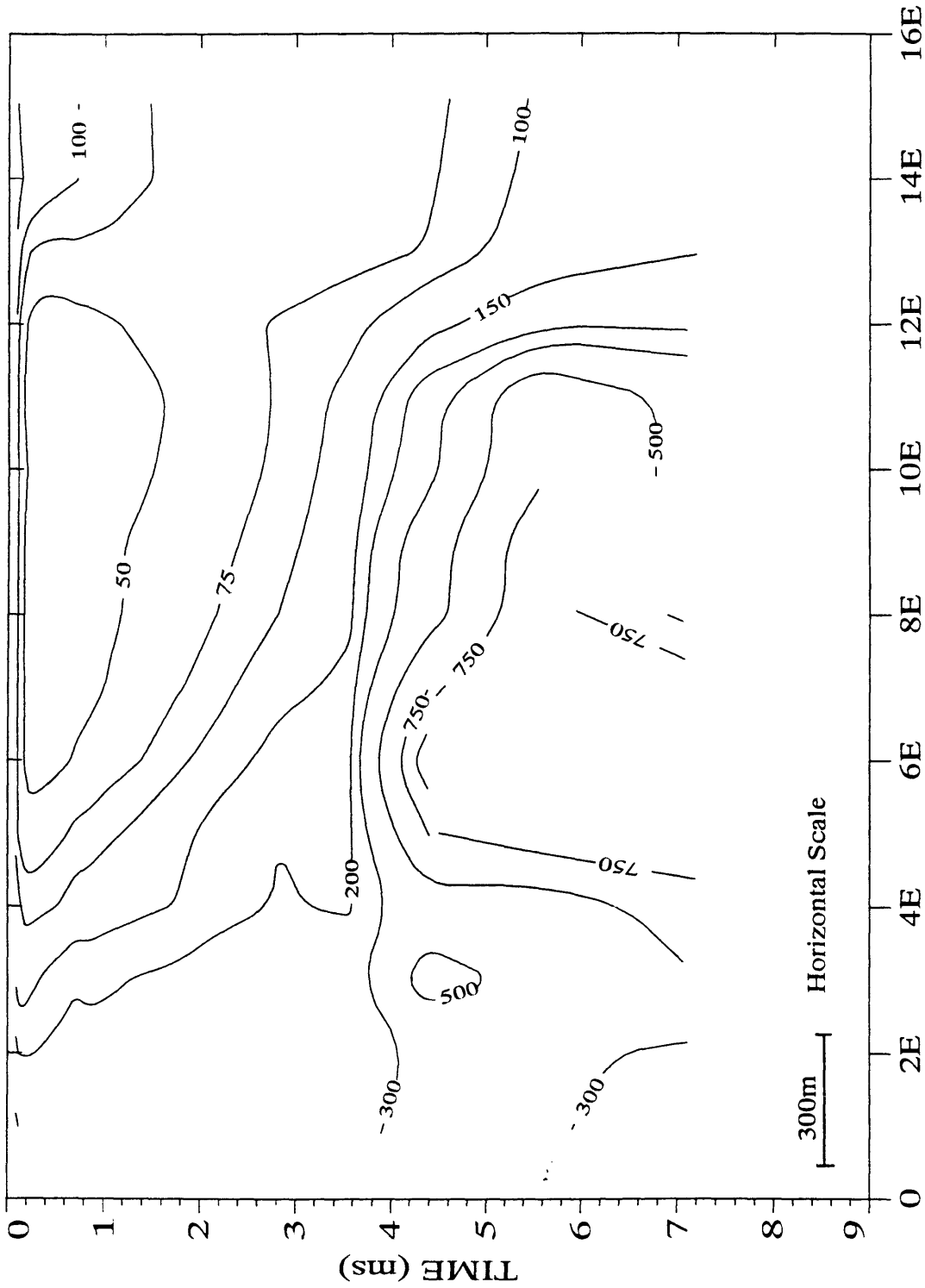
FIG. 2.12 Late time apparent resistivity contour map of Line-3. Contour values in ohm-m.
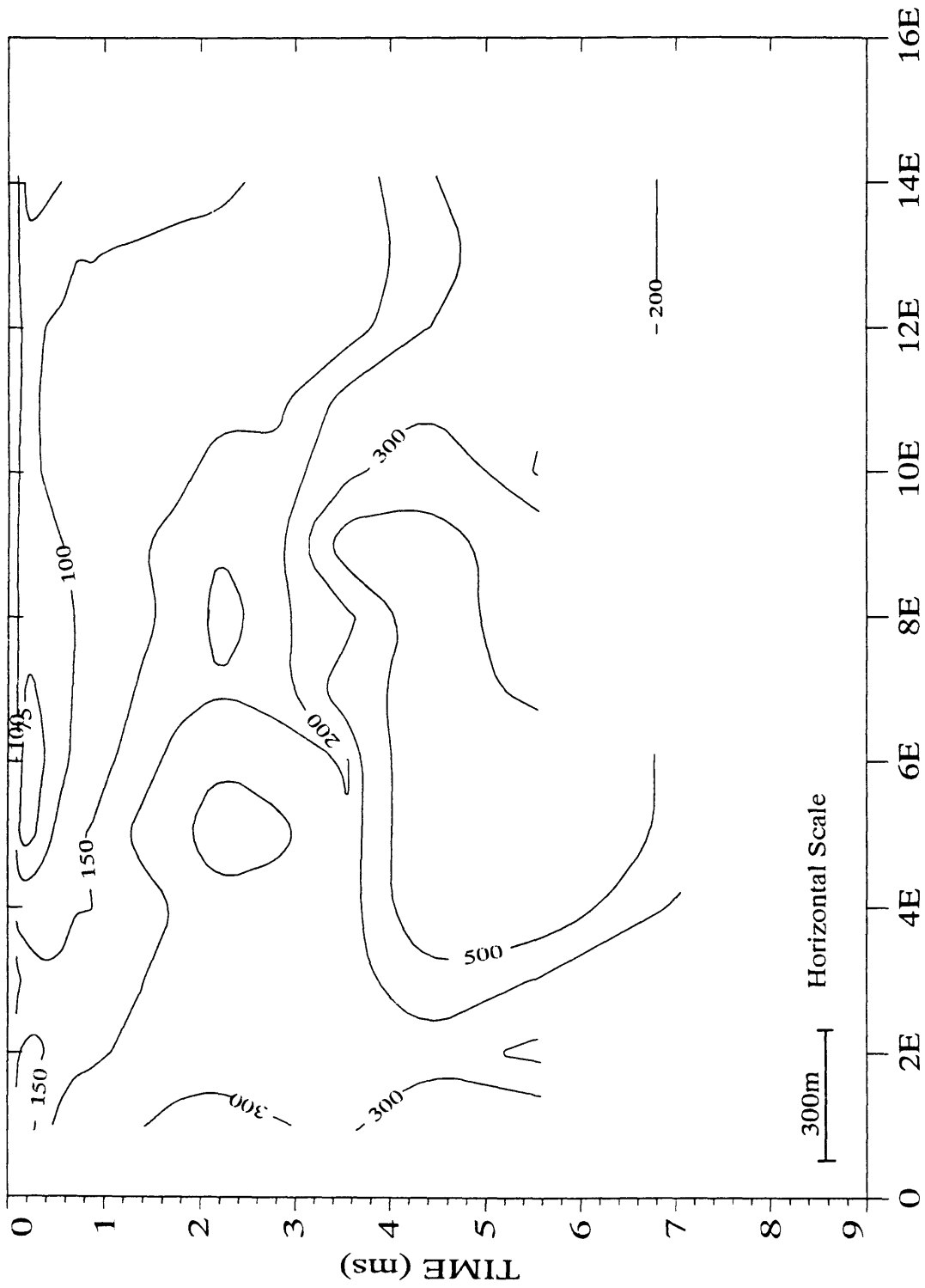
FIG 2.13 Late time apparent resistivity contour map of Line-4. Contour values in ohm-m.

on the west part is placed at early times therefore, the high resistive consolidated rocks could be close to the earth surface. The 200 ohm-m apparent resistivity contour can divide the contour map into two group with a slope which are consolidated rocks, greater than 200 ohm-m, and unconsolidated rocks, lower than 200 ohm-m.

In the last Figure 2.14, the resistivity values lower than 200 ohm-m continue along the line at early times and they thicken to east with increasing time. The high resistivity values are observed at intermediate and late times on the west part of the lines.

From the above discussions, it is clear that these maps are able to give a notion about the geologic setting of the study area. In five contour maps, the low resistivity values are observed at early times on the west and also at early and intermediate times on the east. In addition, these low apparent resistivity contours draw out along the lines with increasing times. It could be interpret that the unconsolidated rocks thicken from west to east. The consolidated rocks lie under this unconsolidated rocks. In order to find the resistivity values of the consolidated and unconsolidated rocks, the following interpretation method will be used.

2.5.2   Curve Matching

First of all, the apparent resistivity curve's type can be determined such as homogeneous or layered medium type. Some theoretical late time apparent resistivity curves are shown in Figure 1.20, 1.21, 1.22 and 1.23. If the field curve is considered as a uniform half-space curve, the resistivity of the uniform half-space can be determined using one of the several different method. As is known the left-hand branch of late-time apparent resistivity curves for a uniform half space is expressed as straight lines with a slope of 10/3. Using this left-hand asymptote, the resistivity of first layer or
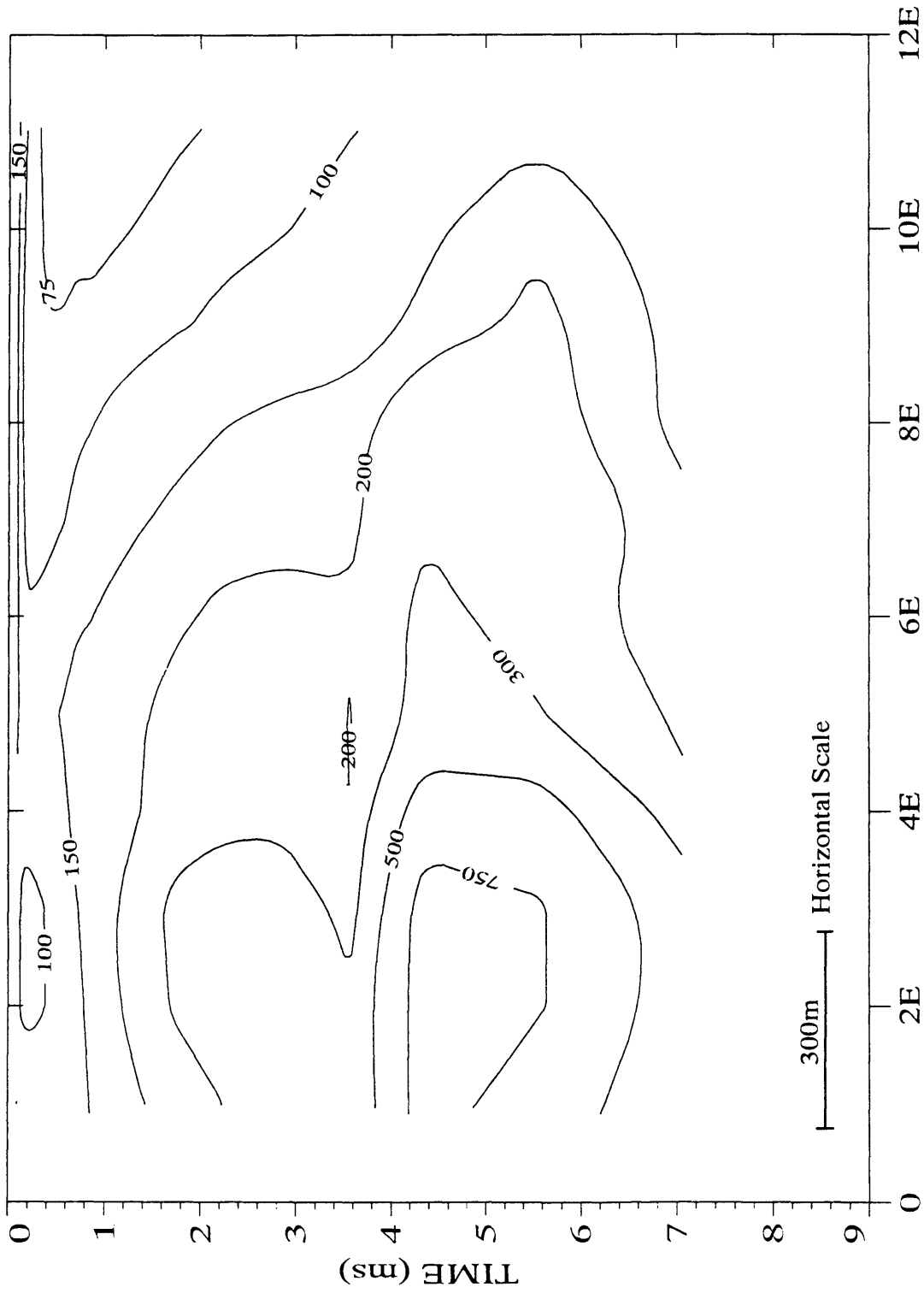
FIG 2.14 Late time apparent resistivity contour map of Line-5. Contour values in ohm-m.

resistivity of a uniform half-space can be determined in following ways:

(1) When the left-hand asymptote of the apparent resistivity curve is matched with straight line, the resistivity, ρ_1, can be calculated as in Figure 2.15 method-1.

(2) Using the abscissa of the intersect of the left-hand asymptote of the apparent resistivity with the axis $\rho_\tau = 1 ohm - m$, the resistivity of the first layer or uniform half-space medium is determined as in Figure 2.15 method-2.

If ρ_1 is not equal to ρ_τ^+ (see Figure 2.15), the medium will not be homogeneous half-space and the curve may be interpreted as a two layer curve. To evaluate two layer curves, the observed curves are matched with one of the two-layer theoretical curves, and a reference point on the theoretical curves, coordinates $\rho_\tau/\rho_1 = 1$ and $\tau/r = 10$, is marked on the observed curves. Thus, the value for ρ_1 is determined from the reference point. The thickness of the first layer can be calculated by using either index r/h_1 or abscissa of the reference point. If these 2 values of h_1 do not match with each other, indicates influence of inhomogeneities, possible mismatch or the value of τ/r is not exactly 10. If this value is slightly different from 10, the values of h_1 is calculated differently. For example, the thickness of the first layer is determined for given example in following way:

$$H_{km} = \sqrt{0.1\rho_1}\sqrt{2\pi t^*} \qquad (2.4)$$

where $\sqrt{2\pi t^*}$ is the abscissa of the reference point for theoretical curve set ($\rho_\tau/\rho_1 = 1$, $\tau_1/H_1 = 10$) on the abscissa of the experimental curve when a match has been obtained. The reference point " $+$ " is obtained in the Figure 2.15, and the thickness of the first layer is;

$H_{km} = \sqrt{0.1135}\sqrt{2\pi}0.015 = 0.138km = 138m.$

And also, ρ_2 is calculated by using index ρ_2/ρ_1, at the theoretical curves. If there
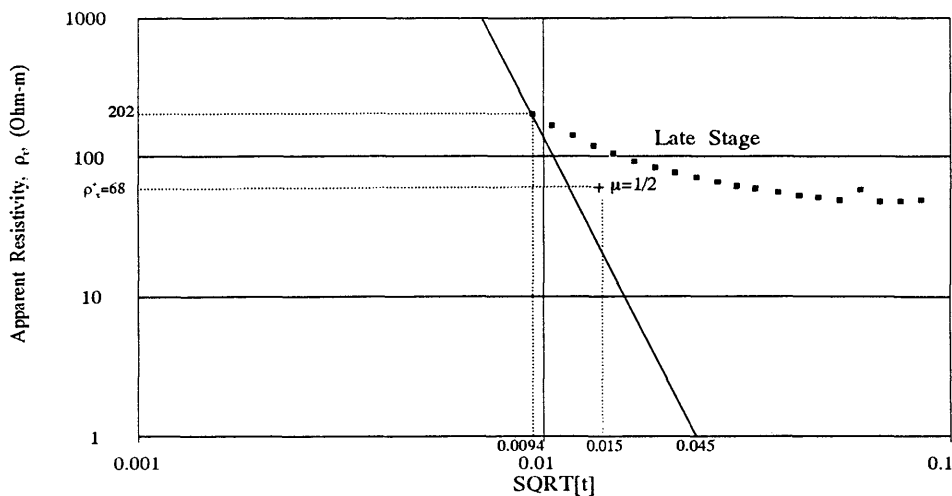
Method 1:
$\rho_1 = 1.647(0.280/\text{SQRT}(2\ \pi)0.094)^5(1/(202)^{3/2}) = 135$ ohm-m

Method 2:
$\rho_1 = 1.647^2(0.28/\ \text{SQRT}(2\pi)0.045)^5 = 155$ ohm-m

FIG. 2.15. Calculation of ρ_1, where r=0.28 km.

is no match between observed curve and two-layer theoretical curves, the observed curve will be matched with a three-layer theoretical curve.

In the interpretation of three layer curves, first the observed curve's type should be determined, such as;

- $\rho_1 > \rho_2 > \rho_3$ Q type

- $\rho_1 < \rho_2 > \rho_3$ K type

- $\rho_1 > \rho_2 < \rho_3$ H type

- $\rho_1 < \rho_2 < \rho_3$ A type

After the observed curves type are found out, they are matched with one of that three layer theoretical curves and ρ_1, ρ_2, ρ_3, h_1 and h_2 are calculated as in two layers case.

Four layer apparent resistivity theoretical curves are used if there is no match with three layer resistivity theoretical curves.

The field curves were interpreted usually as a three layer curves. As seen in the Table 2.3, 2.4, 2.5, 2.6 and 2.7, some of the field curves could not be matched with any theoretical curves. In this case, behavior of the observed resistivity curves may be compared other observed curves along the same survey line and those curves can be interpreted approximately. In the curve matching method, the resistivity of last layer of the curves may be found roughly (see Table 2.3, 2.4, 2.5, 2.6 and 2.7). Moreover, the observed curves may be matched inexactly with a theoretical curve therefore, the curve matching results can not be trustworthy. Thus, an other interpretation method, inversion, is necessary.

2.5.3 Inversion

After the sounding curves were interpreted by the curve matching method, an one-dimensional ridge regression transient inversion (TEMIX Plus by Interpex Limited) program was used. This inversion program requires an initial estimate of the geoelectric section, including the number of layers and the resistivities and thickness of each of the layers. Results from the curve-matching method were given to the inversion program as an initial model. The program then adjusts these parameters so that the model curve converges to be a best fit to the curves formed by the field data set. The inversion program does not change the total number of layers within the model, but allows resistivity and thickness to change freely. An overview of the TEMIX Plus software package is given in Appendix-B.

Table 2.3. Model parameters of Line-1.

							Time Channels From 1 To 20		Current (Amps) 10		Ramp Time (μsec) 80		Frequency (Hz) 30		T ON/OFF (ms) 8.333			
	ρ_1 (ohm-m)		ρ_2 (ohm-m)		ρ_3 (ohm-m)		ρ_4 (ohm-m)		H-1 (m)		H-2 (m)		H-3 (m)			
Location	Matching	Inversion	Matching	Inversion	Matching	Inversion	Matching	Inversion	Matching	Inversion	Matching	Inversion	Matching	Inversion	Fit (%)
1	41	45	164	84	>>41	918	...	...	76	89	76	46	...	...	3.2
2	41	37	164	104	>>41	481	...	...	64	80	64	86	...	...	2.6
3	41	36	164	96	>>41	495	...	...	76	88	76	85	...	...	2.6
4	38	33	152	89	>>38	454	...	...	76	89	76	105	...	...	2.9
5	41	36	164	58	>>41	489	...	...	95	72	95	135	...	...	2.4
6	42	37	168	65	>>42	521	...	...	107	86	107	185	...	...	3.5
7	40	36	80	65	>>40	619	...	...	54	87	216	231	...	...	3.5
8	38	35	76	63	>>38	510	...	...	54	101	216	202	...	...	3.5
9	35	35	70	61	>>35	599	...	...	54	110	216	189	...	...	3.8
10	39	69	78	27	>>39	54	...	552	109	14	109	58	...	231	3.8
11	38	68	76	26	>>38	50	...	628	84	17	168	55	...	292	2.5
12	39	75	78	22	>>39	49	...	427	95	25	190	35	...	295	3.4
13	35	80	70	19	>>35	43	...	215	107	25	214	31	...	301	3.2
14	41	134	82	16	>>41	48	...	210	167	42	214	29	...	301	2.6
15	30	175	60	13	>>30	42	...	211	76	39	152	26	...	274	3.8
16	28	186	56	13	>>28	36	...	204	63	35	126	31	...	274	3.1
17	31	187	124	10	>>31	34	...	254	152	41	152	17	...	269	3.6

2.6 Results

Model parameters of 75 TEM soundings are given in Table 2.3, 2.4, 2.5, 2.6, 2.7. For each sounding, the curve matching results and the inversion results are shown in the Tables and also, the fitting errors between field data and calculated data are shown. Some initial models were started with three layers resulted from matching, and after many iteration of the inversion program, there was not enough convergence to the field data. In such cases, the geoelectrical model was changed to a four layer model instead of a three layer model.

The rocks in study area may be divided into two main part, consolidated and unconsolidated rocks. The possible resistivity of consolidated rocks is greater than 200 ohm-m. This range for unconsolidated rocks is between 1 ohm-m and 200 ohm-

Table 2.4. Model Parameters of Line-2.

		Time Channels From 1 To 20		Current (Amps) 10		Ramp Time (μsec) 80		Frequency (Hz) 30		T ON/OFF (ms) 8.333				
	ρ_1 (ohm-m)		ρ_2 (ohm-m)		ρ_3 (ohm-m)		ρ_4 (ohm-m)		H-1 (m)		H-2 (m)		H-3 (m)		
Location	Matching	Inversion	Matching	Inversion	Matching	Inversion	Matching	Inversion	Matching	Inversion	Matching	Inversion	Matching	Inversion	Fit (%)
1	...	79	...	324	...	6731	...	...	...	33	...	365	...	...	6.8
2	...	85	...	633	...	199	...	269	...	52	...	154	...	76	2.6
3	...	71	...	1159	...	111	...	1121	...	46	...	213	...	129	2.9
4	230	56	115	375	>>230	116	...	506	263	19	132	259	...	115	2.1
5	195	118	97	326	>>195	122	...	2864	266	34	133	103	...	216	3.4
6	160	135	80	235	>>160	105	...	1000	220	39	110	91	...	195	3.5
7	130	92	65	206	>>130	107	...	866	180	69	90	60	...	182	1.8
8	...	189	...	39	...	203	...	...	...	9	...	43	...	...	4.4
9	40	112	160	39	>>40	2089	...	...	38	9	76	93	...	...	4
10	75	95	38	32	>>75	4611	...	...	10	21	60	83	...	...	3.5
11	70	114	35	34	>>70	6866	...	...	11	16	66	116	...	...	3.8
12	68	102	34	24	>>68	55	...	4053	14	30	56	50	...	104	4.5
13	...	88	...	36	...	58	...	1943	...	19	...	82	...	161	3.8
14	...	129	...	24	...	57	...	1892	...	27	...	57	...	198	3.5
15	...	129	...	17	...	61	...	552	...	36	...	36	...	332	3.8
16	...	112	...	10	...	51	...	846	...	44	...	19	...	326	4.2
17	...	137	...	10	...	42	...	648	...	42	...	21	...	271	4.3
18		116		23		40		520		35		67		204	2.9

Table 2.5. Model Parameters of Line-3.

		Time Channels From 1 To 20		Current (Amps) 10		Ramp Time (μsec) 80		Frequency (Hz) 30		T ON/OFF (ms) 8.333				
	ρ_1 (ohm-m)		ρ_2 (ohm-m)		ρ_3 (ohm-m)		ρ_4 (ohm-m)		H-1 (m)		H-2 (m)		H-3 (m)		
Location	Matching	Inversion	Matching	Inversion	Matching	Inversion	Matching	Inversion	Matching	Inversion	Matching	Inversion	Matching	Inversion	Fit (%)
1	...	176	...	302	...	84	...	1743	...	105	...	365	...	68	2.9
2	...	114	...	1006	...	67	...	900	...	105	...	273	...	98	2.1
3	...	64	...	1515	...	44	...	2408	...	65	...	287	...	45	5.2
4	...	110	...	21	...	581	...	...	...	49	...	23	...	...	4.2
5	280	43	35	13	>>280	1158	...	...	10	46	40	10	...	...	3.9
6	180	157	23	7	>>280	10000	...	...	8	37	32	14	...	...	6.7
7	200	141	25	15	>>280	2589	...	...	15	27	60	42	...	...	4.1
8	195	195	24	13	>>195	999	...	...	14	29	54	37	...	...	3.6
9	190	200	24	16	>>190	912	...	...	14	24	56	48	...	...	4.4
10	190	195	24	16	>>190	1001	...	...	14	29	56	55	...	...	2.7
11	185	201	23	14	>>185	1027	...	...	14	26	56	48	...	...	3.4
12	200	191	25	12	>>200	1190	...	...	14	36	56	36	...	...	3.6
13	...	58	...	326	...	28	...	1300	...	184	...	101	...	95	7.1
14	...	95	...	141		19	..	2164	...	208	...	25	...	88	4.4
15		88		270		11		2104	...	162		83		53	3.4

Table 2.6. Model Parameters of Line-4.

Time Channels		Current	Ramp Time	Frequency	T ON/OFF
From	To	(Amps)	(µsec)	(Hz)	(ms)
1	20	10	80	30	8.333

Location	ρ_1 (ohm-m) Matching	Inversion	ρ_2 (ohm-m) Matching	Inversion	ρ_3 (ohm-m) Matching	Inversion	ρ_4 (ohm-m) Matching	Inversion	H-1 (m) Matching	Inversion	H-2 (m) Matching	Inversion	H-3 (m) Matching	Inversion	Fit (%)
1	...	47	...	136	...	3007	...	...	...	38	...	13	...	...	7.8
2	130	95	260	228	>>130	2065	...	...	68	90	68	179	...	...	1.4
3	160	81	320	151	>>160	3407	...	...	76	16	76	250	...	...	2.8
4	102	66	204	286	>>102	971	...	...	76	67	152	206	...	...	5.4
5	...	30	...	139	...	4582	...	...	...	38	...	6	...	...	10
6	23	38	184	278	>>23	10000	...	...	10	59	60	10	...	...	8.0
7	52	46	208	147	>>52	4320	...	...	38	70	38	25	...	...	5.4
8	42	52	168	116	>>42	1893	...	...	38	80	38	30	...	...	2.6
9	...	46	...	120	...	1496	...	...	...	60	...	36	...	...	5.7
10	...	51	...	1650	...	18	...	1465	...	70	...	292	...	35	5.7
11	...	56	...	1481	...	20	...	1496	...	76	...	196	...	38	3.2
12	...	58	...	1379	...	20	...	1465	...	82	...	173	...	42	4.3
13	...	53	...	1508	...	20	...	1504	...	92	...	226	...	47	3.7
14	...	51	...	1543	...	20	...	1545	...	112	...	211	...	38	5.5

Table 2.7. Model Parameters of Line-5.

Time Channels		Current	Ramp Time	Frequency	T ON/OFF
From	To	(Amps)	(µsec)	(Hz)	(ms)
1	20	10	80	30	8.333

Location	ρ_1 (ohm-m) Matching	Inversion	ρ_2 (ohm-m) Matching	Inversion	ρ_3 (ohm-m) Matching	Inversion	H-1 (m) Matching	Inversion	H-2 (m) Matching	Inversion	Fit (%)
1	80	100	160	81	>>80	9030	19	18	76	108	6
2	62	166	496	33	>>62	4112	38	19	38	40	7.5
3	30	194	240	32	>>30	3744	10	18	60	39	9
4	90	190	720	43	...	689	54	18	...	44	3.7
5	100	154	800	60	...	610	54	25	...	59	5.4
6	49	215	196	54	>>49	644	14	21	56	68	6.7
7	36	206	144	16	>>36	1055	10	54	60	22	7.3
8	31	204	124	19	>>31	1122	10	53	60	32	6.7
9	...	202	...	31	...	289	...	43	...	62	4.4
10	56	204	112	44	>>50	662	48	34	96	129	4.5
11	58	213	116	35	>>58	867	54	49	54	115	2.5

m. The unconsolidated rocks are Tertiary alluvium, colluvium, eolian and lacustrine sediments. The resistivity of the rocks may be changed by alteration, fracturing and water content. The resistivity of a rock will be lowered as fracturing increases and also, an increase in the salinity and amount of water within a rock unit will lower its resistivity. Now, let us look at the results of each survey line.

2.6.1 Line 1

The results of Line-1 which are plotted on a two-dimensional geoelectric cross section and the resistivities are shown in Figure 2.16. The first 9 soundings on the Line-1 have best fit with A-type 3-layer model curves. Behaviors of apparent resistivity curves of the eastern most 8 soundings on the profile were fit as a four layer late time apparent resistivity curves. The resistivity of the first layer decreases from $\sim 40 ohm - m$ in the west to less than $20 ohm - m$ in the east. The reasons are probably a reduction in grain size, or increase in water content. At the east end, a more resistive layer is seen at the surface. The second layer's resistivity decreases and its thickness increases from west to east (Figure 2.16). The subdivision in resistivity of unconsolidated rocks may be due to lithological changes, water content and water quality. The depth to basement increases by over 100 meters between soundings 5 and 7 and by 80 meters between soundings 11 and 12. These increases may indicate the presence of faults. In addition the resistivity of the thick second layer, decreases at the same point.

2.6.2 Line 2

The late time apparent resistivity curves and the geoelectric cross section of the Line-2 are shown in Figure 2.17. The behavior of first sounding's apparent resistivity
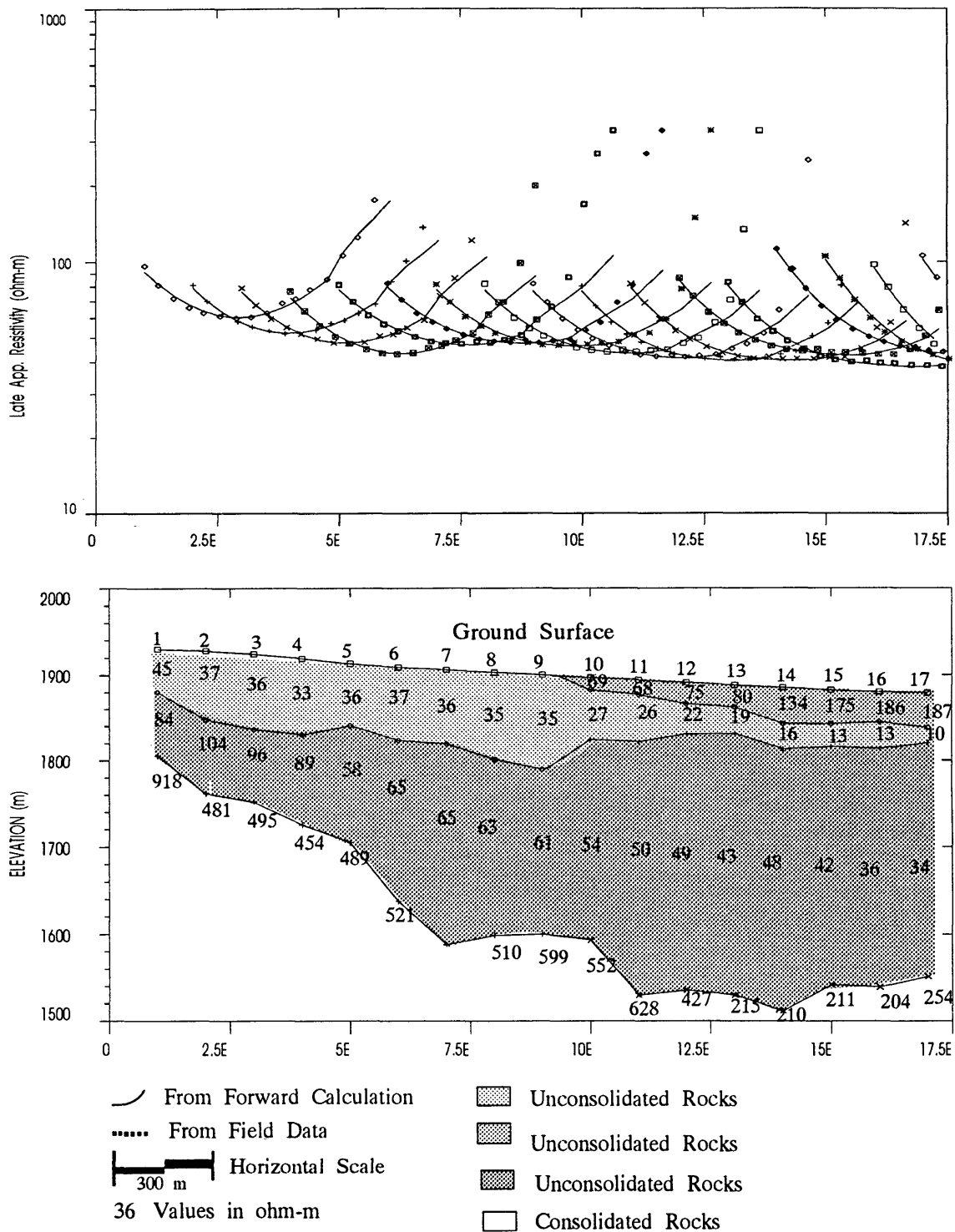
FIG. 2.16. Late time apparent resistivities (above) and 2-D geoelectric section for Line-1.
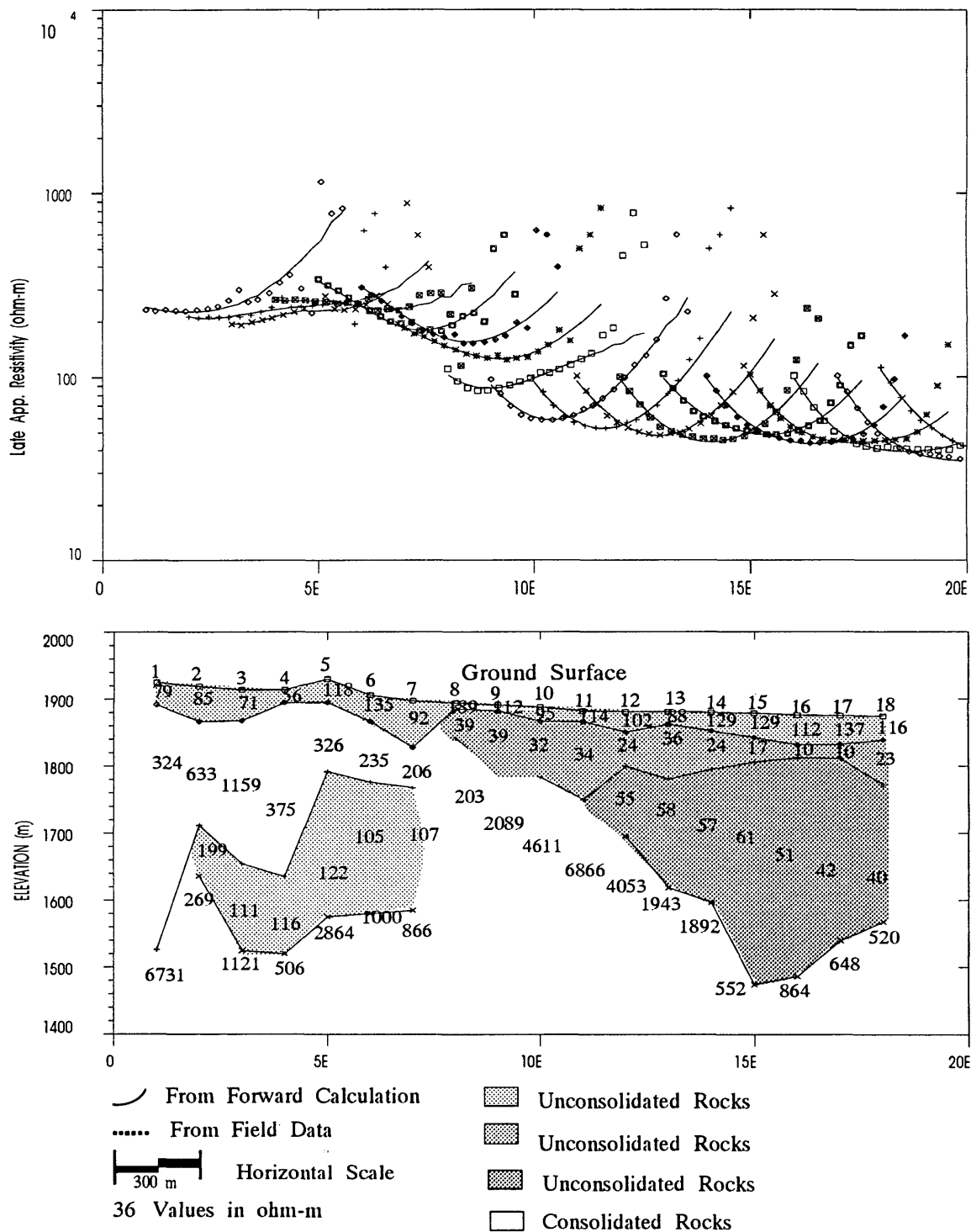
FIG. 2.17. Late time apparent resistivities (above) and 2-D geoelectric section for Line-2.

curve has a sharp changing between the channel-10 and channel-11. It is hard to interpret this kind of curve as two, three or four layers. It may be best way to interpret this curve to compare with adjacent curve so that, the interpretation of such a curve can be trust. Since the fifth sounding is located on the top of hill where the volcanic rock may be grounded, the first layer under this sounding may be evaluated as a unconsolidated rock. As seen in the Figure 2.17, the behavior of late time apparent resistivities for first 7 soundings are different from the behavior of the other curves on the profile. Therefore, from the inversion results it may be thought that there is an alluvial, colluvial sediment inside of volcanic rocks along the sounding 2E through 7E. However, it is difficult to interpret that there is an unconsolidated layer inside the volcanic rock.

The behaviors of the last 11 late time apparent resistivity curves are quite similar to each other. Thus, they can be interpreted as a three and four layers. As seen in the Figure 2.17 under the resistive surface layer, the resistivity increases with depth. Moreover, the resistivity of unconsolidated rock under the resistive surface layer decreases through the east direction. Again, the decreasing of resistivity along the profile may be explained with an increasing of water content and a reduction in grain size. The depth to basement increases by over 100m between soundings 14E and 17E and by 30m between soundings 7 and 8. These increase may display the aspect of faults. In addition, the resistivity of the second layer changes at the same points.

2.6.3   Line 3

The results of transient soundings on the Line-3 are shown in Figure 2.18. The behaviors of the first three and the last three late time apparent resistivities are
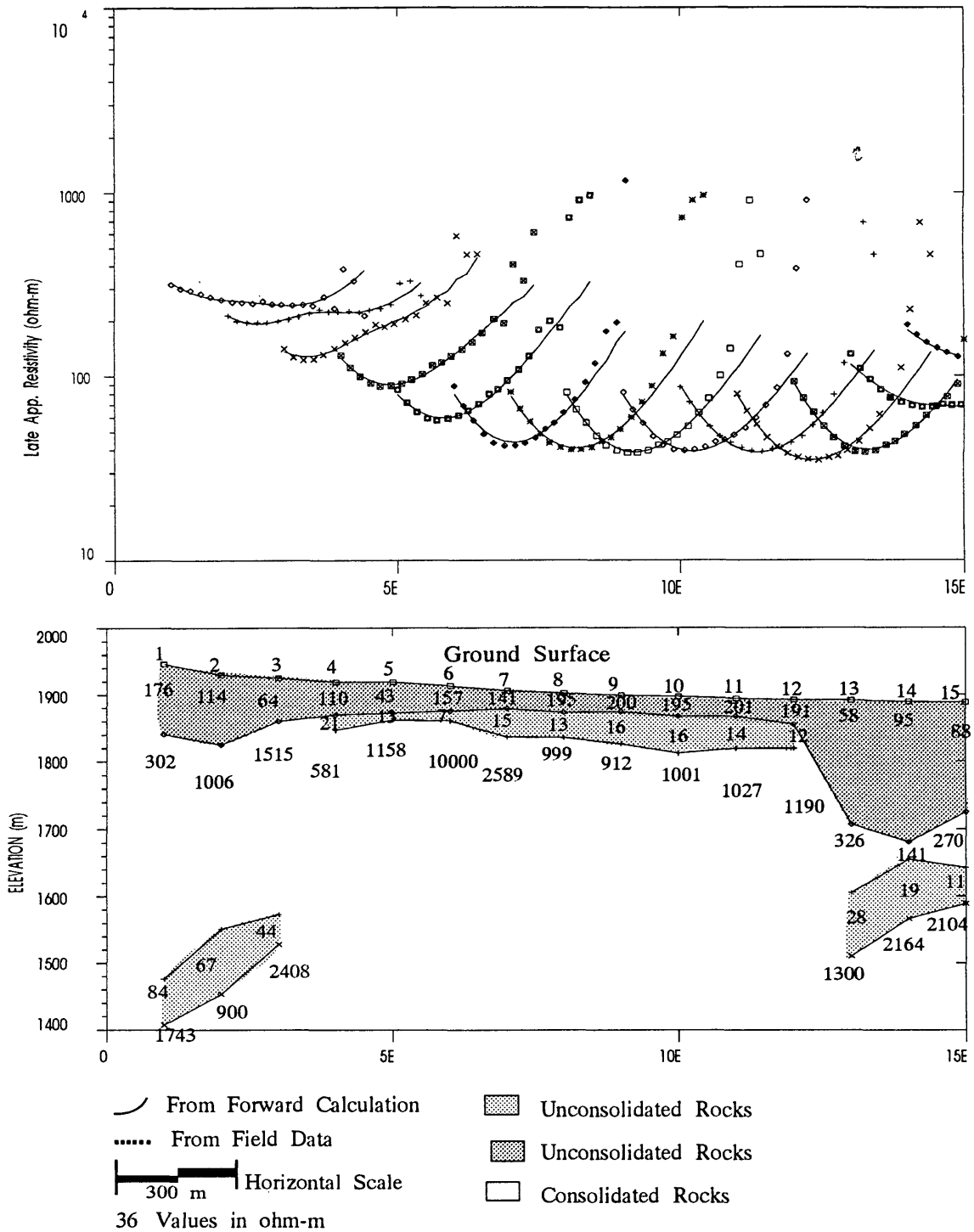
FIG. 2.18. Late time apparent resistivities (above) and 2-D geoelectric section for Line-3.

quite different from the behaviors of other curves on the profile. These apparent resistivity curves are interpreted as a four layers. The other curves on the line are interpreted as a three layers. In contrast the Line-1 and Line-2, the resistive surface layer can be detected along the profile. Between the sounding 4 and 12, the second layer, unconsolidated rock, can be located under the resistive layer with a very low resistivity. There might be a fault under the sounding 4 and 12 because of sharp lateral resistivity change on the second layer. In addition, the depth to basement increases by over 100m between soundings 13 and 15. As was described on the Line-2, the third unconsolidated layer beneath the first and last three sounding can be hardly interpreted.

2.6.4 Line 4

The apparent resistivities and the geoelectric section of the Line-4 are shown in Figure 2.19. The interpretation of data along the Line-4 is more complex than that in the other profiles. As seen in the Table 2.6, the fitting errors between observed data and synthetic data for sounding 1, 5, 6 are much higher then others on the profile. The reason may be that those sounding locations may be on a geologic transition zone along the line. Unlike the Line-2 and 3, the surface layer is not a resistive layer. It can correspond to the unconsolidated rocks and its resistivity decreases through the end of the profile. Again, this lateral resistivity change can depend upon the change of water content. The second layer between the sounding 1 and 9 can be interpreted like not only an unconsolidated rock but also a consolidated rock. It is better to interpret this layer as a consolidated rock because of high resistivity values for second layer under each sounding. The interpretation of the third layer under the sounding 10 through 14 is difficult.
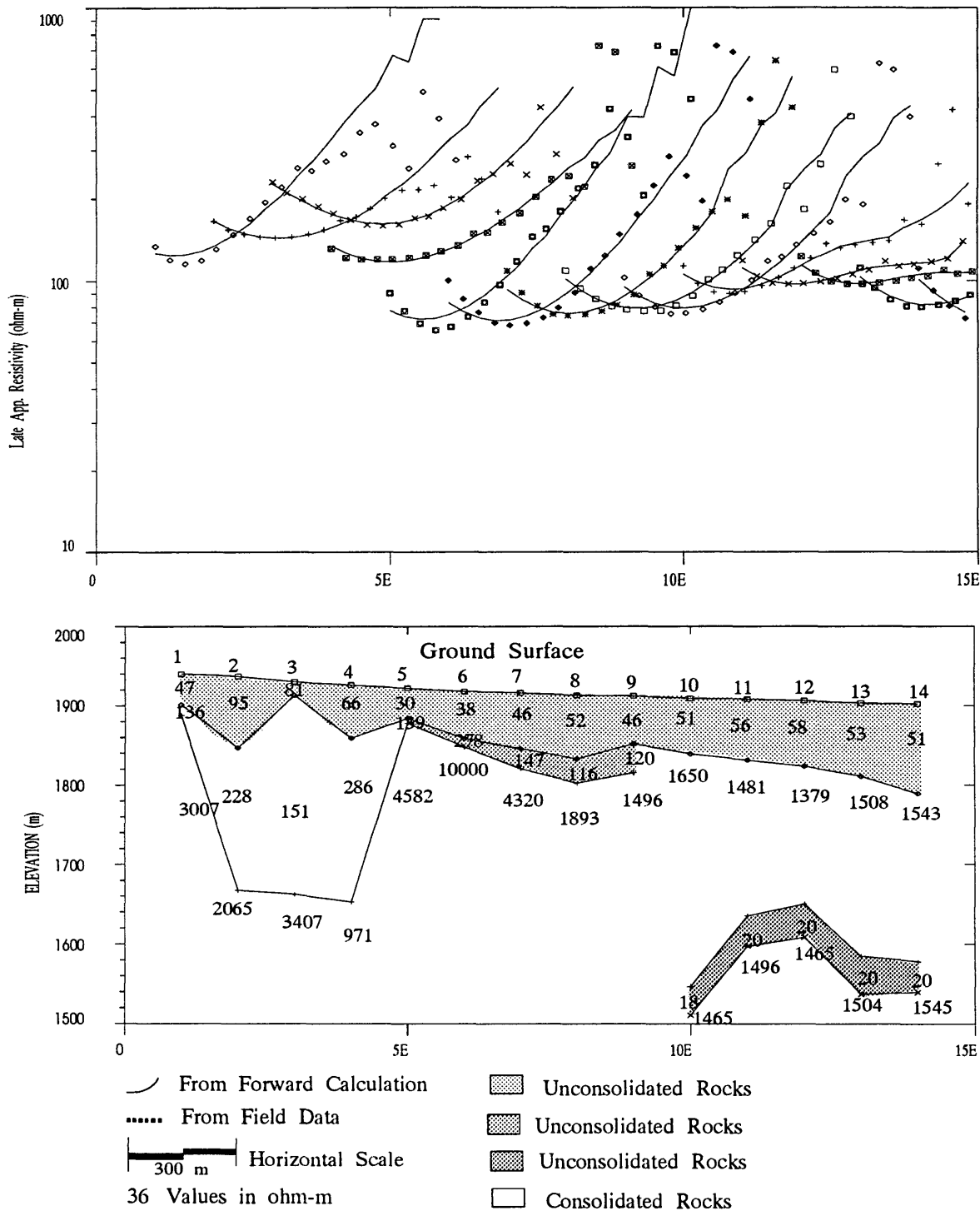
FIG. 2.19. Late time apparent resistivities (above) and 2-D geoelectric section for Line-4.

2.6.5   Line 5

The results of the Line-5 are shown in Figure 2.20. Each sounding, along the line are interpreted as a H-type three layer curve. Resistive surface layer, the second layer and resistive volcanic basement can be defined easily along this line. It may be thought that there are some higher resistivity values, more than 200 ohm-m, on the first layer. In fact, if the resistivity of unconsolidated sediments is less than 200 ohm-m, the equivalent analysis of those interpretation shows that the model parameters can be changed plus or minus a certain amount. This change can be reduced by using more accurate data. The depth to first layer changes by over 30m between soundings 11 and 12 and also the resistivity of the second layer changes at the same points. These changes may indicate the presence of a fault. The depth to basement increases by over 50m between the soundings 1 and 2 and by 50m between sounding 9 and 10. These increases may shows the presence of faults.

2.6.6   Evaluation of TEM Results

The geoelectric cross sections indicated the presence of three and four-layer earth. However, some layers which are the third layer on the western part of the Line-2 and 3 (Figure 2.17, 2.18) and on the eastern part of the Line-3 and 4 (Figure 2.18, 2.19) can not be interpreted easily. Since the main purpose was to map the depth of consolidated volcanic rocks, these uncertain layers can be excluded. In this case, the geoelectric cross sections indicate also two-layer earth. If the subdivision in the resistive layer (≻200 ohm-meters) on the station 1 to 4 (Figure 2.19) can be eliminated, that part of section will indicate also two-layer earth.

In the case of four-layer earth, the sections consist of a moderately resistive surface layer with resistivities between 68 and 187 ohm-meters (eastern part of the
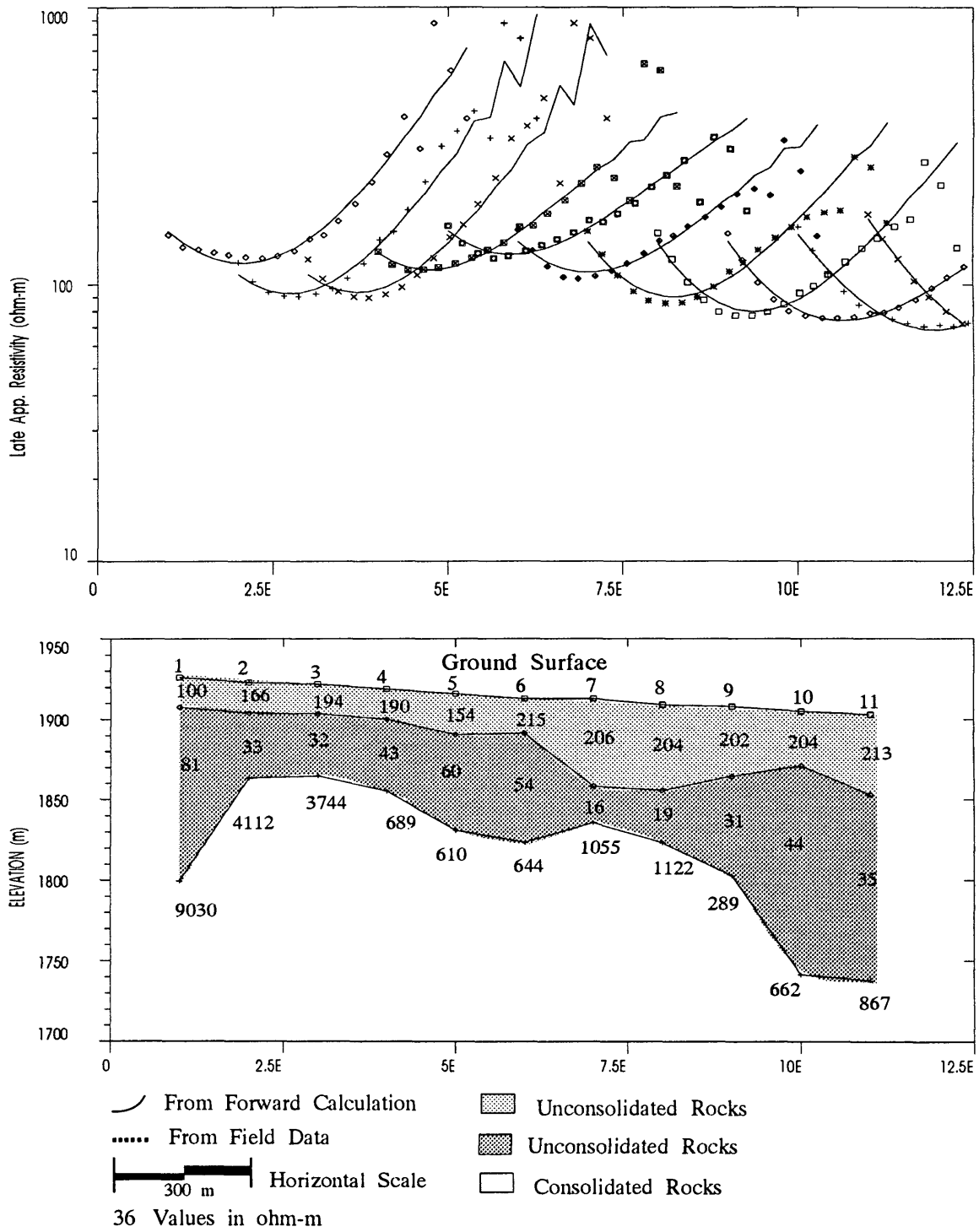
FIG. 2.20. Late time apparent resistivities (above) and 2-D geoelectric section for Line-5.

Line-1 and 2, Figure 2.16, 2.17), underlain by a conductive layer representing prob-

ably coarse grained deposits with resistivities between 10 and 40 ohm-meters. The

third layer appears to be more resistive than the second layer with resistivities be-

tween 34 and 104 ohm-meters. The thicknesses of these three layers vary greatly,

with a tendency for the high values to be in the eastern portion of the study area.

The thicknesses of up to 404 meters were obtained. The fourth layer appeared to be

inhomogeneous, with a wide range of resistivities (≻200 ohm-meters), which probably

indicates the presence of the consolidated basement.

In terms of three-layer earth, the same surface layer appeared on the Line-2, 3

and 5 (Figure 2.17, 2.18, 2.20). The second conductive layer in the four-layer case

appeared as a first layer on the western part of Line-1 (Figure 2.16) and a second

layer on the Line-2 and 3. The third layer in the four-layer case appeared as a second

layer on the Line-5 (Figure 2.20). The thicknesses of these two layers wary up to 318

meters, with a tendency for the high values to be in the eastern portion of the study

area. The last layer appeared to be high resistive basement.

In the case of two-layer earth, the resistive surface layer appeared on the Line-2

and 3 (Figure 2.17, 2.18). The third layer in the four-layer case appeared as a surface

layer on the Line-4 (Figure 2.19). The depth of the relatively resistive basement (≻200

ohm-meters) varies between 10 and 208 meters.

When the uncertain layers on the Line-2, 3 and 4 are excluded, the geoelectric

section of the five lines will be shown in Figure 2.21. As seen in the Figure, the five

geoelectric section shows mainly the boundary of the consolidated rocks under the

unconsolidated rocks. In general, the depth of the consolidated rocks increases from

west to east. The thickness of the unconsolidated rocks decrease not only through

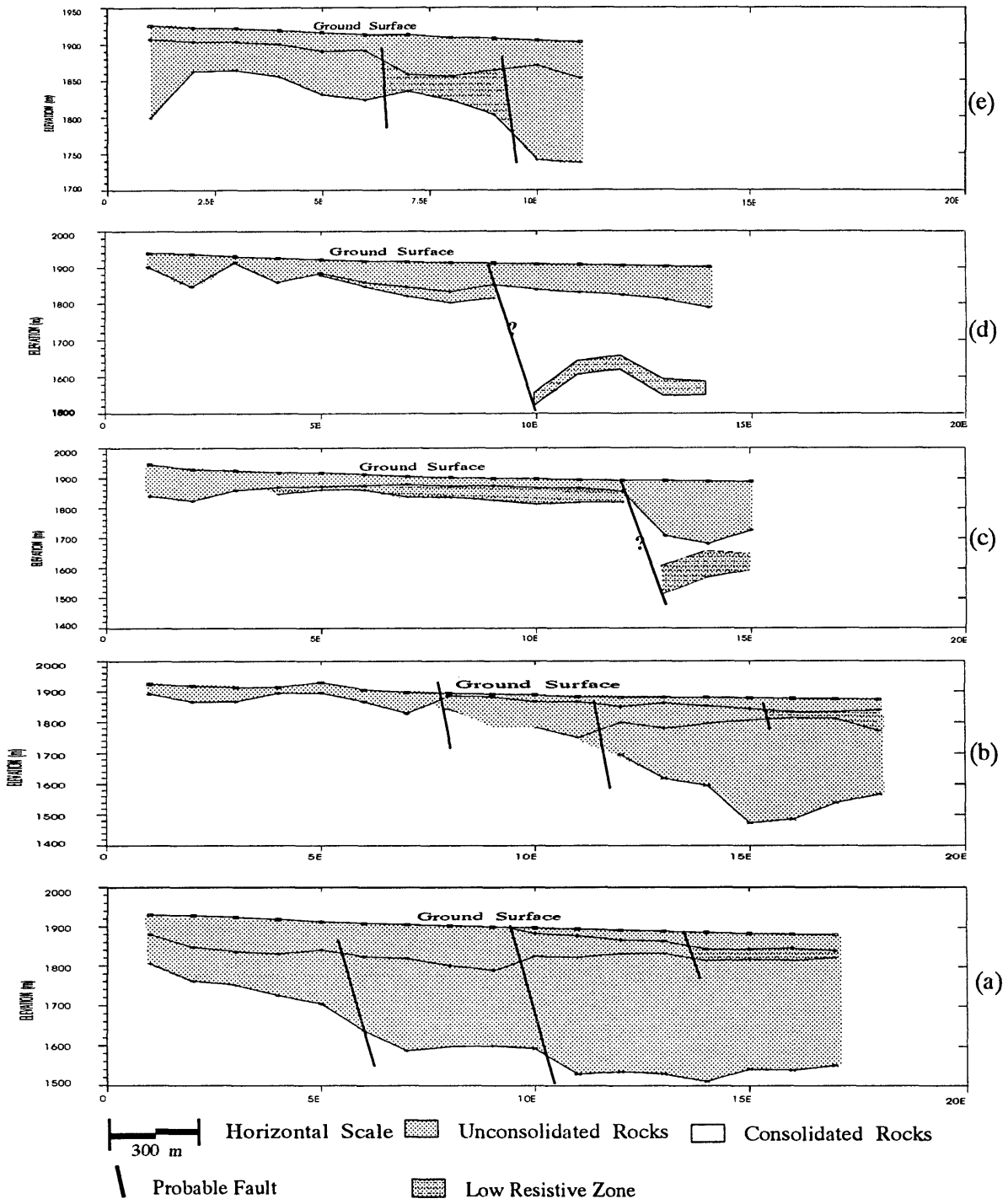the mountain (west) but also on the Line-2, 3 and 4. The Figure 2.21 also shows

FIG. 2.21. 2-D geoelectric section for (a) Line-1, (b) Line-2, (c) Line-3, (d) Line-4 and (e) Line-5.

some possible faults which are determined by sharp changes on the depth and lateral changes on the resistivities, on the geoelectric sections. The topography and depth of the resistive basement surface maps are shown in Figure 2.22. the Figure 2.22b shows the topographic surface map of the study area. As seen in Figure 2.22a, the surface topography of the depth of volcanic rocks more less follows to the surface topography.

2.7   Geologic Interpretation

As it was seen in the previous section, the depth of the unconsolidated rocks which probably correspond to volcanic basement, has been found and its surface map was plotted in Figure 2.22b. At the both side (North and South) of the survey area, the depth of the volcanic rocks changes sharply therefore, two fault may be located between Line-1 and 2, Line-4 and 5. These two faults are plotted approximately on the Figure 2.24. Their orientation may be changed between Line-1 and 2, Line-4 and 5 respectively but, the block between these two faults move up and the blocks on the other side of the faults move down. This fault system can be called *horst* and *graben*. The figure 2.24 shows also other faults from geoelectric sections on each transient line. These faults may continue along the S-N direction. One of them may be plotted as a *basin-bounding fault* and its eastern part moves down and western part moves up (Figure 2.24). There is a evidence of existing of this fault between Line-2 and 3. As is seen in Figure 2.23, the sharp changing of depth along the lithological section allows us put some faults on the section. The approximate location of these faults are plotted on the Figure 2.24 thus, one of these locations matches with the basin-bounding fault.

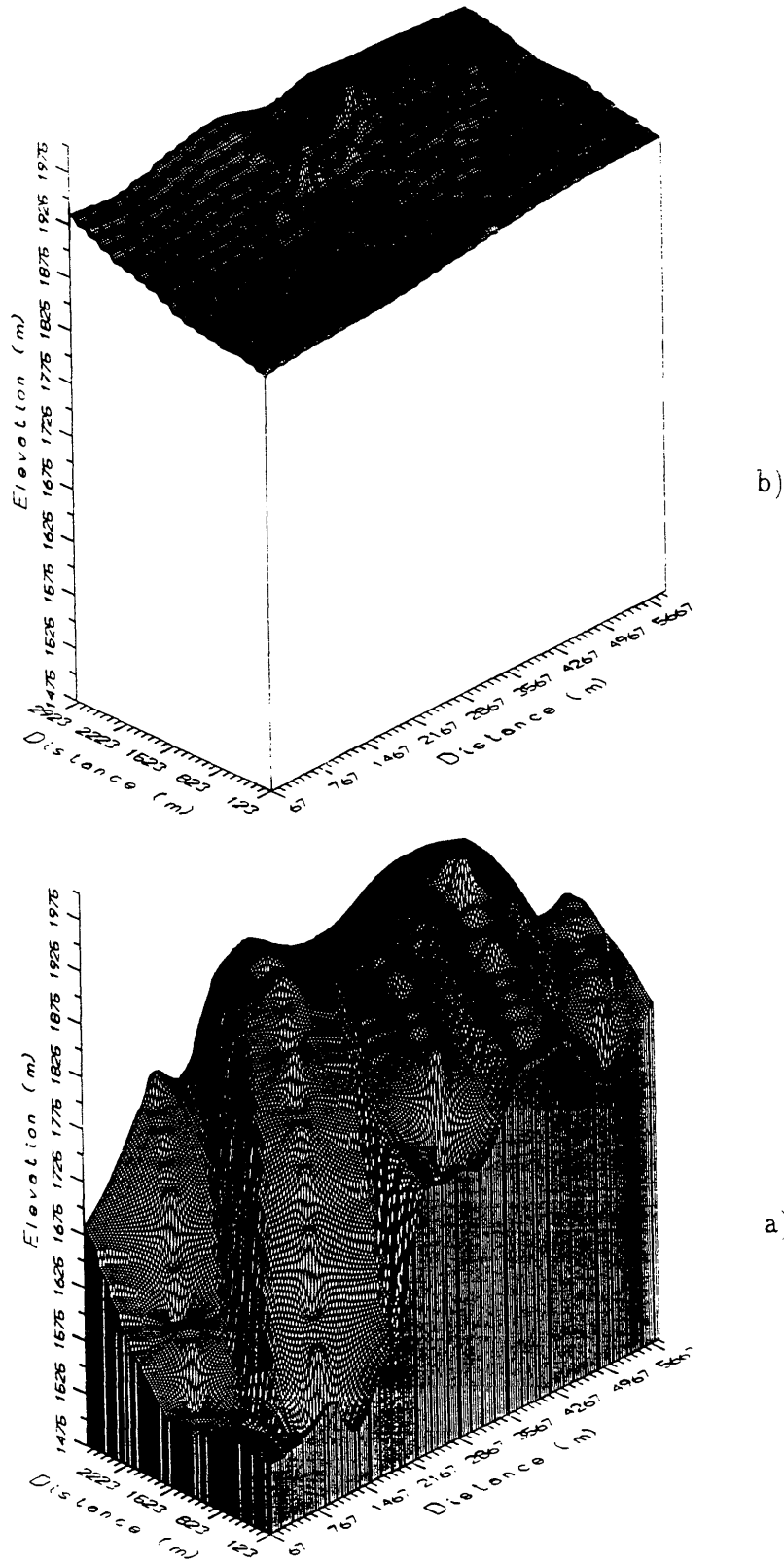On the each geoelectric section, there is a low resistive zone which may correspond

FIG. 2.22. The surface map of (a) depth to resistive basement, (b) topography.
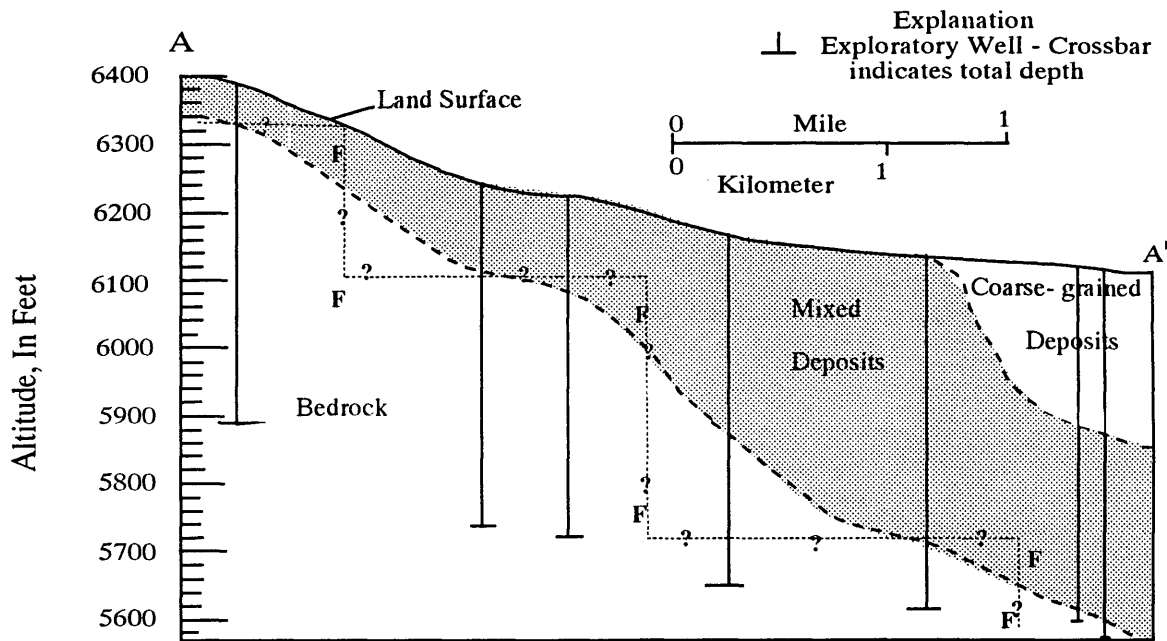
FIG. 2.23. Probable fault location on the Lithological section A-A.

to a hot water zone. The source of hot water zone may be pluton which is interpreted from aeromagnetic survey or hot springs. As is seen in Figure 2.24, two faults, W-E direction, may continue through the pluton and hot springs zone. It is also seen that each hot water zone, on each line, may contact to the basin-bounding fault. As a result, the hot water zone may be associated with basin-bounding fault which may be associated with W-E direction faults. Moreover, the W-E direction faults may continue through the hot springs and igneous intrusion zones.

2.8 Conclusion

The results of this survey demonstrated the ability of the transient electromagnetic method in resolving the depth of the volcanic basement unlike the seismic refraction or aeromagnetic survey.

BASIN and RANGE PROVINCE
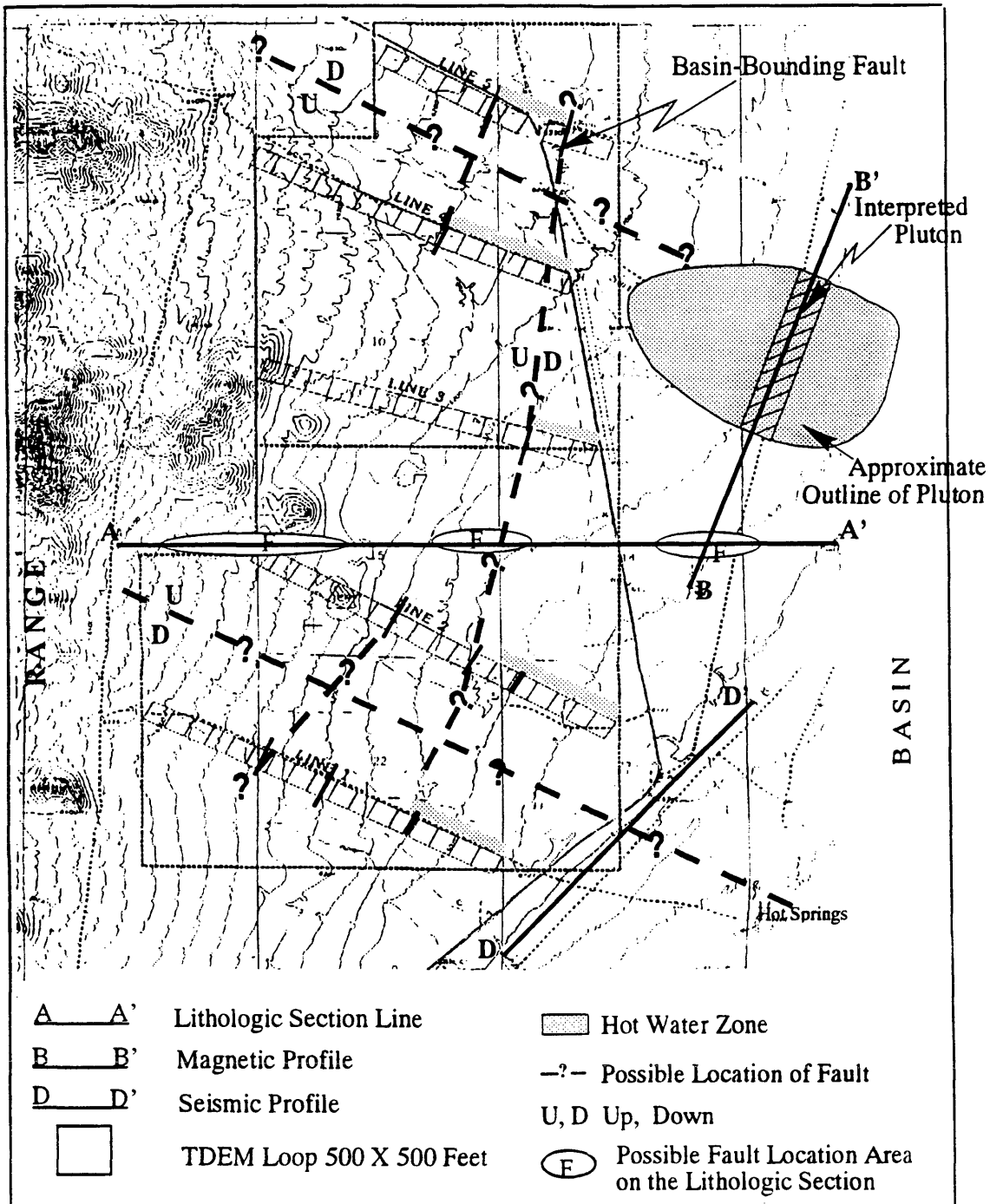
FIG. 2.24. Surveys Location Map.

In addition, the following conclusions are drawn from this thesis:

- The method succeeded in determining the thickness of the unconsolidated heterogeneous rocks which lie on the consolidated volcanic basement.

- The transient electromagnetic method was also able to distinguish the heterogeneous alluvium in three parts, surface, low resistive and relatively resistive layers.

- The changing of depth of alluvium and lateral resistivity changes along the profile were able to delineate the prevailing fault system.

- The low resistive layers associated with faults are caused by movement of hot water.

SELECTED BIBLIOGRAPHY

Abdelmalik, M.B.A., 1988. Vertical resolution capability study of direct current, magnetotelluric and time-domain electromagnetic methods. Thesis T-3327, Colorado School of Mines Golden, CO.

Blackhawk Geosciences, Inc. 1988. Geophysical surveys for mapping salt water encroachment Nassau county, Long Island, New York. Blackhawk Geosciences Inc. Golden, Colorado.

Blackhawk Geosciences, Inc., December 3, 1991. Geophysical survey for characterizing the hydrogeologic regime of the Puu Anahulu area of North Kona Island of Hawaii. Blackhawk Geosciences Inc. Golden, Colorado.

Blackhawk Geosiences, Inc., December 16, 1991. Time domain electromagnetic measurements east-central Florida. Blackhawk Geosciences Inc. Golden, Colorado.

Blackhawk Geosiences, Inc., February 18, 1991. Geophysical survey for ground water exploration adjacent to Anderson elementary school Guam, Mariana Islands. Blackhawk Geosciences Inc. Golden, Colorado.

Blackhawk Geosciences, Inc. 1992. Review of electromagnetic techniques hydrocarbon exploration in support of and reservoir development in the USSR. Blackhawk Geosciences, Inc. Golden, Colorado.

Earth Technology, 1986. Newbery volcano EM-42 report. The Earth Technology Corporation Golden, Colorado.

Fitterman, D., V., Stewart, M., T., 1986. Transient electromagnetic sounding for ground water. Geophysics V. 51, No:4, 995-1004.

Fitterman, D., V., Stanley, W., D., Bisdorf, R., J., 1988. Electrical structure of Newbery volcano, Oregon. Journal of Geophysical Research, Vol.93 No. B9, p10,119-10,134.

Fitterman, D., V., Meekes, J.A.C. and Ritsema, I.L., 1988. Equivalence behavior of three electrical sounding methods as applied to hydrogeological problems. Presented at the 50th Annual Meeting and Technical Exhibition of the European Association of Exploration Geophysicists, June 6-10, 1988. The Haque, Netherlands.

Herring, A. T., 1967. Seismic refraction study of Smith creek valley, Nevada, pt. 6 of Thompson, G.A., and others, geophysical study of basin range structure, Dixie Valley Region, Nevada: Stanford, California, Stanford University Geophysics Department Report, 12p.

Hoekstra, P. and Pesowski, M., 1982. Exploration for conductive targets with transient electromagnetic systems. To be presented at 52nd Annual Meeting SEG, Dallas, TX, October, 1982.

Hoekstra, P., Maimane, M., Kail, D. and Lahti, R., 1989. Geophysical surveys for mapping boundaries of fresh water and salty water in southern Nassau county, Long Island, NY. To be presented at the 3rd Ntl Outdoor Action Conference (NWWA), May 22-25, Orlando, Florida.

Hoekstra, P.,Hild, J., Blohm, M.,1989. Geophysical surveys for precious metal exploration in the Basin and Range, Nevada. Society for Mining, Metallurgy and Exploration Inc., Littleton, Colorado.

Hoekstra, P., Hild, J., Toth, D., 1992. Time domain electromagnetic measurements to determine water quality in the Florida aquifer. To be presented at SAGEEP 1992 (April 27-29).

Hoekstra, P., Blohm, M.W., —. Case histories of time-domain electromagnetic sounding in environmental geophysics. Blackhawk Geosciences, Inc. Golden, Colorado.

Hoekstra, P., Lahti, R., Hild, J., Bates, C.R., Phillips, D., —. Case histories of shallow time domain electromagnetics in environmental site assessment. Blackhawk Geosciences, Inc. Golden, Colorado.

Ibrahim, K.E., 1982. A Time-Domain electromagnetic survey of cochetopa hills and alkali springs, Sagauche county, south-central Colorado. Thesis T-2647, Colorado School of Mines Golden, CO.

Interpex limited, 1992. Transient electromagnetic data interpretation software. TEMIX Plus User's Manual, Golden, Colorado.

Jacobson, J.J., 1969. Deep electromagnetic sounding technique. Thesis T-1252, Colorado School of Mines Golden, CO.

Kaufman, A.,A., and Keller,G.,V., 1983. Frequency and transient sounding. Elsevier.

Kaufman, Alexander A., 1989. A paradox in geoelectromagnetism and its resolution, demonstrating the equivalence of frequency and transient domain methods. Geoexploration, 25 287-317.

Kaufman, A.,A., and Morozova, G.,M., 1970,1972. Theoretical basis for the transient sounding method in the near-zone. Nauka, Novasibirsk, Book-1, Book-2, Book-4, Book-6, Book-7.

Keller, G.,V., Pritchard, J.,I., Jackson, J.,J., Harthill, N., 1984. Megasource time-domain electromagnetic sounding methods. Geophysics vol 49. No.7 p 993-1009.

Kwader, Thomas, 1986. The use of geophysical logs for determining formation water quality. Ground Water, V.24, No: 1, 11-15.

McNeill, J.,D., Bosnar, M. and Levy, G.,M.,1984. Application of simple loop models to the interpretation of transient electromagnetic surveys in a resistive environment. Geonics, Technical Note, TN-12.

McNeill, J.,D., 1980. Application of transient electromagnetic techniques. Geonics Technical Note, TN-7.

Mills, T., Hoekstra, P., Blohm, M., and Evans, L., 1988. Time domain electromagnetic soundings for mapping sea-water intrusion in Monterey county, California. Ground Water, V.26, No:6, 771-782.

Nabighian, M.,N., 1984. Time-domain electromagnetic methods of exploration. Geophysics V.49, No:7, 849-853.

Nabighian, M.,N., 1991. Electromagnetic methods in applied geophysics, Volume-II. Society of Exploration Geophysicists.

Salehi, I. A., 1967. Aeromagnetic survey of Smith creek valley, Nevada: in Thompson, G.A., and others, geophysical study of Basin Range structure, Dixie Valley Region, Nevada: Stanford, California, Stanford University Geophysics Department Report, 20p.

Silva, L.R., 1969. Two-layer master curves for electromagnetic sounding. Thesis T-1250, Colorado School of Mines Golden, CO.

Sinha, A.,K.,1983. Deep transient electromagnetic soundings over the McClean uranium deposits. Geological Survey of Canada, paper 82-11, p273-280.

Souto, J.M., 1980. Test of time-domain electromagnetic exploration for oil and gas. Thesis T-2278, Colorado School of Mines Golden, CO.

Stewart, John H., 1980. Geology of Nevada. Nevada Bureau of Mines and Geology, Special Publication 4.

Stewart, J.H. and Carlson, J.E., 1976. Geology map of north-central Nevada. Nevada Bureau of Mines and Geology, Map 50.

Stewart, J.H. and Carlson, J.E., 1977. Million scale geologic map of Nevada. Nevada Bureau of Mines and Geology, Map 57.

Telford, W.,M., Geldard, L.,P., and Sheriff, R.,E., 1990. Applied geophysics. Cambridge University Press.

Thomas, J.M. Carlton, S.M. and Hines, L.B., 1989. Ground-water hydrology and simulated effects of development in Smith Creek valley, a hydraulically closed basin in Lander County, Nevada. U.S. Geological Survey Professional Paper

1409-E.

APPENDIX A

TEM37 Transmitter

TEM37 transmitter uses a 2.8 KW motor generator as power source and capable of supplying 30 amps into a 300m×600m loop or 8 amps a 1000m ×1500m loop for exploration depths down to 1000m. Specifications of the transmitter are as fallows:

- Current Waveform : Bipolar rectangular current with 50% duty cycle.

- Repetition Rate : 3 Hz, 7.5 Hz or 30 Hz.

- Turn-off Time : 300 μs at 20 amps into 300m×600m. Decreases proportionally with current and transmitter loop length to minimum of 20 μsec.

- Transmitter Loop : Any dimension from 20m×20m to 2000m×2000m single turn loop. Minimum transmitter loop resistance is 0.6 ohms.

- Output Current : 30 amps maximum.

- Output Voltage : 20 to 160 volts in seven steps.

- Synchronization Mode : Reference cable or high stability quartz crystal.

- Motor Generator : 2800 W/120V/400Hz/3 phases. Approximately 8 hours continues operation from full fuel tank.

- Transmitter Protection : Electronic and electromagnetic protection against short circuit.

- Transmitter Wire : Supplies #10 copper wire PVC insulted.

- Transmitter Size : 43×27×40 cm.

- Transmitter Weight : 20 Kg.

- Motor Generator Size : 74×44×51 cm.

- Motor Generator Weight : 66 Kg.

Protem Receiver

Protem receiver is used with a suite of transmitter. Using either cable reference or crystal synchronization this lightweight multi-channel receiver operates any of five switch-selectable base frequencies ranging from 3 Hz to 315 Hz, with twenty logarithmically-spaced time gates at each base frequencies. Four interchangeable receiver coils are used with the Protem receiver. Specifications of receiver are as fallows:

- No. of Channels : 3(multiplexed).

- Measured Quantity : Time rate of decay of magnetic flux along 3 axes.

- Sensors : Different air and ferrite-cored, coils depending on the applications.

- Repetition Rate : 3 Hz, 7.5 Hz, 30 Hz or 315 Hz.

- Time Gate : 20 geometrically spaced time gates for each base frequency gives range from $6\mu s$ to 80 ms.

- Synchronization : Reference cable or high stability quartz crystal.

- Integration Time : 17.5 msec and 70 msec.

- Storage : Solid state memory with capacity for 740 data sets.

- Display : 4 lines × 16 character alphanumerical LCD.

- Data Transfer : Standard RS232 communication port.

- Receiver Batter : 12 volts rechargeable battery for 16 hours continues operation.

- Receiver Size : 34×38×27 cm.

- Receiver Weight : 13 kg.

APPENDIX B

TEMIX Plus is an interactive, graphically oriented, forward and inverse program designed to interpret transient electromagnetic data using 1-dimensional earth models. TEMIX Plus allows you to interpret a consistent TEM data set taken along a profile line. TEMIX Plus reads data from many different field instrument files and provides forward and inverse modeling for six different field geometries. TEMIX Plus accepts data from Crone, Geonics, Sirotem, Zonge, Temix and Ascii files. Lotem data types can be convolved with a system response which represents the transfer function of the filter used in the receiver. Other types of data can be used with ramp turn-off and run-on corrections. TEMIX Plus supports following field geometries.

- Moving loop-loop data for a finite size square TX loop and a vertical axis coil receiver (Slingram).

- Fixed rectangular TX loop with moving vertical axis receiver coil.

- Fixed grounded wire TX with moving vertical axis receiver coil.

- Moving grounded wire for a finite length wire and a vertical axis coil receiver.

- Moving coincident loop using a square loop.

Data are in term of NV/A-m^2 or (μ V/A for coincident loop) at each time and at each station. Unavailable values are represented in the spread sheets by "NONE"(=10^{20}).

Starting models can have up to 5 layers. The data set consists of a single set of time windows, a consistent field geometry and up to 200 sounding curves. Forward modeling calculates a synthetic electromagnetic sounding curves for a model with up to 5 plane layers. The forward modeling routines provide great computational speed

as well as increased accuracy. Anderson-style digital filtering technique supports the Henkel and Fourier transformation that comprise forward modeling.

Inverse modeling produces a model which best fits the data in a least squares sense. Inverse modeling routines use ridge regression to interactively adjust parameters of the starting model. You have to option to constrain some of the parameters of the starting model so they will not be adjusted by the inversion scheme. You also have the option to mask some of the data points so that they will not influence the fitting error or the model adjustments during inversion.

TEMIX Plus calculates sounding curves using filters designed by Anderson. TEMIX Plus accounts for ramp times by convolving the turn-off ramp with the synthetic curve for the specific layered model as described by Fitterman and Anderson. The influence of previous turn-on and turn-off cycles in the transmitter wave train (i.e., run on) is accounted for by summing up the transient voltage from delayed pulses, according to the user's specification of the frequency used in the transmitter current waveform. That is, TEMIX Plus corrects calculated curves for previous pulse and turn-off ramp time rather that removing those effects from the observed data (Interpex, 1992).